



Master Thesis at the Faculty of Physics
Ludwig-Maximilians-Universität München
Technische Universität München



Phenomenology of Asymmetric Dark Sectors

Phänomenologie der asymmetrischen dunklen Sektoren

Mar Císcar Monsalvatje

Supervisors TUM

Prof. Dr. Alejandro Ibarra
Dr. Miguel Escudero Abenza

Supervisor LMU

Prof. Dr. Gerhard Buchalla

Munich, September 2021

Declaration:

I hereby declare that this thesis is my own work, and that I have not used any sources and aids other than those stated in the thesis.

München, 29.09.2021

Abstract

We have astonishingly strong evidence for the existence of dark matter. The fact that there is a matter-antimatter asymmetry in the universe is also very well known. This, together with the fact that the measured energy densities of dark matter and baryons are of the same order of magnitude ($\Omega_{\text{DM}}/\Omega_{\text{b}} \simeq 5$), suggest that dark matter might also be asymmetric, and a possible connection between the asymmetries in the two sectors. We propose a scenario where an asymmetry originally located in the dark sector is transferred to the baryons via the leptonic sector. We develop the necessary computational tools and perform a systematic analysis to find the minimal set of conditions for the transmission of this asymmetry. We find that there must be interactions that simultaneously violate dark number D and lepton number L . Finally, we analyse the parameters of our scenario and their effect on the observed baryon asymmetry, dark matter density and baryon density, setting constraints on their values.

Acknowledgements

I would like to sincerely thank my supervisors Alejandro Ibarra and Miguel Escudero. I very much enjoyed working with them in this project. Since the day of the very first meeting where they told me that ‘there are no hierarchies in this work’, and that I could ‘choose to be a bird or a frog’ as a physicist, they encouraged me to feel comfortable and confident while doing physics. I appreciate all the time they have invested in me. I have learnt a lot from them during these past months, and their guidance was not only academic but also personal. Thank you Alejandro for trusting in me since the beginning and for offering me the opportunity to work with you. Thank you Miguel for all the advice and for always finding time for my questions and concerns, even when you were truly busy.

I would also like to thank Gonzalo, for having offered to read my thesis and for giving me such useful feedback and plenty of support. Thank you to my parents, who have always supported me with everything and given me so many opportunities. And finally, thank you to all the friends who have been there for me during this past year, specially Alejandra, Leonardo, Erik, Sara, Paula, Carmen and Álex. And to Raúl and Silvia, for making this last month in the library so enjoyable.

Contents

1	Introduction	1
2	Theoretical Framework and Motivation	4
2.1	The Dark Sector	4
2.1.1	Observational evidence for dark matter	4
2.1.2	Main dark matter candidates	8
2.1.3	Main mechanisms for dark matter production	9
2.2	An Asymmetric Visible Sector	10
2.2.1	Evidence for a baryon asymmetry	10
2.2.2	Theoretical considerations for baryogenesis	11
2.2.3	Main mechanisms for baryogenesis	13
2.2.4	Bounds for lepton asymmetries	16
2.3	An Asymmetric Dark Sector?	17
2.3.1	Ratio of dark matter and baryon densities	17
3	Thermal Universe	19
3.1	Equilibrium Thermodynamics	19
3.2	Boltzmann Equation	20
3.3	Freeze-out	22
3.3.1	Dark matter freeze-out	23
3.3.2	Asymmetric dark matter freeze-out	25
4	Connections between Dark and Visible Asymmetries	29
4.1	Transmission from Dark to Lepton Asymmetries	29
4.1.1	Systematic analysis	31
	Case 1: All symmetries conserved	31
	Case 2: Breaking CP	32
	Case 3: Breaking lepton number L	32
	Case 4: Breaking lepton number L and CP	33
	Case 5: Breaking dark number D	35
	Case 6: Breaking dark number D and CP	37
	Case 7: Breaking dark number D and lepton number L	38
	Case 8: Breaking dark number D , lepton number L and CP	40
4.1.2	Analytic analysis	42
4.2	Transmission from Lepton to Baryon Asymmetries by Sphalerons	43
4.2.1	Sphaleron rate and chemical equilibrium	43
4.2.2	Boltzmann equations and numerical resolution	45
4.2.3	Comparison with observations	47
4.2.4	Our scenario and some considerations	49
4.2.5	Parameters and results	50

5	Conclusions	53
6	Outlook	55
A	Equilibrium Number Density Expressions	57
B	Calculations for the Boltzmann Equation	59
B.1	Liouville Operator in terms of Number Density	59
B.2	Liouville Operator in terms of Yield	60
B.3	Thermal Average for Decay	60
C	Chemical Equilibration: Baryon and Lepton Asymmetries	64

Chapter 1

Introduction

The Standard Model of Particle Physics (SM) in combination with Quantum Field Theory (QFT) provide a theoretical framework that has been proven to work to a very good accuracy as a low-energy effective model. So far, all laboratory tests have agreed with its predictions with astonishing precision. It has been tested up to TeV energies at the LHC, with no evidence for new particles. The SM has also succeeded in providing experimental predictions such as the existence of the electroweak gauge bosons, the third generation of quarks needed to explain CP-violation in the quark sector, and the Higgs boson which provides a formalism to account for the masses of most particles.

But even though the SM works very well in describing a myriad of observations, we are certain that it is incomplete. The most notable weakness of the model is the fact that it does not provide a description of gravity, only of the three other forces of nature. A complete QFT description of general relativity has not yet been achieved, the formalism breaking down at very high scales. Therefore, the SM does not provide a good description of the very early universe. For a detailed review on quantum gravity the reader is pointed to [1].

Another unsatisfactory aspect of the SM is the so-called hierarchy problem. The Higgs mass, $m_H \simeq 125$ GeV [2], which sets what we call ‘the weak scale’, is much smaller than the Planck scale ($\sim 10^{19}$ GeV). The corrections that m_H receives at loop level diverge quadratically with the cutoff scale instead of being proportional to the mass itself, as happens with fermions and gauge bosons. In order to cancel these contributions and give the small measured value of m_H , there could be some new physics at the TeV scale. The most popular proposal to solve this problem is supersymmetry. To read an extensive review on the hierarchy problem and its possible implications see Ref. [3].

Additionally, there are a number of phenomenological observations that are not explained by the SM, some of which will be more extensively addressed in this work.

- **Dark Matter.** Measurements from the Cosmic Microwave Background (CMB) in combination with the standard cosmological model (Λ CDM), tell us that ~ 85 % of the matter content of the universe is dark matter (DM). There is strong observational evidence that proves the presence of some sort of invisible matter in the universe, as will be further reviewed in section 2.1.1. The most likely solution to this puzzle is the existence of a new fundamental and stable particle (or set of particles) which interacts gravitationally with ordinary matter but that otherwise couples very weakly to it. There are numerous candidates for dark matter, see section 2.1.2, but up to date the searches have yielded inconclusive results. The aim is to find a particle model together

with a production mechanism which results in the observed relic density, as we will detail in section 2.1.3.

- **Neutrino Masses.** Neutrinos are neutral fermionic particles which are completely left-handed as described by the SM. As they do not have a right-handed companion, there is no Yukawa term in the SM lagrangian that would give rise to a neutrino mass. Nevertheless, the phenomenon of neutrino flavour oscillations has been observed in the context of solar, atmospheric and reactor neutrino experiments. These oscillations can only be explained by the fact that the different neutrino flavour eigenstates are a mixture of the mass eigenstates, therefore pointing towards at least two of the SM neutrinos being massive. The nature of these masses is still an open question. See the Particle Data Group section on this topic for a comprehensive review [2].
- **Baryon Asymmetry of the Universe.** Another great puzzle in physics is the origin of the matter-antimatter asymmetry. It is clear that everything we see around us is almost exclusively composed of particles and not antiparticles. There is also evidence against the existence of sizeable amounts of antimatter in the universe. This asymmetry has in fact been measured, and the SM does not provide an explanation for it. The most plausible explanation is that somehow in the early universe, some excess of baryons over antibaryons was generated (baryogenesis). We know that any asymmetric initial condition would have been exponentially diluted away by inflation. For a general overview on baryogenesis see the correspondent chapter in Ref. [4]. We will discuss this issue in detail in section 2.2.
- **Strong CP Problem.** There is no reason for Charge-Parity (CP) to be conserved in the strong sector of the SM. However, strong CP-violation is not seen in experiments, and some really restrictive bounds have been set on the CP violating parameter, $|\bar{\theta}| \lesssim 10^{-10}$ [2]. The smallness of this parameter requires drastic fine-tuning, which is what we call the strong CP problem. One of the most popular mechanisms to solve this puzzle is called the Peccei-Quinn mechanism [5]. For a detailed discussion of this topic see Ref. [6].
- **Dark Energy.** The fact that the expansion of the universe is accelerating [7] indicates the presence in the universe of some unknown kind of energy with negative pressure, dark energy. Dark energy is encoded in the Friedman equations as a cosmological constant Λ . Measurements from the CMB show that dark energy constitutes $\sim 68\%$ of the total energy content of the universe [2], and yet its nature is unknown to us. See Ref. [8] for a compact review on the topic.

A great collection of mechanisms have been proposed to address each of the above fundamental open problems. These mechanisms usually focus on answering each question individually, with the presence of a wide variety of energy scales. Nonetheless, it is conceivable (and appealing) that some of these open questions could be simultaneously addressed in a single framework. In our work we focus on relating dark matter to the baryon asymmetry in the universe, which are both cosmological observational problems.

Motivated by the fact that the measured energy densities of dark matter and baryons are of the same order of magnitude ($\Omega_{\text{DM}} / \Omega_{\text{b}} \simeq 5$), we suggest that dark matter might be asymmetric, and that an excess of dark particles over antiparticles in the early universe could have been transmitted to the visible sector by processes relating both types of particles. We propose a scenario where an asymmetry originally located in the dark sector is transferred to the baryons via the leptonic sector.

First of all, in Chapter 2 we give an introductory motivation for the existence of a dark sector, an asymmetric visible sector, and consequently the possibility of an asymmetric dark sector. Then, in Chapter 3, we review some basic concepts and methodological tools to study the physics of the early Universe. After that, in Chapter 4 we introduce our proposal: a mechanism capable of transmitting a dark asymmetry to the visible sector. We perform a systematic analysis to find the minimal set of conditions needed to transmit an asymmetry from dark matter to the leptons. Then, we study the transmission from the leptons to the baryons by electroweak sphalerons and obtain results consistent with the CMB measurements. Finally, in Chapter 5 we show the conclusions from this work and in Chapter 6 we present the outlook and future prospects.

Chapter 2

Theoretical Framework and Motivation

In this chapter we review the theoretical framework and motivation for this thesis. In section 2.1, we consider the dark sector: the observational evidence for dark matter and the main candidates and mechanisms proposed to account for it. Then, in section 2.2 we discuss the asymmetry in the visible sector. We review evidence for a baryon asymmetry and some of the most popular mechanisms proposed to explain it. We also present the current bounds on lepton asymmetries. Finally, in section 2.3 we entertain the possibility of the dark sector being asymmetric, and motivate the work done in this thesis, where we aim to connect the asymmetries in the dark and visible sectors.

2.1 The Dark Sector

Dark matter is a fundamental open problem in modern physics and yet an integral part of the standard cosmological model. The Standard Model of Particle Physics does not have a suitable dark matter candidate, so dark matter provides evidence for physics beyond the SM. The most plausible explanation is the existence of a new particle or set of particles which are weakly coupled to visible matter, and stable on cosmological timescales (at least one of them). It is also required that they have the correct properties to seed the large scale structures we see today in the universe, which originate from small density fluctuations in the early times and which are dominated by dark matter.

2.1.1 Observational evidence for dark matter

There is strong evidence for the existence of dark matter in the universe. This evidence comes from a variety of sources, phenomena and scales, all of which show the presence some sort of non-luminous matter spread throughout the universe, and which makes $\sim 85\%$ of the matter content of the universe. Some of the observations that demonstrate the existence of dark matter are briefly reviewed next. For more extensive discussions, we refer the reader to Refs. [9, 10].

- **Dynamics of galaxy clusters.** In 1933, applying the virial theorem to the Coma Cluster, F. Zwicky found that the density of the system was at least 400 times higher than would be expected from the amount of visible matter [11]. This could only be explained by an additional non-luminous component that dominated the dynamics of the cluster. It was the first evidence for the existence of dark matter, and it has been verified in many other systems since then.

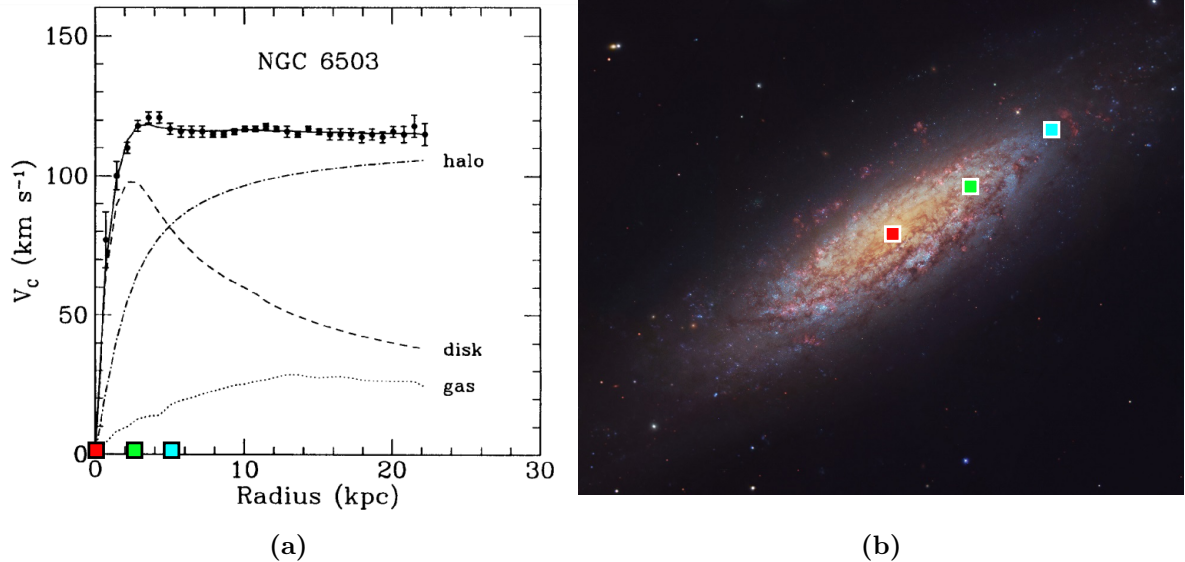


Fig. 2.1: (a) Galactic rotation curve of NGC 6503, from Ref. [13]. The different contributions from the gas and disk are plotted as dotted and dashed lines and the dark matter halo contribution needed to match the data is plotted as a dash-dotted line. (b) Optical image of NGC 6503, taken from the Subaru Telescope (NAOJ) and the Hubble Legacy Archive. The visible radius of the galaxy is 5.35 kpc [14] and the coloured squared markers are placed in both figures for size comparison purposes. We can see that the rotation curve is still flat at radii where there is no longer visible matter.

- **Spiral galaxy rotation curves.** In the 1970s, V. Rubin and K. Ford measured and analysed the fact that rotation curves of spiral galaxies are flatter after certain radius [12]. Rotation curves represent the circular velocities of stars as a function of their distance to the center of the galaxy. The observed rotation curves, as the one shown in Fig. 2.1, exhibit a plateau at distances beyond their visible disks. When the integrated visible mass $M(r)$ stops increasing with r , the circular velocity $v(r) = \sqrt{GM(r)/r}$ should decay as $v \propto 1/\sqrt{r}$. In reality, the fact that $v(r)$ remains constant indicates the presence of a halo with $M(r) \propto r$. This is perhaps the most direct evidence for dark matter on galactic scales.
- **Gravitational lensing.** According to Einstein's theory of General Relativity, the propagation of light can deviate from straight lines when passing near intense gravitational fields, which act as lenses. This distortion depends on the mass distribution of matter within the lens and is independent of its nature. The light from bright distant objects is bent by gravitational lenses and there might be multiple images of the same object, or an increment on its brightness. Lensing measurements confirm the existence of large amounts of dark matter in galaxies and clusters of galaxies. For a review on weak gravitational lensing see Ref. [15].

Collisions of galaxy clusters also give relevant information about dark matter. A reconstruction of the gravitational potential map of the clusters after the collision, like the one in Fig. 2.2, can be performed using gravitational lensing. This analysis shows that most of the total matter density remains where the individual clusters were before colliding, while the visible matter is focused in the collision region. The fact that dark matter is unaffected by the collision implies that it should be weakly interacting with visible matter and with itself.

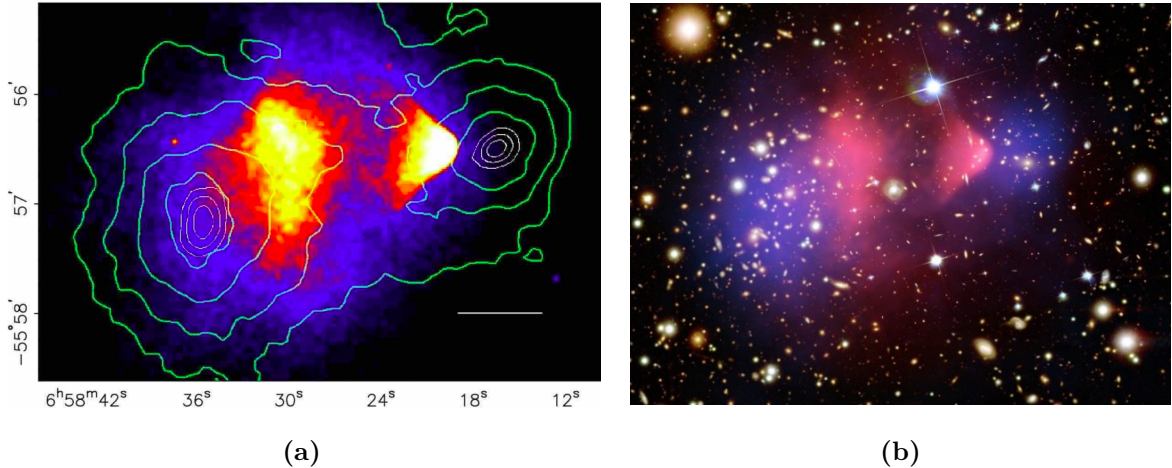


Fig. 2.2: (a) Color image from the Magellan images of the colliding Bullet cluster, 1E0657-558 [16]. The green contours show the lensing density reconstructions and the color gradient shows the X-ray emission map, which does not match the centers of the gravitational potential. (b) Composite image of the Bullet cluster. The pink region conforms the hot baryonic gas in the X-ray spectrum [17] and the blue region corresponds to the dark matter distribution obtained from the lensing maps [16]. The fact that dark matter is unaffected by the collision implies that it should be weakly interacting with visible matter and with itself.

- **Cosmic Microwave Background.** Moving to cosmological scales, perhaps the most powerful evidence for the existence of dark matter are the small CMB anisotropies. The position and shape of the peaks of the CMB power spectrum probe the photon-baryon oscillations just before the decoupling of light and matter (recombination), at the time of 3.8×10^5 years after the Big Bang. They could not be explained without the presence of dark matter. The density anisotropies, which were of order $\sim 10^{-5}$ at the time of recombination, could not have grown enough to give rise to the galaxies that we see today without a cold dark matter component which does not significantly couple to photons. While the galaxy dynamics, rotation curves and gravitational lensing give no information about the total amount of dark matter in the universe, CMB measurements are very precise probes of the dark matter energy density. Global fits to the precise CMB data from the Planck collaboration [18], within the framework of the standard cosmological model Λ CDM, tell us that $\sim 26\%$ of the total energy density of the universe is dark matter [2]

$$\Omega_{\text{DM}} = \frac{\rho_{\text{DM}}}{\rho_{\text{crit}}} = 0.265(7). \quad (2.1.1)$$

- **Structure formation.** Finally, evidence for dark matter can also be found in the study of structure formation in the universe. In the Λ CDM paradigm, primordial density fluctuations originated by inflation are the seeds of the large scale structure that we see today. Cosmological simulations show that dark matter is needed for these primordial anisotropies to develop into the observed present galaxy distribution. For detailed discussions on this topic the reader is referred to Ref. [19].
- ★ **Primordial nucleosynthesis.** Big Bang nucleosynthesis (BBN) is not an evidence for dark matter on its own, but together with the CMB measurements provides relevant information about its nature. BBN is the formation of light nuclei (D, ^3He , ^4He , and ^7Li), which takes place around 3 min after the Big Bang. BBN offers a deep reliable

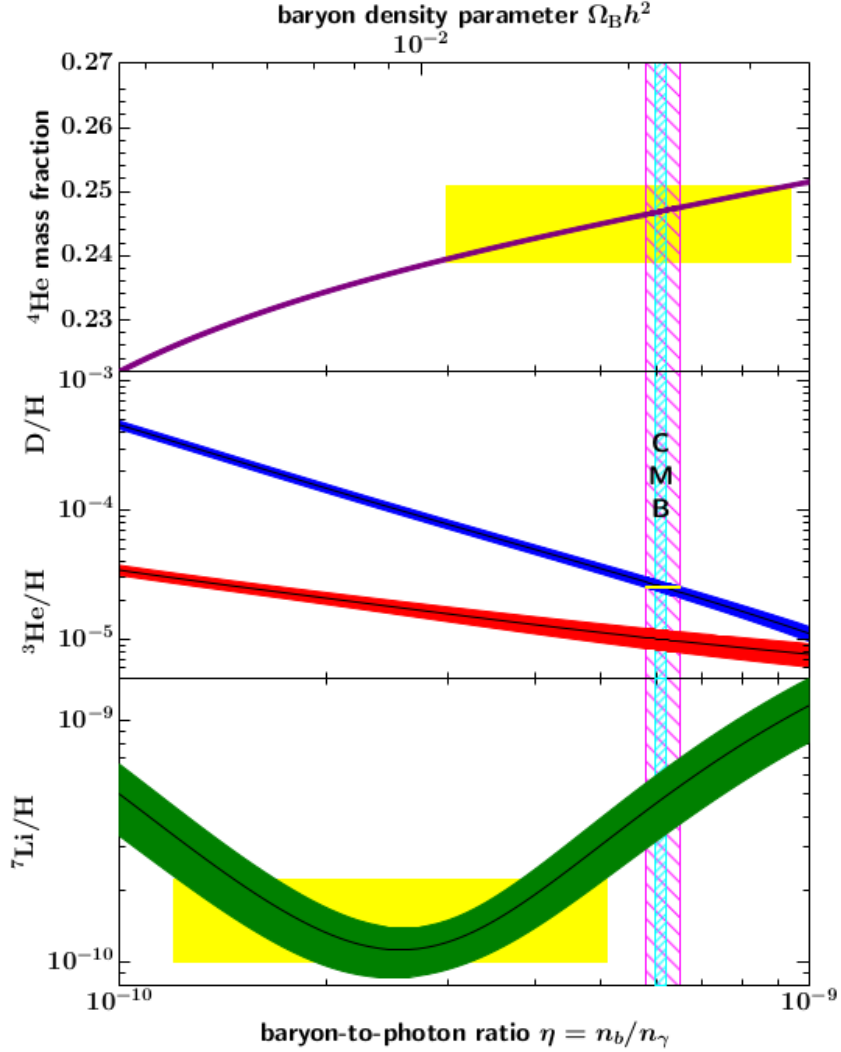


Fig. 2.3: The primordial abundances of ${}^4\text{He}$, D , ${}^3\text{He}$, and ${}^7\text{Li}$ as predicted by BBN. The bands show the 95% CL range. The yellow boxes indicate the measured abundances. The vertical blue band corresponds to the CMB measure of the baryon density, while the vertical pink band corresponds to the BBN $\text{D}+{}^4\text{He}$ concordance range at 95% CL. Figure taken from [2].

probe of the early universe, as there is a remarkable concordance between most of its predictions and the observed element abundances. The abundances of these elements depend on the baryon density at the time, as we can see in Fig. 2.3. Particularly, the Deuterium and Helium abundances have been measured up to a precision of 1% and the high sensitivity of the deuterium abundance to the baryon energy density allows us to strongly constrain it [2]

$$0.021 \leq \Omega_b h^2 \leq 0.024 \quad (95\% \text{ CL}), \quad (2.1.2)$$

where $h \equiv H_0/100 \text{ km s}^{-1} \text{ Mpc}^{-1}$. For a value of $h \sim 0.7$, this results in $0.043 \lesssim \Omega_b \lesssim 0.049$. The comparison of these constraints with the measurements of the total density provided by the CMB ($\Omega_m \simeq 0.3$), prove that most matter in the universe is not only dark, but also takes a non-nucleonic form. See the review on [2] for a broader analysis on the topic.

2.1.2 Main dark matter candidates

There is a large number of candidates for dark matter. As we have seen in the previous section, the evidence for its existence is convincing at an array of astrophysical and cosmological scales. The allowed range for dark matter masses is also extremely wide, ranging from $\sim 10^{-30}$ to $\sim 10^{57}$ GeV [2]. The most motivated dark matter candidates have been linked to other problems in particle physics, such as the electroweak hierarchy problem, the strong CP problem, or the neutrino masses.

As already mentioned, most likely the nature of dark matter is some fundamental particle. Many particle candidates have been proposed, such as WIMPs, axions and sterile neutrinos, which are described below. Further examples of the numerous particle candidates for dark matter are FIMPs [20], SIMPs [21], dark photons [22] and gravitinos [23]. Other possibilities that have been proposed include primordial black holes [24]. Furthermore, modification of gravity at galactic scales has been also proposed to explain the spiral galaxy rotation curves [25], but fails to explain the CMB [26]. Here we review some of the leading particle candidates for dark matter. For a wider review see [9, 27].

WIMPs

Weakly Interacting Massive Particles are hypothetical particles in the MeV-TeV mass range, which interact with visible matter as weakly or more weakly than the weak nuclear force in the SM. These particles would annihilate with one another into light thermal particles via $2 \leftrightarrow 2$ interactions in the early universe. At early times when the rates are high, WIMPs are in thermal equilibrium with the rest of the cosmic plasma. Later, as the universe expands and the interaction rates decrease, WIMPs decouple from the thermal plasma and its comoving density remains constant until today, setting the relic abundance.

The relic abundance is determined by the annihilation cross-section, $\langle\sigma v\rangle_{\text{ann}}$, and the value which gives the correct abundance is $\langle\sigma v\rangle \simeq 2.6 \times 10^{-9} \text{ GeV}^{-2}$, which is very close to the characteristic cross-section of the weak interactions. This coincidence is known as ‘the WIMP miracle’, and the required cross section stays almost constant for a wide range of dark matter masses [28]. This hints for a connection between weak-scale physics and dark matter, which is one of the properties that has made WIMPs popular candidates for dark matter. Another reason for their popularity is their theoretical motivation. They emerge in a variety of SM extensions, and particularly they are a natural prediction of the Minimal Supersymmetric Standard Model with R parity conservation, where they appear as the lightest neutralino. For comprehensive reviews on WIMPs see Refs. [9, 29].

Weak processes are difficult to detect, but not impossible. This constitutes another motivation for WIMPs, as it is an scenario that could be experimentally tested. There are three main ways to search for WIMP-like particles:

1. Direct detection. Consists in looking for the signatures of DM-nucleus or DM-electron scatterings inside underground detectors.
2. Indirect detection. Consists in detecting the product particles resulting from the annihilation or decays of WIMPs in astrophysical environments such as the Sun, the center of the Milky Way, or its satellite galaxies.
3. Collider searches. They consist in finding the correspondent missing energy in a collider event.

At the present moment no strong evidence for a dark matter signal compatible with all complementary constraints has been found. For the current status and future prospects of WIMP dark matter we refer the reader to Ref. [30].

Axions

Axion particles arise as a natural consequence of the Peccei-Quinn mechanism, which is the most popular attempt to solve the strong CP problem of the SM [5]. In addition, axions can be good dark matter candidates. They are pseudo-Goldstone bosons arising from the breaking of a new global symmetry, the $U(1)_{\text{PQ}}$. Dynamically, the vacuum of the theory is CP-conserving, therefore solving the strong CP problem. See Refs. [6, 31] for extensive reviews on this topic.

The mass and the relic abundance of axions is not predicted directly by the Peccei-Quinn mechanism, but it depends on the assumptions made regarding their production and the energy scale at which the $U(1)_{\text{PQ}}$ symmetry breaks. However, laboratory searches, stellar cooling and the dynamics of supernova 1987A together with the CMB could be used to constrain the mass of axions to be very small, $m_a \lesssim 0.1$ eV [32, 2]. The coupling of axions to ordinary matter is also model dependent, but they are expected to be extremely weak. In the KSVZ model [33, 34], the axion to photon coupling is expected to range from $\sim 10^{-10}$ to $\sim 10^{-18}$ GeV^{-1} depending on the axion mass [35]. It is possible to find an adequate range of parameters which are in agreement with the observational constraints for dark matter and hence represent a good dark matter candidate. For a review on the ongoing axion searches see Ref. [36].

Sterile neutrinos

As already described in Chapter 1, there is evidence for neutrino flavour oscillations, firstly considered by Bruno Pontecorvo [37]. This points to the fact that at least two of the SM neutrinos have a mass, requiring physics beyond the SM. One of the natural ways to account for neutrino masses is the addition of a right-handed companion N_R for the left-handed SM neutrino ν_L . N_R is called a sterile neutrino because it would carry no quantum numbers under the SM symmetry groups. The most popular mechanism for neutrino mass generation is the seesaw mechanism [38], which consists in including a Majorana mass term for N_R in addition to the Yukawa couplings with ν_L in the Lagrangian. This mechanism associates the light masses of active neutrinos with high scales for the masses of N_R .

It has been shown that sterile neutrinos of masses around the keV could account for dark matter [39]. Such dark matter particles would originate in the early universe via oscillations with light active neutrinos. This scenario is theoretically very appealing, but most of the parameter space for it has been already ruled out by a combination of cosmological considerations and X-ray searches. For a review on the current status of sterile neutrino dark matter see Ref. [40].

2.1.3 Main mechanisms for dark matter production

The landscape of mechanisms which attempt to explain the generation of dark matter is quite wide. Each mechanism has very different features depending on the model they are framed into. Here we briefly comment on three of the most popular mechanisms.

- **Freeze-out mechanism.** This scenario usually accounts for WIMP-like particles. The dark matter is initially in equilibrium with the thermal bath of particles from the visible sector through its coupling to lighter particles in the plasma. At some point, the rate for interactions involving dark matter and SM particles becomes smaller than the rate at which the universe is expanding. Then, the dark matter decouples from the thermal plasma ‘freezing out’. From this moment on, the comoving number density of dark matter particles remains constant. This mechanism will be detailed in section 3.3.
- **Freeze-in mechanism.** Maybe dark matter was never in thermal equilibrium with the plasma. In this context the freeze-in mechanism emerges [20]. It involves a Feebly Interacting Massive Particle (FIMP), which is decoupled from the thermal bath. It is assumed that the abundance of dark matter is initially negligible. The interactions with the bath lead to some production of dark matter until it freezes in, remaining constant afterwards. As opposed to the freeze-out case, the abundance at the moment of freeze-in increases with the strength of the interactions. Another difference with freeze-out is that here the relic abundance is dependent on the initial conditions.
- **Misalignment mechanism.** This is the mechanism through which axion-like dark matter would be generated. It consists in the production of axions in the early universe as a result of coherent oscillations of the axion field, which result in zero-momentum bosonic condensates behaving as cold dark matter. For a quantitative and comprehensive description of the phenomena see Ref. [6].

2.2 An Asymmetric Visible Sector

Our universe is predominantly made of matter, and the fact that there is much more matter than antimatter is known as the baryon asymmetry. This does not seem to agree with the fact that CP is almost a perfect symmetry as we measure it at colliders. The baryon asymmetry is one of the most relevant open problems in physics today, and finding a baryogenesis mechanism is not at all a trivial task.

2.2.1 Evidence for a baryon asymmetry

Even though antimatter is rare around us, we have observed it in small quantities on Earth: it is produced in the decay of some radioactive nuclei and it has been produced and stored in particle physics laboratories. We also know that the solar system is made of matter, as the space exploration probes that visited the planets would not have survived otherwise. Moving to galactic scales, we can probe material from all the galaxy and beyond by cosmic rays. Tiny amounts of antiprotons are seen here, at the level of $\sim 10^{-4}$ compared to the amount of protons [4]. But these antiprotons are believed to come from reactions of said rays with the interstellar material¹, and they evidence that there is a galactic asymmetry between baryons and antibaryons.

The nucleon-antinucleon annihilation cross section is rather large, keeping them in thermal equilibrium with the cosmic plasma until very low temperatures ($T \sim 22$ MeV). This implies that if the universe was locally baryon symmetric, the nucleon-antinucleon annihilation would have been going on for such a long time during its thermal history, that now the relic abundance of nucleons (and antinucleons) would be around

¹They might also come from dark matter annihilation [41]

$n_b/s = n_{\bar{b}}/s \approx 7 \times 10^{-20}$ [4]. This number is nine orders of magnitude smaller than the measured value. One could argue that maybe the universe is baryon symmetric, but distributed in different matter or antimatter separated bubbles, us living inside a huge matter region. This is also ruled out as it has been shown that annihilation near regional boundaries would produce a signal exceeding observational limits [42]. The conclusion is, therefore, that the universe is not baryon symmetric.

The easiest explanation is that in the early universe there was already some excess of baryons over antibaryons. The baryon-antibaryon annihilation then took place leaving only baryons in the universe. It is unlikely that the asymmetry was an initial condition, as it would have been erased by inflation. We assume then that some mechanism must have existed in the very early universe to generate the excess of baryons, and this still unknown mechanism we call baryogenesis.

The ratio of the number density of baryons to photons in the universe, η_B , is most precisely measured from the height of the power spectrum peaks of the CMB [18]

$$\eta_B \equiv \frac{n_b}{n_\gamma} = (6.12 \pm 0.04) \times 10^{-10}. \quad (2.2.1)$$

Since the existence of significant amounts of antimatter in the universe is excluded, η_B is also a measure of the matter-antimatter asymmetry,

$$\eta_B \equiv \frac{n_b}{n_\gamma} = \frac{n_b - n_{\bar{b}}}{n_\gamma}. \quad (2.2.2)$$

The measured value shown in Eq. (2.2.1) is a very small number, and it corresponds to a very tiny quark-antiquark asymmetry in the early universe: one extra quark for every 30 million.

2.2.2 Theoretical considerations for baryogenesis

Sakharov conditions

Sakharov wrote his famous paper on baryogenesis in 1967 [43], shortly after the discovery of CP-violation in K^0 decays. There he presented a model where three necessary conditions for the generation of a baryon asymmetry in the Universe were outlined.

1. **Baryon number violation.** We must need B -violation in order to generate a net baryon number $B \neq 0$. We know that the inflationary conditions do not allow an initial baryon number, and so if all the interactions in the universe preserve B , it seems impossible to depart from $B = 0$.
2. **C and CP violation.** The conservation of charge conjugation (C), and the product of charge conjugation and parity (CP), imply that the reaction rate for two processes related by the exchange of particles and antiparticles would be the same. Even in the presence of B non-conserving interactions, without C or CP violation, the rate of processes involving baryons would be as large as that of processes involving antibaryons. Without this necessary mismatch, a net baryon number cannot be generated.

3. **Departure from thermal equilibrium.** In thermal equilibrium the phase space density of baryons and antibaryons is effectively the same, implying that no asymmetry can be generated. We can also think of it in terms of rates. In thermal equilibrium the interaction rates are very fast compared to the expansion of the universe, so we effectively have that the interaction rate of a process equals that of the inverse process. This produces a generation and a washing-out of the baryon number at the same speed, with a zero net effect. We therefore need departure from thermal equilibrium for an asymmetry generation.

These three conditions are crucial if we want to generate a baryon asymmetry from scratch, but as we will see in chapter 4, not all of them are necessary if we generate the baryon asymmetry by transmitting it from another sector. The C and CP violating interactions could be exempted if we start from a CP non-conserving medium (asymmetric initial conditions) and the B -violating interactions would not be necessary if dark matter also carried baryon number. The only compulsory condition for the purpose of symmetry generation is the departure from thermal equilibrium.

Electroweak Sphalerons

In the Standard Model, baryon number B and lepton number L are global symmetries $U(1)_B$ and $U(1)_L$. These symmetries are said to be ‘accidental’, meaning that there is no fundamental principle for them to be conserved. They are conserved at tree level

$$\partial_\mu J_B^\mu = \partial_\mu J_L^\mu = 0. \quad (2.2.3)$$

But it was discovered by 't Hooft in 1976 [44] that quantum effects give rise to the chiral anomaly and induce B and L violation by non-perturbative effects

$$\partial_\mu J_B^\mu = \partial_\mu J_L^\mu = \frac{N_F}{32\pi^2} \left(g^2 W_{\mu\nu}^a \tilde{W}^{a\mu\nu} - g'^2 B_{\mu\nu} \tilde{B}^{\mu\nu} \right), \quad (2.2.4)$$

where N_F is the number of families, $W_{\mu\nu}$ and $B_{\mu\nu}$ are the $SU(2)_L$ and $U(1)_Y$ field strengths, g and g' their coupling constants. The notation $\tilde{A}^{\mu\nu}$ is defined as $\tilde{A}^{\mu\nu} \equiv (1/2)\epsilon^{\mu\nu\sigma\rho} A_{\sigma\rho}$. It is easy to see that $B - L$ is conserved in the SM, even at quantum level

$$\partial_\mu (J_B^\mu - J_L^\mu) = \partial_\mu J_B^\mu - \partial_\mu J_L^\mu = 0. \quad (2.2.5)$$

while the orthogonal combination $B + L$ does not,

$$\partial_\mu (J_B^\mu + J_L^\mu) \neq 0. \quad (2.2.6)$$

The change in B and L is related to the change in the topological charge or the Chern-Simons number N_{CS} as [45]

$$B(t) - B(0) = N_F [N_{CS}(t) - N_{CS}(0)]. \quad (2.2.7)$$

There is an infinite number of degenerate vacuum states with a different Chern-Simons integer number as illustrated in Fig. 2.4, where the minima are the vacuum states. To change N_{CS} by one unit, the system needs to go over an energy barrier, which are the

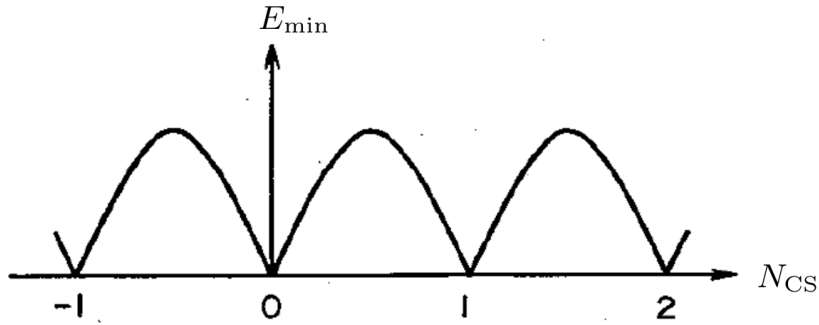


Fig. 2.4: Minimal field energy for given value of the Chern-Simons number N_{CS} , from Ref. [46]. The energy barriers are the so-called electroweak sphalerons.

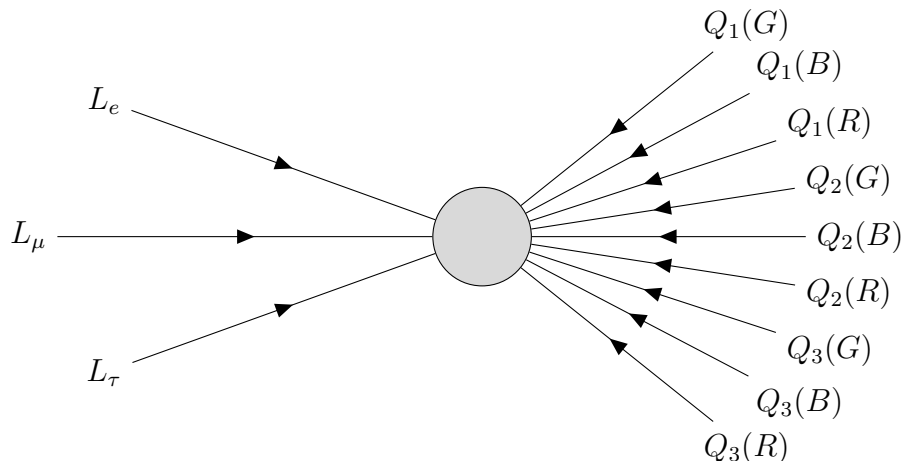


Fig. 2.5: Electroweak sphaleron interactions, involving 12 left-handed fermions: 9 quarks and 3 leptons.

static solutions to the equations of motion, called sphalerons. The transition from one vacuum to a different one is associated with a change in baryon and lepton numbers by a multiple of $N_{\text{F}} = 3$, as can be seen from Eq. (2.2.7). At low energies, the N_{CS} -changing transitions can only occur via tunneling, while at high temperatures thermal fluctuations can take the system over the sphaleron barriers. The number of transitions per unit time and unit volume is known as the Chern-Simons diffusion rate or sphaleron rate, Γ_{sph} . Sphaleron transitions are associated to interactions that involve 12 left-handed fermions: 9 quarks and 3 leptons, as shown in the diagram in Fig. 2.5. For more extensive discussions on the topic of electroweak sphalerons, we refer the reader to Refs. [4, 45]. The electroweak sphaleron processes will be relevant later in this thesis as they will be in charge of transmitting the asymmetry from the leptonic to the baryonic sector, see section 4.2.

2.2.3 Main mechanisms for baryogenesis

There is a number of mechanisms attempting to explain the generation of the baryon asymmetry of the universe, where the main action happens at many different energy scales ranging from 10^2 to 10^{16} GeV. Here we give a short review on two of the most popular and best motivated: electroweak baryogenesis and leptogenesis. Some other important proposals are GUT baryogenesis, provided by Grand Unified Theories, which were the earliest well-motivated scenarios for implementing Sakharov's ideas. In these theories,

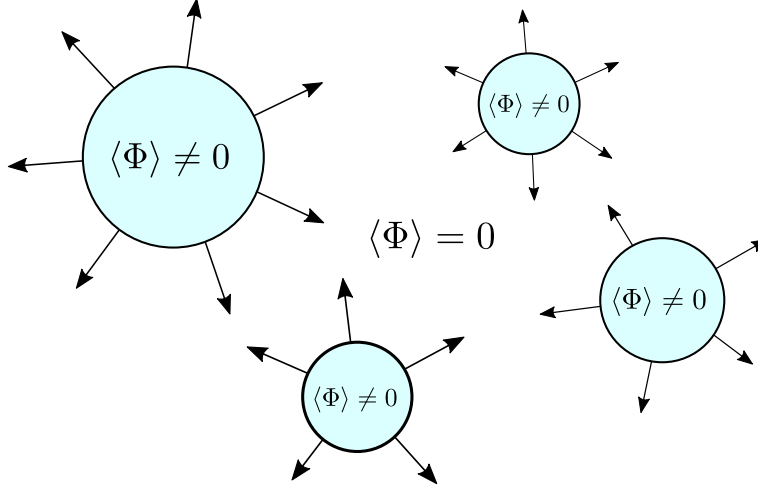


Fig. 2.6: First-order electroweak phase transition. Expanding bubbles from the broken phase with $\langle \Phi \rangle \neq 0$ within the surrounding plasma in the symmetric phase with $\langle \Phi \rangle = 0$.

quarks and leptons appear as members of a common irreducible representation of the gauge group, and B and L violation comes naturally. $SU(5)$ GUT models were excluded as the sphaleron processes would completely wash-out the generated asymmetry, see Refs. [4, 47]. Another worth-mentioning mechanism is Affleck-Dine baryogenesis [48], which can be highly efficient and presupposes low energy supersymmetry. Here, the ordinary quarks and leptons are accompanied by scalar quarks and leptons also carrying L and B numbers. Their decay into fermions in the early universe can change the net baryon number. For an in-depth review on this mechanism see Ref. [47].

Electroweak baryogenesis

Electroweak baryogenesis (EWBG) refers to any mechanism in which the baryon asymmetry is generated during the electroweak phase transition (EWPT). There have been many different proposed realizations for EWBG, but all of them share some common features [49]. The initial conditions for all the EWBG scenarios consist of a net zero baryon charge in a radiation-dominated universe which is symmetric under the electroweak symmetry group $SU(2)_L \times U(1)_Y$.

For EWBG to be successful, the EWPT must be first-order [50]. These kind of phase transitions proceed via bubble nucleation: bubbles with non-zero Higgs vacuum expectation value (VEV), $\langle \Phi \rangle \neq 0$, expand within the symmetric phase space with $\langle \Phi \rangle = 0$ to eventually collide and fill all space, as illustrated in Fig. 2.6. The sphaleron rate is highly effective outside the bubbles (symmetric phase), but exponentially suppressed inside them (broken phase). The asymmetry generation takes place near the bubble walls in 3 steps.

1. The particles in the plasma scatter with the bubble walls. CP-violation in these walls leads to different amounts of reflection/absorption for right- and left-handed quarks and antiquarks, leading to a chiral asymmetry in the vicinity of the wall. This is schematically shown in Fig. 2.7. The net effect is that outside the bubbles, the number of $(\bar{q}_L + q_R)$ is higher than the number of $(\bar{q}_R + q_L)$.

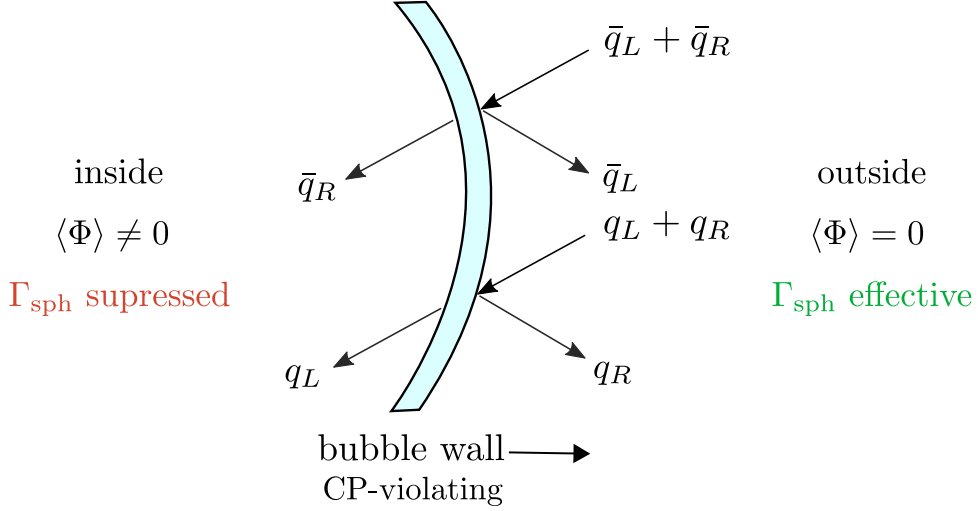


Fig. 2.7: Schematic baryon asymmetry production near the bubble walls. CP-violation in these walls leads to different amounts of reflection/absorption for right- and left-handed quarks and antiquarks.

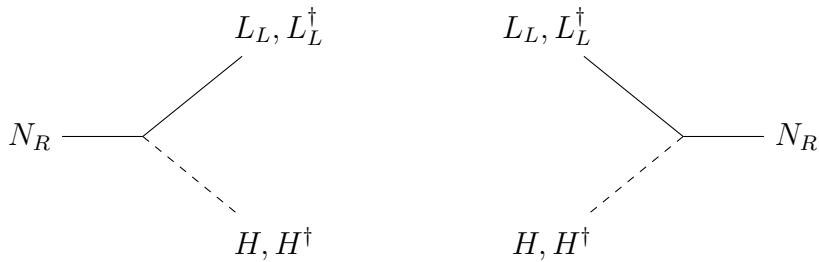
2. Electroweak sphalerons, which are effective outside the bubbles, generate the baryon asymmetry as they are biased to produce more baryons than antibaryons. Sphalerons only affect the left-handed quarks, and due to the chiral asymmetry generated in step 1, the interaction rate $\Gamma(\bar{q}_L \rightarrow 8q_L + 3l_L)$ with $\Delta B = +3$ is higher than $\Gamma(q_L \rightarrow 8\bar{q}_L + 3\bar{l}_L)$ with $\Delta B = -3$. A net B asymmetry is generated.
3. Finally, the generated net baryon number diffuses into the bubbles as they expand. Because the sphaleron rate is strongly suppressed in the broken phase, the asymmetry is not washed out. We have now a net B in a broken-phase universe.

These three steps satisfy the Sakharov's conditions. Although all ingredients involved are present in the SM, we need physics beyond the SM to explain the observed baryon asymmetry. In the first place, in order for EWPT to be first-order, the mass of the Higgs boson should be $m_H \lesssim 70$ GeV [51], much smaller than the value measured in experiments, $m_H = (125.10 \pm 0.14)$ GeV [2]. In addition, the CP-violation induced by the CKM phase in the quark sector of the SM is not enough to generate a sufficient chiral asymmetry [52]. It would result in a baryon asymmetry of order $\sim 10^{-20}$, which is tiny compared with the observed value in Eq. (2.2.1). For extensive reviews on EWBG, the reader is referred to Refs. [53, 45].

Leptogenesis

The main idea behind thermal leptogenesis is the generation of a baryon asymmetry through the generation of a lepton asymmetry, which is then transmitted by the electroweak sphaleron processes.

As already mentioned in section 2.1.2, the introduction of right-handed sterile neutrinos, N_R , is a usual procedure to account for the problem of neutrino masses. The seesaw mechanism [38] could explain the smallness of the observed light neutrino mass scale when the Majorana mass is much larger than the electroweak scale. The key feature of the sterile neutrino for leptogenesis is that it can participate in L -violating interactions. Its decay and inverse decay through the Dirac mass term into the lepton doublet L_L and the Higgs H has a change of $\Delta L = 1$:



Some scattering processes also have $\Delta L = 1$ or $\Delta L = 2$. These interactions generate a net $B - L$ number that will be partially transmitted from L to B by sphalerons.

The condition of CP-violation is also fulfilled in N_R decays and inverse decays at one-loop level, when there are two or more generations of sterile neutrinos. However, it is not guaranteed that the C and CP violation would be large enough for leptogenesis. Departure from thermal equilibrium is also guaranteed due to the expansion of the universe, for Majorana masses of order $10^{10} - 10^{16}$ GeV. For a more extensive review on leptogenesis see Ref. [45].

2.2.4 Bounds for lepton asymmetries

We are able to measure the baryon asymmetry of the universe very accurately from the CMB power spectrum. However, we have very loose bounds for the lepton asymmetry. Because of the global charge neutrality of the universe, we know the lepton asymmetry associated to the charged leptons. Now, the asymmetry related to the neutrinos could be a priori much larger. This means that the lepton asymmetry is effectively encoded in the neutrino-antineutrino asymmetry, η_ν . Therefore, it is quite hard to observe.

Luckily, the light element abundances produced in primordial nucleosynthesis are quite sensitive to the lepton asymmetry, see Ref. [54]. The reason for this is that these abundances depend sensitively on the neutron-to-proton ratio at the time where the weak interactions among them freeze out. The excess of electron neutrinos over antineutrinos shift the equilibrium between neutrons and protons via reactions of the type

$$p^+ + e^- \leftrightarrow n + \nu_e,$$

making the neutron fraction sensitive to the lepton asymmetry. Moreover, the energy density of neutrinos, increased by the neutrino asymmetry, affects the cosmic expansion. This provides another way of constraining the lepton asymmetry, by constraining the effective number of neutrinos N_{eff} .

We expect neutrinos to quickly oscillate before BBN, which equilibrates the asymmetry among the different flavours [55]. A detailed BBN analysis shows that [56]

$$\xi_\nu \equiv \mu_\nu/T_\nu = 0.001 \pm 0.016, \quad (2.2.8)$$

with

$$\eta_\nu \equiv \frac{n_\nu - n_{\bar{\nu}}}{n_\gamma} \approx \frac{1}{12\zeta(3)} \left(\frac{T_\nu}{T}\right)^3 (\pi^2 \xi_\nu + \xi_\nu^3). \quad (2.2.9)$$

This translates into the following bounds for lepton-to-photon ratio, η_L , and lepton asymmetry, $Y_L \equiv (n_l - n_{\bar{l}}) / s$, today:

$$\begin{aligned} |\eta_L| &\lesssim 4 \times 10^{-3}, \\ |Y_L| &\lesssim 6 \times 10^{-4}. \end{aligned} \tag{2.2.10}$$

The constraints on the lepton asymmetry are $\sim 10^7$ orders of magnitude more relaxed than those on the baryon asymmetry, see Eq. (2.2.1). These bounds will be relevant later in this thesis as we will be generating a lepton asymmetry together with the baryon asymmetry.

2.3 An Asymmetric Dark Sector?

In section 2.1.2 we reviewed some of the candidates for symmetric dark matter. As we saw on section 2.2.1, the visible sector is asymmetric. It is natural therefore to consider a dark sector for which the abundances of particles and antiparticles are not identical: Asymmetric Dark Matter (ADM). We will give a technical review on ADM freeze-out in section 3.3.2.

2.3.1 Ratio of dark matter and baryon densities

Another strong motivation for considering an asymmetric dark sector comes from the fact that the dark matter and baryon abundances are observationally very similar [18]

$$\Omega_{\text{DM}} \simeq 5 \Omega_{\text{b}}, \tag{2.3.1}$$

suggesting a possible common mechanism relating both sectors.

These two quantities are a priori unrelated. On the one side we have the WIMP freeze-out paradigm for dark matter, where the relic density is fixed by the time at which the interaction rate drops below the Hubble expansion. On the other side, in baryogenesis the relic density of baryons is given by the CP-violation parameters and by the out-of-equilibrium dynamics related to the B non-conserving processes. Since these conditions are not related to each other, it seems surprising that the energy densities of dark and visible matter are of the same order of magnitude.

One way of relating both sectors is by considering an asymmetry in the dark sector which is related to the baryon asymmetry. Both asymmetries might have a common origin, generated simultaneously by the same mechanism. Alternatively, an asymmetry could arise in one of the two sectors and then be transmitted to the other one. At some point, the processes which communicate the two sectors (or at least the processes which communicate their asymmetries) would decouple, isolating the asymmetry in each sector. Eventually, if the dark matter was thermalized, the symmetric part of its abundance must annihilate away as happens with the baryons and antibaryons.

In this thesis we will focus on the situation in which an asymmetry was first originated in the dark sector and then it is transmitted to the visible sector via interactions among dark matter and leptons. The transmission from the leptonic to the baryonic sector is then carried out by the electroweak sphalerons. The reason for choosing an initial dark asymmetry is that it is easier to generate it in the dark sector than in the visible one. We know much less about the dark sector, which translates into fewer constraints. Finding a model and a mechanism to generate an asymmetry in the dark sector would be much simpler. Most of the mechanisms proposed for this purpose are analogous to those introduced for baryogenesis, see section 2.2.3. For complete reviews on the ADM see Refs. [57, 58].

Chapter 3

Thermal Universe

The purpose of this chapter is giving a review on some of the theoretical elements to analyse the physics in the early universe. In section 3.1 we briefly discuss some aspects of equilibrium thermodynamics. Then, in section 3.2 we introduce the Boltzmann equation for a generic interaction. Finally, we review the physics of the freeze-out mechanism in section 3.3, for symmetric and asymmetric dark matter. The reader is referred to Refs. [4, 59] for extensive reviews on these topics.

3.1 Equilibrium Thermodynamics

In the early universe, the particles were forming a hot dense plasma which was in thermal equilibrium. At temperatures over a few GeVs, all standard model particles have energies well above their rest mass

$$E \approx \sqrt{m^2 + |\vec{p}|^2} \approx |\vec{p}|,$$

so they can be considered as relativistic (they behave as radiation). In this context, the only relevant parameter is the temperature of the plasma. For species in kinetic equilibrium, their phase space distributions are given by the Fermi-Dirac distribution for fermions or Bose-Einstein distribution for bosons

$$f_{\pm} = \frac{1}{e^{(E-\mu)/T} \pm 1}, \quad (3.1.1)$$

where the + sign corresponds to fermions and the - sign to bosons. μ is the chemical potential of the particle species. Sometimes we can approximate the chemical potential of the SM particles in the early universe to be zero, $\mu = 0$, as it is negligible compared to the temperature. However, this would imply that the number of particles and antiparticles is the same, which is not exactly true. Moreover, if the species are in chemical equilibrium, we can set a relation between the chemical potential of the particles involved in certain interactions. For an interaction $a + b \rightarrow i + j$, the relation between the chemical potentials would be $\mu_a + \mu_b = \mu_i + \mu_j$.

In order to obtain the number density n and the energy density ρ of a particle species with g internal degrees of freedom, we perform the integrals

$$n = \frac{g}{(2\pi)^3} \int f(E) d^3p, \quad (3.1.2)$$

and

$$\rho = \frac{g}{(2\pi)^3} \int E f(E) d^3p, \quad (3.1.3)$$

where $E^2 = |\vec{p}|^2 + m^2$. The dependence of the number density n with the temperature is explicitly shown on appendix A.

3.2 Boltzmann Equation

We now know how to describe the evolution of a particle species when it is in equilibrium with the thermal plasma of the universe. The evolution of the abundance around the epoch of decoupling is nevertheless more challenging.

To understand the evolution of the particle species we focus on the evolution of its phase space distribution, which evolves according to the Boltzmann equation. The Boltzmann equation can be written generically in the form

$$\hat{L}[f] = \hat{C}[f], \quad (3.2.1)$$

where \hat{C} is the collision operator and \hat{L} is the Liouville operator. For the Friedmann-Lemaître-Robertson-Walker (FLRW) metric, the Liouville operator takes the form

$$\hat{L}[f(E, t)] = E \frac{\partial f}{\partial t} - \frac{\dot{a}}{a} |\vec{p}|^2 \frac{\partial f}{\partial E}. \quad (3.2.2)$$

Recalling the definition of the number density in terms of the phase space density (3.1.2), dividing by E and integrating Eq. (3.2.2) by parts, one arrives to

$$\dot{n} + 3Hn = \frac{g}{(2\pi)^3} \int \frac{d^3p}{E} \hat{C}[f], \quad (3.2.3)$$

where H is the Hubble parameter. To see this step explicitly, see appendix B.1.

Now, developing the collision term on the right-hand side of the equation for a generic interaction ($\psi + a + b + \dots \leftrightarrow i + j + \dots$) where we are focusing on particle ψ ,

$$\begin{aligned} \frac{g_\psi}{(2\pi)^3} \int \hat{C}[f] \frac{d^3p_\psi}{E_\psi} &= -g_\psi \int d\Pi_\psi d\Pi_a d\Pi_b \dots d\Pi_i d\Pi_j \dots \\ &\times (2\pi)^4 \delta^4(p_\psi + p_a + p_b + \dots - p_i - p_j \dots) \\ &\times \left[|M|_{\psi+a+b \dots \rightarrow i+j \dots}^2 f_\psi f_a f_b \dots (1 \pm f_i)(1 \pm f_j) \dots \right. \\ &\quad \left. - |M|_{i+j \dots \rightarrow \psi+a+b \dots}^2 f_i f_j \dots (1 \pm f_\psi)(1 \pm f_a)(1 \pm f_b) \dots \right] \end{aligned} \quad (3.2.4)$$

with f_ψ, f_a , etc. the phase space distributions for each particle, given by (3.1.1). Here, + applies to bosons and - to fermions. The delta function ensures energy-momentum conservation. The matrix element squared $|M|_{\psi+a+b \dots \rightarrow i+j \dots}^2$ is averaged over the initial

and the final spins, and takes into account the proper factors for identical particles. The Lorentz invariant phase space factors $d\Pi$ are defined as

$$d\Pi \equiv \frac{1}{(2\pi)^3} \frac{d^3p}{2E}. \quad (3.2.5)$$

We can make some assumptions to simplify greatly this equation:

1. Time reversal T-invariance (or equivalently CP invariance), which implies that

$$|M|_{\psi+a+b\dots\rightarrow i+j\dots}^2 = |M|_{i+j\dots\rightarrow\psi+a+b\dots}^2 \equiv |M|^2.$$

Even if CP is broken, the form of equilibrium distribution functions remains the same and this relation can effectively be considered [60].

2. We are interested in temperatures smaller than $E - \mu$, which happens for high temperatures. In this limit, the exponential in the Bose-Einstein or Fermi-Dirac distribution is large and dwarves the ∓ 1 in the denominator,

$$f = \frac{1}{e^{(E-\mu)/T} \mp 1} \approx e^{-(E-\mu)/T} \longrightarrow 1 \pm f \approx 1, \quad (3.2.6)$$

regardless of the nature of the particle (fermionic or bosonic). Even if we are not in the high temperature regime, this will translate into a correction of less than $\sim 20\%$ in the rate.

With this two assumptions, and putting together Eqs. (3.2.3) and (3.2.4), the Boltzmann equation can be rewritten as

$$\begin{aligned} \dot{n}_\psi + 3Hn_\psi = & -g_\psi \int d\Pi_\psi d\Pi_a d\Pi_b \dots d\Pi_i d\Pi_j \dots (2\pi)^4 |M|^2 \times \\ & \times \delta^4(p_\psi + p_a + p_b + \dots - p_i - p_j \dots) [f_\psi f_a f_b \dots - f_i f_j \dots], \end{aligned} \quad (3.2.7)$$

where the term $3Hn_\psi$ accounts for the dilution of the number density due to the expansion of the universe, and the right-hand side encompasses the change in particle number due to the interactions with other particles. It is usual to write the Boltzmann equation in terms of the comoving number density, removing in this way the expansion term. For these purposes a new variable called yield is defined, as

$$Y_\psi \equiv \frac{n_\psi}{s}, \quad (3.2.8)$$

with s the entropy density, given by

$$s = \frac{2\pi^2}{45} g_{\star S} T^3, \quad (3.2.9)$$

where $g_{\star S}$ are the effective number of relativistic degrees of freedom at temperature of the thermal plasma T . The entropy density scales as $s \propto T^3$ with the temperature, as opposed to the scale factor $a \propto T^{-1}$. In absence of particle creation or annihilation, the number

density also scales like $n \propto T^3$ and the yield remains constant. Using the conservation of entropy S , which translates into the condition $sa^3 = \text{constant}$, we can relate the left-hand side of Eq. (3.2.7) to the Yield as

$$\dot{n}_\psi + 3Hn_\psi = s\dot{Y}. \quad (3.2.10)$$

The explicit derivation of this relation can be found in appendix B.2. Introducing the variable $x \equiv m_\psi/T$, with $\frac{dx}{dt} = xH(x)$ and $H(x) = H(x=1)x^{-2}$ we get to

$$\dot{n} + 3Hn = sxH(x)\frac{dY}{dx} = \frac{sH(x=1)}{x}\frac{dY}{dx}. \quad (3.2.11)$$

We remember that the Hubble parameter in the radiation dominated epoch, the epoch in which we are interested, is given by

$$H = \pi\sqrt{\frac{g_\star}{90}}\frac{T^2}{M_{\text{Pl}}}, \quad (3.2.12)$$

where $M_{\text{Pl}} = 2.435 \times 10^8$ GeV is the reduced Planck mass. Using relation (3.2.11) we can turn our Eq. (3.2.7) into

$$\begin{aligned} \frac{dY_\psi}{dx} = & -\frac{xg_\psi}{H(1)s} \int d\Pi_\psi d\Pi_a d\Pi_b \dots d\Pi_i d\Pi_j \dots (2\pi)^4 |M|^2 \times \\ & \times \delta^4(p_\psi + p_a + p_b + \dots - p_i - p_j \dots) [f_\psi f_a f_b \dots - f_i f_j \dots], \end{aligned} \quad (3.2.13)$$

which is the Boltzmann equation for a generic interaction.

3.3 Freeze-out

When the temperature of the thermal plasma drops below the mass of a certain particle species, this species stops behaving relativistically. The annihilation of the particle-antiparticle pairs to lighter species is favoured in comparison to the inverse reaction: the production of particle-antiparticle pairs from lighter ones. In this instant, the equilibrium comoving number density of the particle, which previously was constant, starts decreasing exponentially, as we can see from Eq. (A.2) in appendix A. Because of this exponential suppression, if the particle species remained in thermal equilibrium until today, its number density would be totally negligible. This is what would happen in a non-expanding universe. In reality, the expansion of the universe dictates when a particle species departs from thermal equilibrium, and therefore, the evolution of its number density.

The criteria that defines whether some particle species is in thermal equilibrium or not, is the ratio between the interaction rate, Γ , with other particles in the thermal plasma, and the rate at which the universe is expanding, H . If the particles interact much more rapidly than the universe is expanding

$$\Gamma \gg H, \quad (3.3.1)$$

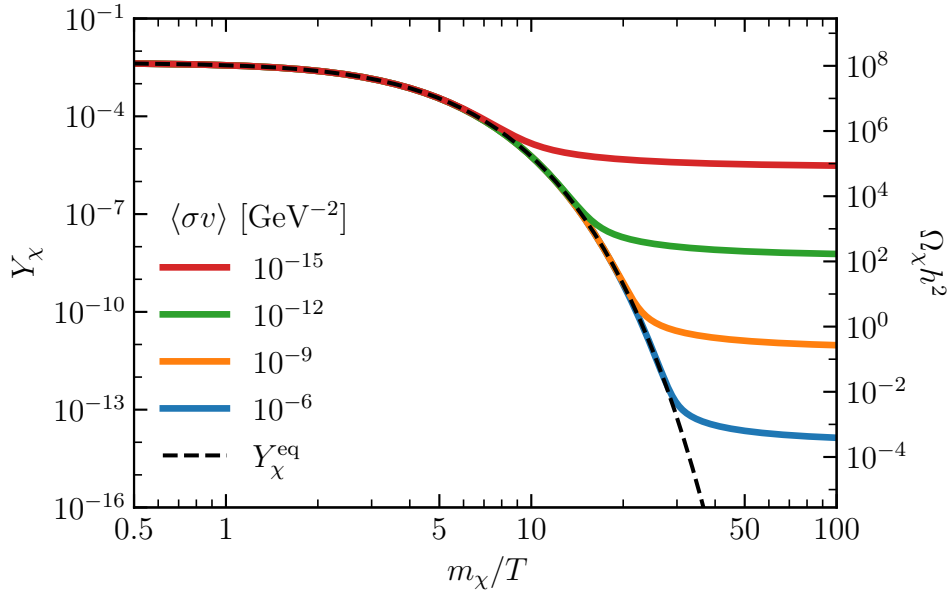


Fig. 3.1: Freeze-out of a massive particle species χ for different annihilation cross-sections and for $m_\chi = 100$ GeV. The dashed black line is the equilibrium abundance while the solid lines are the actual abundances for each annihilation strength given by the interaction cross-section $\langle\sigma v\rangle$. On the right side of the plot, the correspondence to the relic density of the species today is shown. We can see that the stronger the annihilation rate, the later the particle species freezes out and the smaller the relic abundance is. Here, and from now on, we are considering only s-wave annihilation for which $\langle\sigma v\rangle$ does not have a dependence with the velocity.

then they do not feel the expansion and they remain in equilibrium with the thermal plasma. On the contrary, the rate of interaction drops below the expansion rate

$$\Gamma < H, \quad (3.3.2)$$

then particles and anti-particles cannot find each other any more and the annihilation stops. When this happens, the species departs equilibrium with the rest of the particles and freezes-out. The comoving number density remains then constant. The stronger the interactions are, the later the particle species will freeze-out. This behaviour is shown in Fig. 3.1. When a particle species freezes out, its energy is deposited in the rest of the particle species, increasing the temperature of the plasma and therefore slowing down the cool-down of the universe.

3.3.1 Dark matter freeze-out

Let us now study more carefully the evolution of the dark matter abundance along the thermal history of the universe. Considering dark matter particles χ that are stable, massive and weakly interacting with SM particles, we have the following particle-antiparticle annihilation/production process

$$\chi \bar{\chi} \longleftrightarrow \psi \bar{\psi}, \quad (3.3.3)$$

where ψ denotes all the species into which χ can annihilate. The number of dark matter particles is changed by two units in this interaction.

We can assume that the SM particles will be in thermal equilibrium with the plasma at the temperatures relevant to the dark matter freeze-out. This assumption is based on the fact that they will have additional interactions with other particles, which will be stronger than the one in Eq. (3.3.3). Therefore, ψ and $\bar{\psi}$ will have thermal distributions with zero chemical potentials.

The Boltzmann equation for the particles χ can be specified from Eq. (3.2.13) as

$$\begin{aligned} \frac{dY_\chi}{dx} = & -\frac{xg_\chi}{H(1)s} \int d\Pi_\chi d\Pi_{\bar{\chi}} d\Pi_\psi d\Pi_{\bar{\psi}} (2\pi)^4 |M|^2 \times \\ & \times \delta^4(p_\chi + p_{\bar{\chi}} - p_\psi - p_{\bar{\psi}}) [f_\chi f_{\bar{\chi}} - f_\psi f_{\bar{\psi}}]. \end{aligned} \quad (3.3.4)$$

As the product particles have thermal equilibrium distributions with vanishing chemical potentials, their phase space distributions become

$$\begin{aligned} f_\psi &= f_\psi^{\text{eq}} = \exp(-E_\psi/T) \\ f_{\bar{\psi}} &= f_{\bar{\psi}}^{\text{eq}} = \exp(-E_{\bar{\psi}}/T). \end{aligned} \quad (3.3.5)$$

Also, the energy part of the δ -function in the Boltzmann equation enforces $E_\chi + E_{\bar{\chi}} = E_\psi + E_{\bar{\psi}}$, so that

$$f_\psi^{\text{eq}} f_{\bar{\psi}}^{\text{eq}} = \exp\left(-\frac{E_\psi + E_{\bar{\psi}}}{T}\right) = \exp\left(-\frac{E_\chi + E_{\bar{\chi}}}{T}\right) = f_\chi^{\text{eq}} f_{\bar{\chi}}^{\text{eq}}. \quad (3.3.6)$$

This trick is called ‘detailed balance’, and allows us to make the substitution

$$[f_\chi f_{\bar{\chi}} - f_\psi f_{\bar{\psi}}] \longrightarrow [f_\chi f_{\bar{\chi}} - f_\chi^{\text{eq}} f_{\bar{\chi}}^{\text{eq}}]$$

in Eq. (3.3.4). Now we can develop the interaction term of the Boltzmann equation arriving to an expression in terms of the abundances of χ ,

$$\dot{n}_\chi + 3Hn_\chi = -\langle\sigma v\rangle_{\text{ann}} [n_\chi^2 - n_{\chi,\text{eq}}^2], \quad (3.3.7)$$

or alternatively in terms of the yields, using the relation on Eq. (3.2.11)

$$\frac{dY_\chi}{dx} = -\frac{xs\langle\sigma v\rangle_{\text{ann}}}{H(1)} [Y_\chi^2 - Y_{\chi,\text{eq}}^2]. \quad (3.3.8)$$

Here we have assumed that there is not an asymmetry between the abundances of χ and $\bar{\chi}$, setting $n_\chi = n_{\bar{\chi}}$. In these expressions, $\langle\sigma v\rangle_{\text{ann}}$ is the thermally averaged annihilation cross section times velocity, summed over all possible final states, given by

$$\begin{aligned} \langle\sigma v\rangle_{\text{ann}} &= \sum_{\psi\bar{\psi}} \langle\sigma v\rangle_{\chi\bar{\chi}\rightarrow\psi\bar{\psi}}, \\ \langle\sigma v\rangle_{\chi\bar{\chi}\rightarrow\psi\bar{\psi}} &= \frac{g_\chi}{n_{\chi,\text{eq}}^2} \int d\Pi_\chi d\Pi_{\bar{\chi}} d\Pi_\psi d\Pi_{\bar{\psi}} (2\pi)^4 \delta^4(p_\chi + p_{\bar{\chi}} - p_\psi - p_{\bar{\psi}}) |M|^2 f_\chi f_{\bar{\chi}}. \end{aligned} \quad (3.3.9)$$

The calculations necessary to arrive to Eqs. (3.3.7) and (3.3.8) are not trivial. In appendix B.3 the thermal average is solved analytically for the simpler case of a decay into two massless particles.

One can now numerically calculate the evolution of the number density of the particle χ as it was done for Fig. 3.1. After the freeze-out of the particle, the yield Y_χ^f remains constant. This is because there are no more number-changing interactions, so it will be the same until today

$$Y_\chi^f = \frac{n_\chi^f}{s(x_f)} \simeq Y_\chi^0 = \frac{n_\chi^0}{s(x_0)}. \quad (3.3.10)$$

where f means freeze-out and 0 means today. We therefore can obtain the present relic density of dark matter in the universe, which can be then compared with the measured value in Eq. (2.1.1). In this way we can constrain the unknown parameters which are the dark matter mass and the annihilation cross section, $\langle\sigma v\rangle_{\text{ann}}$. One can also approximately calculate the relic density today assuming an instantaneous freeze-out.

3.3.2 Asymmetric dark matter freeze-out

As we already mentioned, symmetric WIMPs have been one of the leading dark matter candidates for many years. Another popular proposal Asymmetric Dark Matter (ADM). This candidate particle is different from its antiparticle, and therefore it is possible to have different abundances for particles and antiparticles. The assumption is that this asymmetry is generated well before the dark matter annihilation reactions freeze out. As we introduced in section 2.3.1, this scenario is motivated by the similarity of the dark matter and baryon densities in the universe, which suggest that a common mechanism might have given rise to both the baryon and the hypothetical dark matter asymmetries.

Let us consider a dark matter particle χ and its antiparticle $\bar{\chi}$. Assuming that only $\chi\bar{\chi}$ pairs can annihilate into SM particles and following Eq. (3.3.8), we can write the following Boltzmann equations for their number densities

$$\begin{aligned} \frac{dY_\chi}{dx} &= -\frac{\lambda\langle\sigma v\rangle_{\text{ann}}}{x^2} \left(Y_\chi Y_{\bar{\chi}} - Y_\chi^{\text{eq}} Y_{\bar{\chi}}^{\text{eq}} \right), \\ \frac{dY_{\bar{\chi}}}{dx} &= -\frac{\lambda\langle\sigma v\rangle_{\text{ann}}}{x^2} \left(Y_\chi Y_{\bar{\chi}} - Y_\chi^{\text{eq}} Y_{\bar{\chi}}^{\text{eq}} \right), \end{aligned} \quad (3.3.11)$$

where

$$\lambda \equiv \frac{4\pi}{\sqrt{90}} m_\chi M_{\text{Pl}} \sqrt{g_{\star S}}. \quad (3.3.12)$$

The yield of equilibrium comes from the number density in Maxwell-Boltzmann approximation given in Eq. (A.3) divided by the entropy density s defined in Eq. (3.2.9),

$$Y_{\chi, \bar{\chi}}^{\text{eq}} = \frac{45}{4\pi^4} \frac{g_\chi}{g_{\star S}} x^2 K_2(x) e^{\pm\xi}. \quad (3.3.13)$$

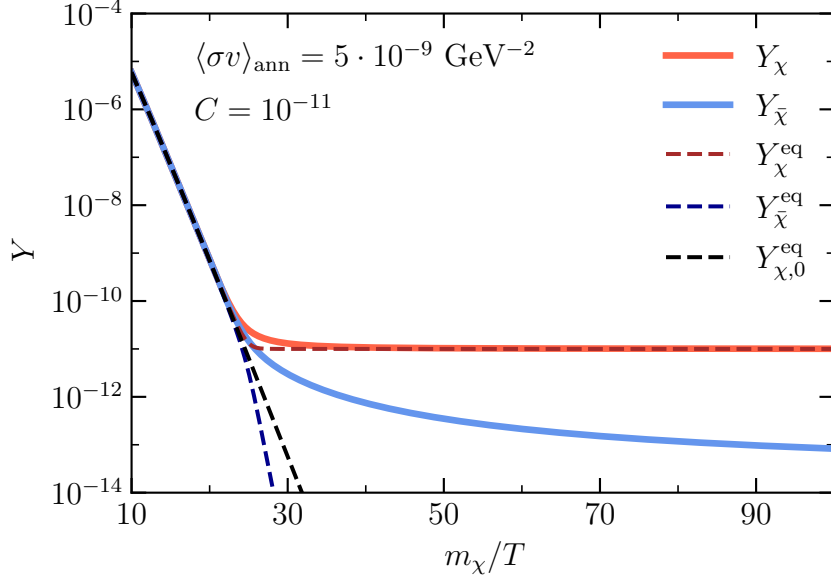


Fig. 3.2: Evolution of the χ and $\bar{\chi}$ abundances for $m_\chi = 100$ GeV, $\langle\sigma v\rangle_{\text{ann}} = 5 \times 10^{-9}$ GeV $^{-2}$ and $C = 10^{-11}$. The dashed black line is the equilibrium abundance for the case where there is no asymmetry ($C = 0$), the red and blue dashed lines are the χ and $\bar{\chi}$ equilibrium abundances for $C = 10^{-11}$, and the solid lines are the actual abundances. Our results in this plot agree with those of Ref. [61].

We take $g_\chi = 2$ for fermionic dark matter. In this expression, ξ is defined as $\xi \equiv \mu/T$, but the dependence with the chemical potential will be cancelled in Eqs. (3.3.11) as it only appears in the form $Y_\chi^{\text{eq}} Y_{\bar{\chi}}^{\text{eq}}$.

Notice that the Eqs. (3.3.11) are identical, which means that if we subtract them,

$$\frac{dY_\chi}{dx} - \frac{dY_{\bar{\chi}}}{dx} = 0,$$

which implies

$$Y_\chi - Y_{\bar{\chi}} = C, \quad (3.3.14)$$

where C is a constant. The difference between the comoving number densities of particles and antiparticles is conserved, as we would anticipate by the fact that they can only annihilate in $\chi\bar{\chi}$ pairs. This could be due to the conservation of some dark matter charge. Taking this into consideration, we can rewrite the two Boltzmann equations into a decoupled form

$$\begin{aligned} \frac{dY_\chi}{dx} &= -\frac{\lambda\langle\sigma v\rangle_{\text{ann}}}{x^2} \left(Y_\chi^2 - CY_\chi - Y_\chi^{\text{eq}} Y_{\bar{\chi}}^{\text{eq}} \right), \\ \frac{dY_{\bar{\chi}}}{dx} &= -\frac{\lambda\langle\sigma v\rangle_{\text{ann}}}{x^2} \left(Y_{\bar{\chi}}^2 + CY_{\bar{\chi}} - Y_\chi^{\text{eq}} Y_{\bar{\chi}}^{\text{eq}} \right). \end{aligned} \quad (3.3.15)$$

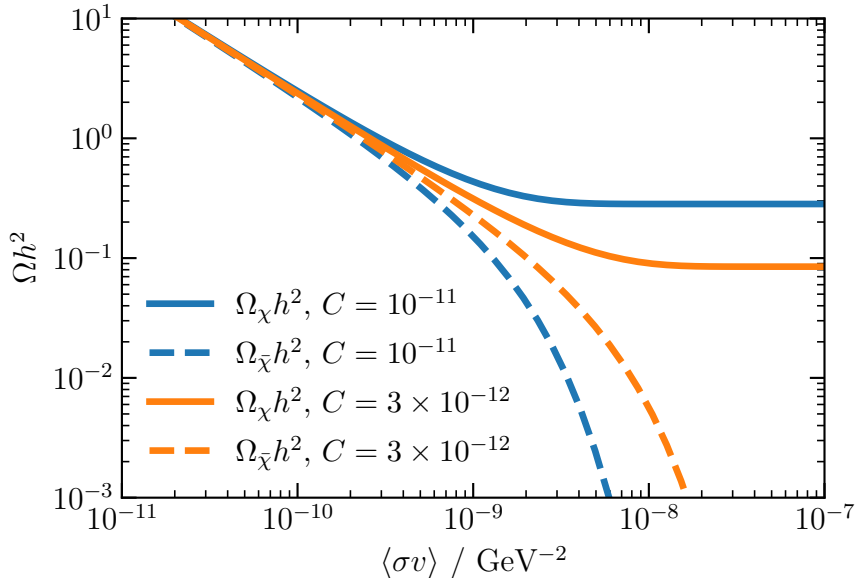


Fig. 3.3: Relic densities Ωh^2 for χ and $\bar{\chi}$ with $m_\chi = 100$ GeV, for increasing $\langle\sigma v\rangle_{\text{ann}}$ and two different values of the asymmetry: $C = 10^{-11}$ and $C = 3 \times 10^{-12}$. Only s-wave annihilation is taken into account. Our results in this plot agree with those of Ref. [61].

We can solve these equations numerically to obtain the evolution of the χ and $\bar{\chi}$ number densities, as shown in Fig. 3.2. The parameters to be chosen are the initial asymmetry C , which will remain constant as shown in (3.3.14), and the annihilation cross-section $\langle\sigma v\rangle_{\text{ann}}$, which we will assume to be in s-wave and therefore, constant. This case is different than the WIMP or symmetric freeze-out, shown in Fig. 3.1. As now the equilibrium abundances depend on the chemical potential, they are different for χ and $\bar{\chi}$. The yield Y_χ (solid red line in Fig. 3.2) is bounded from below by Y_χ^{eq} (dashed red line) to the value of the asymmetry C , as this is the excess of χ particles that cannot find $\bar{\chi}$ partners to annihilate with.

Another feature of this case is that, due to this lower bound for the χ particles, we still have a considerable number of them after freeze-out. This affects the population of $\bar{\chi}$ in the sense that they will find a non-negligible number of χ particles to annihilate with even after the decoupling temperature and they will keep decreasing for big x , as we can see in Fig. 3.2.

We can also study the dependence of the final relic abundance on the annihilation cross-section. In Fig. 3.3 we plot the value of Ωh^2 as a function of $\langle\sigma v\rangle_{\text{ann}}$, taken to be constant (s-wave annihilation). The two different colors correspond to two different asymmetries. As expected, the lower the annihilation cross section, the bigger the impact on the relic density. For small values of $\langle\sigma v\rangle_{\text{ann}}$, the value of the asymmetry C does not play a big role, as Y_χ and $Y_{\bar{\chi}}$ do not decrease fast enough to notice the lower bound imposed by the asymmetry. For large values of $\langle\sigma v\rangle_{\text{ann}}$, the value of C does affect the relic abundance and we see that when we go above certain value of the cross-section, the relic abundance of χ does not vary any more as it adopts the lowest possible value given by the asymmetry. We can also notice that for larger values of asymmetry C , the larger the difference in the relic abundance of χ and $\bar{\chi}$ is.

We note that for ADM, both χ and $\bar{\chi}$ contribute to the relic density, and their contributions have to be added,

$$\Omega_{\text{DM}} = \Omega_{\chi} + \Omega_{\bar{\chi}}. \quad (3.3.16)$$

This results in the required annihilation cross-section to be approximately twice as large as that for the WIMP case (Majorana dark matter), where there is only the contribution of Ω_{χ} to the relic density. The larger cross-section in the case of ADM reduces the relic density of each χ and $\bar{\chi}$, compensating the fact that we have two species contributing the observed relic abundance.

Chapter 4

Connections between Dark and Visible Asymmetries

In this Chapter we will introduce our proposed scenario: a mechanism capable of transmitting an initial dark asymmetry to the visible sector. First, in section 4.1, we perform a systematic analysis to find the minimal set of conditions needed to transmit an asymmetry from dark matter to the leptons. Then, in section 4.2, we study the transmission from the leptonic to the baryonic sector by electroweak sphalerons. Finally we obtain results consistent with the CMB measurements, and set constraints on our parameters.

4.1 Transmission from Dark to Lepton Asymmetries

In this section, we will explore how an asymmetry in the dark sector can be transferred into the leptonic one. For this purpose we assume an asymmetric dark matter sector consisting on a particle χ and its antiparticle $\bar{\chi}$. In general, the dark sector may consist of a variety of dark particles fulfilling some symmetry group, but for our purposes we will focus only on this particle species that couples weakly with some SM particles. We will consider that dark matter is coupled to leptons, which we denote by l , and l^c its antiparticle. These leptons will be coupled to the SM thermal bath by interactions stronger than their coupling to dark matter, therefore remaining in thermal equilibrium with the plasma in the range of temperatures taken into consideration. For now we will treat them as generic leptons, and later on we will define their nature.

The SM is invariant under a global symmetry $U(1)_L$ associated to the so called lepton number L . As this is an accidental symmetry, we can write interaction terms that break it in the Lagrangian. We also want to define a similar global symmetry $U(1)_D$ with a quantum number D carried by our dark matter particles χ and $\bar{\chi}$.

We consider an initial asymmetry C_0 between dark matter particles and antiparticles, that we will try to convert into an asymmetry in the leptonic abundances, initially taken to be symmetric. The reason for choosing an initial dark asymmetry is that the dark sector is less constrained than the visible one, and therefore it is easier to create a model where this asymmetry arises. For the purpose of asymmetry transmission, we can already anticipate that the breaking of some global symmetry will be needed. This is hinted by the Sakharov conditions listed in section 2.2.2, which also suggest that we might need some kind of CP-violation.

Case	Broken symmetries			Asymmetry transfer
	L	D	CP	
1				No
2			×	No
3	×			No
4	×		×	No
5		×		No
6		×	×	No
7	×	×		Yes
8	×	×	×	Yes

Table 4.1: List of cases we will take into account in our analysis. The crosses mark the corresponding broken symmetries for each case. L and D are the quantum numbers associated to the global symmetries $U(1)_L$ and $U(1)_D$. CP stands for charge-parity. In the right column we state whether the asymmetry will be successfully transferred for that case or not.

The approach I will follow is to systematically review the different breaking possibilities to find the minimal set of conditions needed for the transmission of the asymmetry. The list of cases that will be considered is shown in Table 4.1, where we specify which symmetries are broken in each case. This table can be considered as an index for this chapter. In Table 4.2 we list the cross-sections for the different processes that will appear along our analysis, and the notations used for them. We will refer to this table repeatedly during this section.

All conserving	$\langle\sigma v\rangle(\chi\bar{\chi} \rightarrow ll^c) \equiv \langle\sigma v\rangle_{\text{ann}}$
L -violating	$\langle\sigma v\rangle(\chi\bar{\chi} \rightarrow ll) \equiv \langle\sigma v\rangle_{L1}, \quad \langle\sigma v\rangle(\chi\bar{\chi} \rightarrow l^c l^c) \equiv \langle\sigma v\rangle_{L2}$
D -violating	$\langle\sigma v\rangle(\chi\chi \rightarrow ll^c) \equiv \langle\sigma v\rangle_{D1}, \quad \langle\sigma v\rangle(\bar{\chi}\bar{\chi} \rightarrow ll^c) \equiv \langle\sigma v\rangle_{D2}$
L - and D -violating but $D + L$ preserving	$\langle\sigma v\rangle(\chi\chi \rightarrow ll) = \langle\sigma v\rangle(\bar{\chi}\bar{\chi} \rightarrow l^c l^c) \equiv \langle\sigma v\rangle_{DL1}$
L - and D -violating but $D - L$ preserving	$\langle\sigma v\rangle(\chi\chi \rightarrow l^c l^c) = \langle\sigma v\rangle(\bar{\chi}\bar{\chi} \rightarrow ll) \equiv \langle\sigma v\rangle_{DL2}$

Table 4.2: List of cross-sections that will be considered in this section, the notations used for them and the quantum numbers broken by their interactions.

4.1.1 Systematic analysis

Case 1: All symmetries conserved

Let us start briefly reviewing the all-conserving annihilation from the standard ADM scenario, but also showing the equations and the evolution of the SM particles coupled to the dark matter. We can already foresee that no asymmetry will be transmitted in this scenario, but it is a good exercise to understand better the physics of the later more complex scenarios.

As we already mentioned, the generic leptons to which dark matter couples interact strongly with the the SM thermal bath of particles, which keeps them in thermal equilibrium with the plasma. For exemplifying purposes, in what follows we will consider the dark matter mass to be $m_\chi = 100$ GeV. The complete set of equations, considering only the process ($\chi\bar{\chi} \leftrightarrow ll^c$) and the decay of the leptons to lighter SM particles ($ll^c \leftrightarrow \text{SM}$), will be

$$\begin{aligned}
 \frac{dY_\chi}{dx} &= -\frac{\lambda}{x^2} \langle\sigma v\rangle_{\text{ann}} \left(Y_\chi Y_{\bar{\chi}} - Y_\chi^{\text{eq}} Y_{\bar{\chi}}^{\text{eq}} \right), \\
 \frac{dY_{\bar{\chi}}}{dx} &= -\frac{\lambda}{x^2} \langle\sigma v\rangle_{\text{ann}} \left(Y_\chi Y_{\bar{\chi}} - Y_\chi^{\text{eq}} Y_{\bar{\chi}}^{\text{eq}} \right), \\
 \frac{dY_l}{dx} &= +\frac{\lambda}{x^2} \left[\langle\sigma v\rangle_{\text{ann}} \left(Y_\chi Y_{\bar{\chi}} - Y_\chi^{\text{eq}} Y_{\bar{\chi}}^{\text{eq}} \right) - \langle\sigma v\rangle_{ll^c \rightarrow \text{SM}} \left(Y_l Y_{l^c} - Y_l^{\text{eq}} Y_{l^c}^{\text{eq}} \right) \right], \\
 \frac{dY_{l^c}}{dx} &= +\frac{\lambda}{x^2} \left[\langle\sigma v\rangle_{\text{ann}} \left(Y_\chi Y_{\bar{\chi}} - Y_\chi^{\text{eq}} Y_{\bar{\chi}}^{\text{eq}} \right) - \langle\sigma v\rangle_{ll^c \rightarrow \text{SM}} \left(Y_l Y_{l^c} - Y_l^{\text{eq}} Y_{l^c}^{\text{eq}} \right) \right].
 \end{aligned}
 \tag{4.1.1}$$

As in section 3.3.2, we notice that

$$\frac{dY_\chi}{dx} - \frac{dY_{\bar{\chi}}}{dx} = 0,
 \tag{4.1.2}$$

and

$$\frac{dY_l}{dx} - \frac{dY_{l^c}}{dx} = 0,
 \tag{4.1.3}$$

which means that the initial asymmetries will remain constant during the evolution of the number densities. This allows us to relate $Y_{\bar{\chi}}(x) = Y_\chi(x) - C$ and $Y_l(x) = Y_{l^c}(x)$ as we consider that the leptons do not have an initial asymmetry. The asymmetry will not be transmitted in this case as we anticipated.

Solving numerically Eqs. (4.1.1) we get the evolution of the involved particle abundances. In Fig. 4.1 these abundances are shown for two different values of annihilation cross section and dark matter asymmetries. In the two upper plots, the asymmetry between the abundance of χ and $\bar{\chi}$ is $C = 10^{-11}$, smaller than in the two lower plots, where $C = 10^{-9}$. We can see that for the same value of $\langle\sigma v\rangle_{\text{ann}}$, left or right, the different value of C influences the evolution of the abundance because it sets a lower bound for Y_χ , as explained in section 3.3.2. Comparing horizontally we can also see clearly how lowering the annihilation cross section gives a higher relic abundance. The cross-section $\langle\sigma v\rangle_{ll^c \rightarrow \text{SM}}$ takes values of $\sim 10^{-6}$ GeV $^{-2}$, which keeps the leptons effectively in thermal equilibrium.

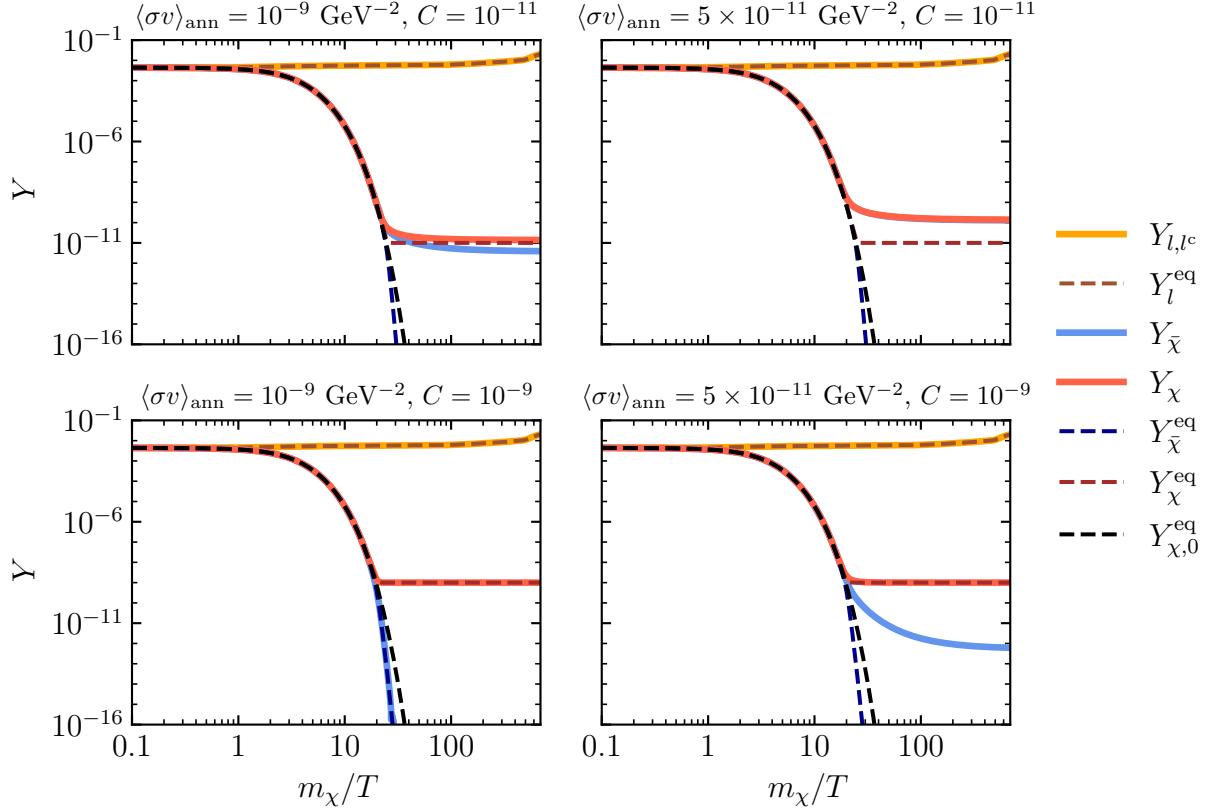


Fig. 4.1: Evolution of the comoving abundances of χ , $\bar{\chi}$, l and l^c in [Case 1](#) and assuming $m_\chi = 100$ GeV. The system is solved for different values of $\langle\sigma v\rangle_{\text{ann}}$ and the asymmetry C indicated above each plot.

Case 2: Breaking CP

The case where D and L are preserved but CP is violated cannot be considered in this analysis, as the only process allowed, the annihilation ($\chi\bar{\chi} \leftrightarrow ll^c$), is its own conjugate.

Case 3: Breaking lepton number L

In our attempt to transmit the asymmetry from the dark sector to the leptonic one we might expect the need to break the lepton number L . The yield quantifying lepton number is $Y_L \equiv Y_l - Y_{l^c}$. As we defined at the beginning of this section, the quantum number D corresponding to the global symmetry $U(1)_D$ is carried by our dark matter particles χ and $\bar{\chi}$. The yield quantifying this dark quantum number is $Y_D \equiv Y_\chi - Y_{\bar{\chi}}$, which we have been calling C when it is constant. In this section we will still only consider interactions that preserve D .

In addition to the process ($\chi\bar{\chi} \leftrightarrow ll^c$), we also have ($\chi\bar{\chi} \leftrightarrow ll$) and ($\chi\bar{\chi} \leftrightarrow l^c l^c$) which break L . First we try the case where CP is conserved. Conservation of CP means that the two reactions that break lepton number have the same cross section, $\langle\sigma v\rangle_{L1} = \langle\sigma v\rangle_{L2} \equiv \langle\sigma v\rangle_L$.

In order for the L violating interactions to take place without violating electromagnetic charge we need to impose our leptons to be electromagnetically neutral. We will still address them as generic leptons, which could be the SM left-handed neutrinos, some kind of light sterile neutrinos, or other type of particle. We will go back to this matter in [section 4.2](#).

The Boltzmann equations for this case are

$$\begin{aligned}
\frac{dY_\chi}{dx} &= -\frac{\lambda}{x^2} \left(\langle \sigma v \rangle_{\text{ann}} + 2\langle \sigma v \rangle_L \right) \left(Y_\chi Y_{\bar{\chi}} - Y_\chi^{\text{eq}} Y_{\bar{\chi}}^{\text{eq}} \right), \\
\frac{dY_{\bar{\chi}}}{dx} &= -\frac{\lambda}{x^2} \left(\langle \sigma v \rangle_{\text{ann}} + 2\langle \sigma v \rangle_L \right) \left(Y_\chi Y_{\bar{\chi}} - Y_\chi^{\text{eq}} Y_{\bar{\chi}}^{\text{eq}} \right), \\
\frac{dY_l}{dx} &= +\frac{\lambda}{x^2} \left[\left(\langle \sigma v \rangle_{\text{ann}} + 2\langle \sigma v \rangle_L \right) \left(Y_\chi Y_{\bar{\chi}} - Y_\chi^{\text{eq}} Y_{\bar{\chi}}^{\text{eq}} \right) - \langle \sigma v \rangle_{ll^c \rightarrow \text{SM}} \left(Y_l Y_{l^c} - Y_l^{\text{eq}} Y_{l^c}^{\text{eq}} \right) \right], \\
\frac{dY_{l^c}}{dx} &= +\frac{\lambda}{x^2} \left[\left(\langle \sigma v \rangle_{\text{ann}} + 2\langle \sigma v \rangle_L \right) \left(Y_\chi Y_{\bar{\chi}} - Y_\chi^{\text{eq}} Y_{\bar{\chi}}^{\text{eq}} \right) - \langle \sigma v \rangle_{ll^c \rightarrow \text{SM}} \left(Y_l Y_{l^c} - Y_l^{\text{eq}} Y_{l^c}^{\text{eq}} \right) \right].
\end{aligned} \tag{4.1.4}$$

We notice that again

$$\begin{aligned}
\frac{dY_D}{dx} &\equiv \frac{dY_\chi}{dx} - \frac{dY_{\bar{\chi}}}{dx} = 0 \\
\frac{dY_L}{dx} &\equiv \frac{dY_l}{dx} - \frac{dY_{l^c}}{dx} = 0
\end{aligned} \tag{4.1.5}$$

which means that the asymmetries of each sector do not evolve with time. Therefore, we move on to the next case where we will try breaking CP.

Case 4: Breaking lepton number L and CP

Here we consider the same annihilation processes as in [Case 3](#), but now we have $\langle \sigma v \rangle_{L1} \neq \langle \sigma v \rangle_{L2}$ due to CP-violation. See [Table 4.2](#) for the cross-section to process correspondence. The Boltzmann equation for this case take the form

$$\begin{aligned}
\frac{dY_\chi}{dx} &= -\frac{\lambda}{x^2} \left(\langle \sigma v \rangle_{\text{ann}} + \langle \sigma v \rangle_{L1} + \langle \sigma v \rangle_{L2} \right) \left(Y_\chi Y_{\bar{\chi}} - Y_\chi^{\text{eq}} Y_{\bar{\chi}}^{\text{eq}} \right), \\
\frac{dY_{\bar{\chi}}}{dx} &= -\frac{\lambda}{x^2} \left(\langle \sigma v \rangle_{\text{ann}} + \langle \sigma v \rangle_{L1} + \langle \sigma v \rangle_{L2} \right) \left(Y_\chi Y_{\bar{\chi}} - Y_\chi^{\text{eq}} Y_{\bar{\chi}}^{\text{eq}} \right), \\
\frac{dY_l}{dx} &= +\frac{\lambda}{x^2} \left[\left(\langle \sigma v \rangle_{\text{ann}} + 2\langle \sigma v \rangle_{L1} \right) \left(Y_\chi Y_{\bar{\chi}} - Y_\chi^{\text{eq}} Y_{\bar{\chi}}^{\text{eq}} \right) - \langle \sigma v \rangle_{ll^c \rightarrow \text{SM}} \left(Y_l Y_{l^c} - Y_l^{\text{eq}} Y_{l^c}^{\text{eq}} \right) \right], \\
\frac{dY_{l^c}}{dx} &= +\frac{\lambda}{x^2} \left[\left(\langle \sigma v \rangle_{\text{ann}} + 2\langle \sigma v \rangle_{L2} \right) \left(Y_\chi Y_{\bar{\chi}} - Y_\chi^{\text{eq}} Y_{\bar{\chi}}^{\text{eq}} \right) - \langle \sigma v \rangle_{ll^c \rightarrow \text{SM}} \left(Y_l Y_{l^c} - Y_l^{\text{eq}} Y_{l^c}^{\text{eq}} \right) \right].
\end{aligned} \tag{4.1.6}$$

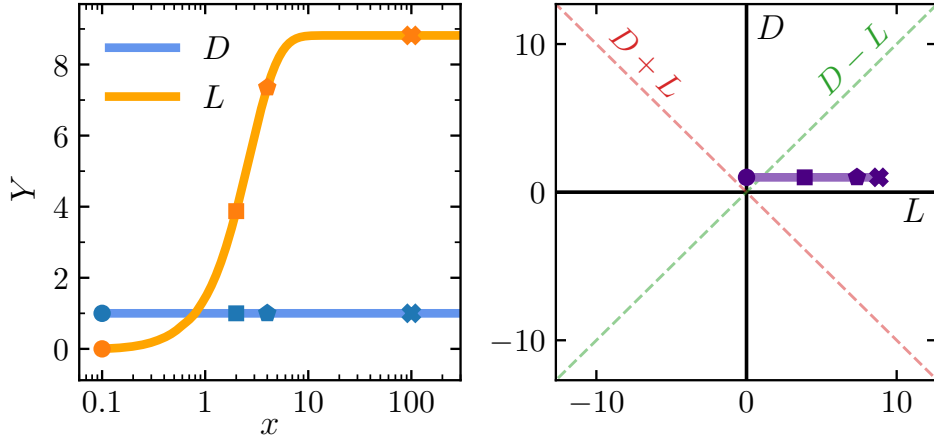


Fig. 4.2: Evolution of the dark matter asymmetry $Y_D(\equiv D)$ and the lepton asymmetry $Y_L(\equiv L)$ in Case 4, assuming $m_\chi = 100$ GeV. The system is solved for cross-sections $\langle\sigma v\rangle_{\text{ann}} = 10^{-10}$ GeV^{-2} , $\langle\sigma v\rangle_{L1} = 2 \times 10^{-18}$ GeV^{-2} and $\langle\sigma v\rangle_{L2} = 10^{-18}$ GeV^{-2} , and initial asymmetries $Y_D^{\text{in}} = 10^{-11}$ and $Y_L^{\text{in}} = 0$. The vertical axis on the left plot and both axes on the right plot are scaled by a factor of 10^{-11} . Here the notation D and L is used for the asymmetry yields. The left plot shows the asymmetries as a function of the evolution of the universe $x = m_\chi / T$. On the right plot a more schematic view of the asymmetries is shown, as a DL plane. The horizontal axis of this right plot corresponds to the change in L , and the vertical one to the change in D , which in this case stays constant. The red and green dashed lines mark the directions of preserved number $D+L$ and $D-L$ respectively, and all the directions parallel to these lines have the same conserved quantities. The purple solid line describes the evolution of the asymmetries for the chosen parameters. Finally, the markers shown in both plots mark some specific points along the evolution of the universe to help identify the correspondence between the two plots. Here the markers correspond to $x = 0.1, 2, 4$ and 100 .

Now, as the equations for the lepton and antilepton abundances are different, the evolution of the asymmetries is

$$\frac{dY_D}{dx} = 0, \tag{4.1.7}$$

$$\frac{dY_L}{dx} = 2 \frac{\lambda}{x^2} (\langle\sigma v\rangle_{L1} - \langle\sigma v\rangle_{L2}) (Y_\chi Y_{\bar{\chi}} - Y_\chi^{\text{eq}} Y_{\bar{\chi}}^{\text{eq}}).$$

These equations tell us that the asymmetry in the dark sector will not evolve but the one in the leptonic sector will. We therefore cannot say that the asymmetry will be transmitted, but rather directly generated in the visible sector. We can see this graphically in Fig. 4.2. There, we numerically solved the evolution of Eqs. (4.1.7) for cross-sections $\langle\sigma v\rangle_{\text{ann}} = 10^{-10}$ GeV^{-2} , $\langle\sigma v\rangle_{L1} = 2 \times 10^{-18}$ GeV^{-2} and $\langle\sigma v\rangle_{L2} = 10^{-18}$ GeV^{-2} ¹, and initial asymmetries $Y_D^{\text{in}} = 10^{-11}$ and $Y_L^{\text{in}} = 0$. As we predicted by looking at the evolution equations, the yield of the asymmetry in dark matter ($Y_D \equiv D$) remains constant while the leptonic one ($Y_L \equiv L$) evolves from zero to a non-negligible value. We notice that Y_L grows towards positive values because we have chosen $\langle\sigma v\rangle_{L1} > \langle\sigma v\rangle_{L2}$. In the opposite

¹ The reason for using such small values for some cross-sections is that we encountered numerical problems for larger values. These are Riccati equations, which are numerically very unstable. Taking small values for the parameters does not affect the physics of the asymmetry transfer and so it allows us to qualitatively understand the behaviour of the system. For these reasons, from here on, we will take small values for the cross-sections.

case $\langle\sigma v\rangle_{L1} < \langle\sigma v\rangle_{L2}$, the asymmetry would go towards negative values, corresponding to a larger number of antileptons than leptons.

It should be pointed out that even though the magnitude of the symmetry-conserving annihilation cross-section $\langle\sigma v\rangle_{\text{ann}}$ does not appear in the equations of the asymmetries (4.1.7), it indirectly affects the size of the generated asymmetry. This is due to the fact that $\langle\sigma v\rangle_{\text{ann}}$ plays an important part on how close will Y_χ and $Y_{\bar{\chi}}$ get to the equilibrium distributions Y_χ^{eq} and $Y_{\bar{\chi}}^{\text{eq}}$, as the first two equations in Eqs. (4.1.6) show. This affects the term $(Y_\chi Y_{\bar{\chi}} - Y_\chi^{\text{eq}} Y_{\bar{\chi}}^{\text{eq}})$ in Eqs. (4.1.7). In the same way, also the values of the cross-sections $\langle\sigma v\rangle_{L1}$ and $\langle\sigma v\rangle_{L2}$ matter, and not only their difference.

We then conclude that the breaking of L and CP creates a lepton asymmetry, but it is not a sufficient condition to allow the transmission of the asymmetry from one sector to the other. In the next case we will try breaking the dark matter number D .

Case 5: Breaking dark number D

In this case, in addition to the process $(\chi\bar{\chi} \leftrightarrow ll^c)$, we also consider $(\chi\chi \leftrightarrow ll^c)$ and $(\bar{\chi}\bar{\chi} \leftrightarrow ll^c)$, which break D by two units. First we analyse the case in which there is no CP violation. This implies that $\langle\sigma v\rangle_{D1} = \langle\sigma v\rangle_{D2} \equiv \langle\sigma v\rangle_D$ are of the same magnitude. See Table 4.2 for the cross-section to process correspondence. The Boltzmann equations are in this case

$$\begin{aligned}
\frac{dY_\chi}{dx} &= -\frac{\lambda}{x^2} \left[\langle\sigma v\rangle_{\text{ann}} (Y_\chi Y_{\bar{\chi}} - Y_\chi^{\text{eq}} Y_{\bar{\chi}}^{\text{eq}}) + 2\langle\sigma v\rangle_D (Y_\chi^2 - Y_{\chi,\text{eq}}^2) \right], \\
\frac{dY_{\bar{\chi}}}{dx} &= -\frac{\lambda}{x^2} \left[\langle\sigma v\rangle_{\text{ann}} (Y_\chi Y_{\bar{\chi}} - Y_\chi^{\text{eq}} Y_{\bar{\chi}}^{\text{eq}}) + 2\langle\sigma v\rangle_D (Y_{\bar{\chi}}^2 - Y_{\bar{\chi},\text{eq}}^2) \right], \\
\frac{dY_l}{dx} &= +\frac{\lambda}{x^2} \left[\langle\sigma v\rangle_{\text{ann}} (Y_\chi Y_{\bar{\chi}} - Y_\chi^{\text{eq}} Y_{\bar{\chi}}^{\text{eq}}) + \langle\sigma v\rangle_D (Y_\chi^2 + Y_{\bar{\chi}}^2 - Y_{\chi,\text{eq}}^2 - Y_{\bar{\chi},\text{eq}}^2) \right. \\
&\quad \left. - \langle\sigma v\rangle_{ll^c \rightarrow \text{SM}} (Y_l Y_{l^c} - Y_l^{\text{eq}} Y_{l^c}^{\text{eq}}) \right], \\
\frac{dY_{l^c}}{dx} &= +\frac{\lambda}{x^2} \left[\langle\sigma v\rangle_{\text{ann}} (Y_\chi Y_{\bar{\chi}} - Y_\chi^{\text{eq}} Y_{\bar{\chi}}^{\text{eq}}) + \langle\sigma v\rangle_D (Y_\chi^2 + Y_{\bar{\chi}}^2 - Y_{\chi,\text{eq}}^2 - Y_{\bar{\chi},\text{eq}}^2) \right. \\
&\quad \left. - \langle\sigma v\rangle_{ll^c \rightarrow \text{SM}} (Y_l Y_{l^c} - Y_l^{\text{eq}} Y_{l^c}^{\text{eq}}) \right].
\end{aligned} \tag{4.1.8}$$

The evolution of the asymmetries is

$$\begin{aligned}
\frac{dY_D}{dx} &= -\frac{2\lambda}{x^2} \langle\sigma v\rangle_D (Y_\chi^2 - Y_{\bar{\chi}}^2 - Y_{\chi,\text{eq}}^2 + Y_{\bar{\chi},\text{eq}}^2), \\
\frac{dY_L}{dx} &= 0.
\end{aligned} \tag{4.1.9}$$

In this case, we have the opposite situation to the one in Case 4. The lepton asymmetry does not change, while the dark matter asymmetry will evolve.

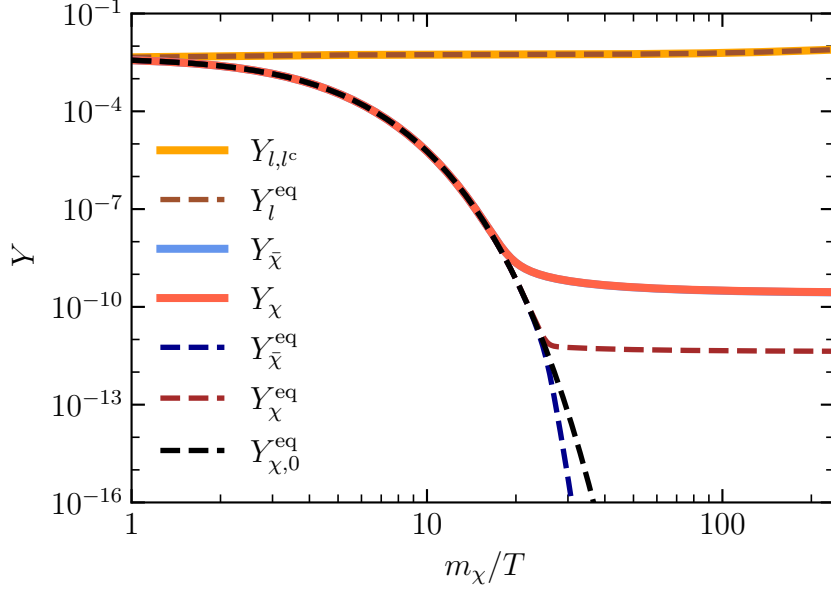


Fig. 4.3: Evolution of the comoving abundances of χ , $\bar{\chi}$, l and l^c in **Case 5**, assuming $m_\chi = 100$ GeV, $\langle\sigma v\rangle_{\text{ann}} = 2 \times 10^{-11}$ GeV $^{-2}$, $\langle\sigma v\rangle_D = 2 \times 10^{-12}$ GeV $^{-2}$, and $Y_D^{\text{in}} = 10^{-10}$. The dashed lines correspond to the equilibrium distributions and the solid ones to the actual yields. In this particular case the blue solid line corresponding to $Y_{\bar{\chi}}$ is hidden behind the red solid line.

Now that the yield of the dark matter asymmetry $Y_D(\equiv Y_\chi - Y_{\bar{\chi}})$ is not a constant any more, we need to inspect carefully how this will affect the equilibrium distributions $Y_{\chi,\bar{\chi}}^{\text{eq}}$. The equilibrium yields depend on the chemical potential of the χ and $\bar{\chi}$ particles as seen in Eq. (3.3.13), where the parameter $\xi \equiv \mu/T$ is related to the asymmetry of such particles as

$$2 \sinh \xi(x) = \frac{Y_D(x)}{Y_{\chi,0}^{\text{eq}}}, \quad (4.1.10)$$

where $Y_{\chi,0}^{\text{eq}}$ is the equilibrium distribution in the symmetric case, namely when $Y_\chi - Y_{\bar{\chi}} = 0$.

Solving numerically the system of differential equations (4.1.8) for $\langle\sigma v\rangle_{\text{ann}} = 2 \times 10^{-11}$ GeV $^{-2}$, $\langle\sigma v\rangle_D = 2 \times 10^{-12}$ GeV $^{-2}$, and $Y_D^{\text{in}} = 10^{-10}$, and taking into account the chemical potential dependence on the asymmetry, we obtain the evolution of the comoving abundances shown in Fig. 4.3. Here we notice how the equilibrium yield Y_χ^{eq} (dashed red line) does not stabilize at the value $Y_D^{\text{in}} = 10^{-10}$, but decreases down to $\sim 5 \times 10^{-12}$ due to the asymmetry wash-out that takes place.

Let us now see graphically the evolution of the asymmetries. As we said earlier, we expect from Eqs. (4.1.9) that only the dark asymmetry will evolve. This is shown in Fig. 4.4, where we numerically solved the system for cross-sections $\langle\sigma v\rangle_{\text{ann}} = 4 \times 10^{-19}$ GeV $^{-2}$ and $\langle\sigma v\rangle_D = 2 \times 10^{-19}$ GeV $^{-2}$, and initial asymmetries $Y_D^{\text{in}} = 10^{-11}$ and $Y_L^{\text{in}} = 0$. Here the choice of parameters is different than in Fig. 4.3 for illustrative purposes, but the behaviour will be analogous. The asymmetry between the χ and $\bar{\chi}$ abundances is washed-out. The magnitude of the wash-out depends on the value of $\langle\sigma v\rangle_D$ and the relative strength of $\langle\sigma v\rangle_{\text{ann}}$ compared to $\langle\sigma v\rangle_D$. In a case where $\langle\sigma v\rangle_D$ is larger, we can have almost a complete wash-out of Y_D

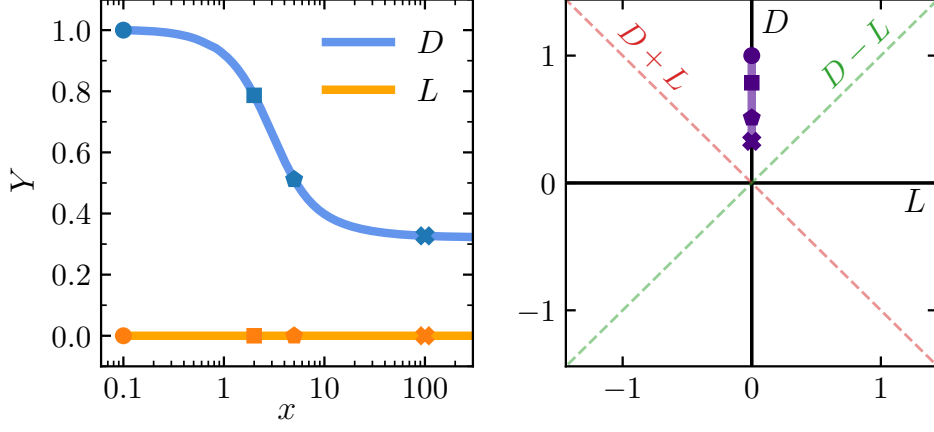


Fig. 4.4: Evolution of the dark matter asymmetry $Y_D(\equiv D)$ and the lepton asymmetry $Y_L(\equiv L)$ in [Case 5](#), assuming $m_\chi = 100$ GeV. The system is solved for cross-sections $\langle\sigma v\rangle_{\text{ann}} = 4 \times 10^{-19}$ GeV $^{-2}$ and $\langle\sigma v\rangle_D = 2 \times 10^{-19}$ GeV $^{-2}$, and initial asymmetries $Y_D^{\text{in}} = 10^{-11}$ and $Y_L^{\text{in}} = 0$. The vertical axis on the left plot and both axes on the right plot are scaled by a factor of 10^{-11} . The markers correspond to $x = 0.1, 2, 5$ and 100 . The notations are the same as in [Fig. 4.2](#).

We have therefore shown that breaking the dark number D on its own can wash-out the initial asymmetry in this sector, but will not be able transmit the asymmetry to the visible sector. Next, we will try the case where in addition to D , CP is also broken.

Case 6: Breaking dark number D and CP

In this case one might foresee from symmetry arguments that the dark matter asymmetry also cannot be transmitted to the visible sector. Nevertheless, let us corroborate this expectation using the Boltzmann equations. Making use of the notation described in [Table 4.2](#), the processes corresponding to $\langle\sigma v\rangle_{\text{ann}}$, $\langle\sigma v\rangle_{D1}$ and $\langle\sigma v\rangle_{D2}$ are active. We write the Boltzmann equations, which take the form

$$\begin{aligned}
\frac{dY_\chi}{dx} &= -\frac{\lambda}{x^2} \left[\langle\sigma v\rangle_{\text{ann}} (Y_\chi Y_{\bar{\chi}} - Y_\chi^{\text{eq}} Y_{\bar{\chi}}^{\text{eq}}) + 2\langle\sigma v\rangle_{D1} (Y_\chi^2 - Y_{\chi,\text{eq}}^2) \right], \\
\frac{dY_{\bar{\chi}}}{dx} &= -\frac{\lambda}{x^2} \left[\langle\sigma v\rangle_{\text{ann}} (Y_\chi Y_{\bar{\chi}} - Y_\chi^{\text{eq}} Y_{\bar{\chi}}^{\text{eq}}) + 2\langle\sigma v\rangle_{D2} (Y_{\bar{\chi}}^2 - Y_{\bar{\chi},\text{eq}}^2) \right], \\
\frac{dY_l}{dx} &= +\frac{\lambda}{x^2} \left[\langle\sigma v\rangle_{\text{ann}} (Y_\chi Y_{\bar{\chi}} - Y_\chi^{\text{eq}} Y_{\bar{\chi}}^{\text{eq}}) + \langle\sigma v\rangle_{D1} (Y_\chi^2 - Y_{\chi,\text{eq}}^2) \right. \\
&\quad \left. + \langle\sigma v\rangle_{D2} (Y_{\bar{\chi}}^2 - Y_{\bar{\chi},\text{eq}}^2) - \langle\sigma v\rangle_{ll^c \rightarrow \text{SM}} (Y_l Y_{l^c} - Y_l^{\text{eq}} Y_{l^c}^{\text{eq}}) \right], \\
\frac{dY_{l^c}}{dx} &= +\frac{\lambda}{x^2} \left[\langle\sigma v\rangle_{\text{ann}} (Y_\chi Y_{\bar{\chi}} - Y_\chi^{\text{eq}} Y_{\bar{\chi}}^{\text{eq}}) + \langle\sigma v\rangle_{D1} (Y_\chi^2 - Y_{\chi,\text{eq}}^2) \right. \\
&\quad \left. + \langle\sigma v\rangle_{D2} (Y_{\bar{\chi}}^2 - Y_{\bar{\chi},\text{eq}}^2) - \langle\sigma v\rangle_{ll^c \rightarrow \text{SM}} (Y_l Y_{l^c} - Y_l^{\text{eq}} Y_{l^c}^{\text{eq}}) \right].
\end{aligned} \tag{4.1.11}$$

The evolution of the asymmetries reads

$$\begin{aligned}\frac{dY_D}{dx} &= -\frac{2\lambda}{x^2} \left[\langle \sigma v \rangle_{D1} (Y_\chi^2 - Y_{\chi, \text{eq}}^2) - \langle \sigma v \rangle_{D2} (Y_{\bar{\chi}}^2 - Y_{\bar{\chi}, \text{eq}}^2) \right], \\ \frac{dY_L}{dx} &= 0.\end{aligned}\tag{4.1.12}$$

Again only the asymmetry in the dark sector will evolve, as in case [Case 5](#). As we are interested in the transmission, we then understand that the minimal case for transmitting the asymmetry will necessarily have to simultaneously break both D and L .

Case 7: Breaking dark number D and lepton number L

Finally we got to the conclusion that we need at least the simultaneous breaking of both L and D . In this scenario we have all the processes described in the previous sections, in addition to the four processes which break both global symmetries at once, labelled by the cross-sections $\langle \sigma v \rangle_{DL1}$ and $\langle \sigma v \rangle_{DL2}$ (see [Table 4.2](#)). In this case, we preserve CP, so $\langle \sigma v \rangle_{L1} = \langle \sigma v \rangle_{L2} \equiv \langle \sigma v \rangle_L$ and $\langle \sigma v \rangle_{D1} = \langle \sigma v \rangle_{D2} \equiv \langle \sigma v \rangle_D$. The set of Boltzmann equations for this case have the following form

$$\begin{aligned}\frac{dY_\chi}{dx} &= -\frac{\lambda}{x^2} \left[(\langle \sigma v \rangle_{\text{ann}} + 2\langle \sigma v \rangle_L) (Y_\chi Y_{\bar{\chi}} - Y_{\chi, \text{eq}} Y_{\bar{\chi}, \text{eq}}) \right. \\ &\quad \left. + 2(\langle \sigma v \rangle_D + \langle \sigma v \rangle_{DL1} + \langle \sigma v \rangle_{DL2}) (Y_\chi^2 - Y_{\chi, \text{eq}}^2) \right], \\ \frac{dY_{\bar{\chi}}}{dx} &= -\frac{\lambda}{x^2} \left[(\langle \sigma v \rangle_{\text{ann}} + 2\langle \sigma v \rangle_L) (Y_\chi Y_{\bar{\chi}} - Y_{\chi, \text{eq}} Y_{\bar{\chi}, \text{eq}}) \right. \\ &\quad \left. + 2(\langle \sigma v \rangle_D + \langle \sigma v \rangle_{DL1} + \langle \sigma v \rangle_{DL2}) (Y_{\bar{\chi}}^2 - Y_{\bar{\chi}, \text{eq}}^2) \right], \\ \frac{dY_l}{dx} &= +\frac{\lambda}{x^2} \left[(\langle \sigma v \rangle_{\text{ann}} + 2\langle \sigma v \rangle_L) (Y_\chi Y_{\bar{\chi}} - Y_{\chi, \text{eq}} Y_{\bar{\chi}, \text{eq}}) + (\langle \sigma v \rangle_D + 2\langle \sigma v \rangle_{DL1}) (Y_\chi^2 - Y_{\chi, \text{eq}}^2) \right. \\ &\quad \left. + (\langle \sigma v \rangle_D + 2\langle \sigma v \rangle_{DL2}) (Y_{\bar{\chi}}^2 - Y_{\bar{\chi}, \text{eq}}^2) - \langle \sigma v \rangle_{ll^c \rightarrow \text{SM}} (Y_l Y_{l^c} - Y_l^{\text{eq}} Y_{l^c}^{\text{eq}}) \right], \\ \frac{dY_{l^c}}{dx} &= +\frac{\lambda}{x^2} \left[(\langle \sigma v \rangle_{\text{ann}} + 2\langle \sigma v \rangle_L) (Y_\chi Y_{\bar{\chi}} - Y_{\chi, \text{eq}} Y_{\bar{\chi}, \text{eq}}) + (\langle \sigma v \rangle_D + 2\langle \sigma v \rangle_{DL2}) (Y_\chi^2 - Y_{\chi, \text{eq}}^2) \right. \\ &\quad \left. + (\langle \sigma v \rangle_D + 2\langle \sigma v \rangle_{DL1}) (Y_{\bar{\chi}}^2 - Y_{\bar{\chi}, \text{eq}}^2) - \langle \sigma v \rangle_{ll^c \rightarrow \text{SM}} (Y_l Y_{l^c} - Y_l^{\text{eq}} Y_{l^c}^{\text{eq}}) \right].\end{aligned}\tag{4.1.13}$$

and the evolution of the asymmetries reads

$$\begin{aligned}\frac{dY_D}{dx} &= -\frac{2\lambda}{x^2} (\langle \sigma v \rangle_D + \langle \sigma v \rangle_{DL1} + \langle \sigma v \rangle_{DL2}) (Y_\chi^2 - Y_{\bar{\chi}}^2 - Y_{\chi, \text{eq}}^2 + Y_{\bar{\chi}, \text{eq}}^2), \\ \frac{dY_L}{dx} &= +\frac{2\lambda}{x^2} (\langle \sigma v \rangle_{DL1} - \langle \sigma v \rangle_{DL2}) (Y_\chi^2 - Y_{\bar{\chi}}^2 - Y_{\chi, \text{eq}}^2 + Y_{\bar{\chi}, \text{eq}}^2).\end{aligned}\tag{4.1.14}$$

Both Y_D and Y_L evolve in this scenario, which is what allows for the transmission of the asymmetry from one sector to the other. The fact that both equations in (4.1.14) contain the cross-sections $\langle\sigma v\rangle_{DL1}$ and $\langle\sigma v\rangle_{DL2}$ is pointing to the fact that the asymmetry is indeed transmitted and that the interactions associated to them: $(\chi\chi \leftrightarrow ll)$, $(\bar{\chi}\bar{\chi} \leftrightarrow l^c l^c)$, $(\chi\chi \leftrightarrow l^c l^c)$ and $(\bar{\chi}\bar{\chi} \leftrightarrow ll)$ are the ones which accomplish the transmission. The interactions associated to $\langle\sigma v\rangle_D$ indirectly affect the magnitude of the transmission, but they are not actually transmitting the asymmetry. In this particular case, we moreover see that both Eqs. (4.1.14) are proportional to each other, showing that the evolution of both asymmetries can be related as

$$Y_D = - \left(\frac{\langle\sigma v\rangle_D + \langle\sigma v\rangle_{DL1} + \langle\sigma v\rangle_{DL2}}{\langle\sigma v\rangle_{DL1} - \langle\sigma v\rangle_{DL2}} \right) Y_L + Y_D^{\text{in}}. \quad (4.1.15)$$

We can conclude that the minimal scenario to transmit the asymmetry from the dark sector to the leptonic sector is to simultaneously break D and L . However, there is no need to violate C or CP in the interactions involving dark matter and leptons because we are already starting from a CP non-conserving medium: an asymmetric sector. As long as one of the cross-sections $\langle\sigma v\rangle_{DL1}$ or $\langle\sigma v\rangle_{DL2}$ is non-zero, we are successful in the transmission.

Notice that the interactions $(\chi\chi \leftrightarrow ll)$ and $(\bar{\chi}\bar{\chi} \leftrightarrow l^c l^c)$, associated to $\langle\sigma v\rangle_{DL1}$, preserve $D + L$, while $(\chi\chi \leftrightarrow l^c l^c)$ and $(\bar{\chi}\bar{\chi} \leftrightarrow ll)$, associated to $\langle\sigma v\rangle_{DL2}$, preserve $D - L$. We could build a model in which one of these combinations is anomaly free (or a similar combination including baryon number B), allowing their interactions to take place.

In Fig. 4.5 four different examples are shown with different choices of cross-sections $\langle\sigma v\rangle_{\text{ann}}$, $\langle\sigma v\rangle_{DL1}$ and $\langle\sigma v\rangle_{DL2}$. We set $\langle\sigma v\rangle_L = \langle\sigma v\rangle_D = 0$ to simplify the analysis and focus only on the transmitting interactions. The initial asymmetries are taken to be $Y_D^{\text{in}} = 10^{-11}$ and $Y_L^{\text{in}} = 0$.

- In Fig. 4.5a the system is solved for cross-sections $\langle\sigma v\rangle_{\text{ann}} = 10^{-18} \text{ GeV}^{-2}$, $\langle\sigma v\rangle_{DL1} = 0$ and $\langle\sigma v\rangle_{DL2} = 3 \times 10^{-19} \text{ GeV}^{-2}$. The only violating interactions that are active are the ones corresponding to $\langle\sigma v\rangle_{DL2}$, which preserve $D - L$. This is clearly seen on the right plot, where the evolution of the purple line is parallel to the green $D - L$ direction. It can also be noted on the left plot that both the dark and lepton asymmetries have analogous evolutions, which could be easily predicted by checking Eq. (4.1.15), where the coefficient becomes $+1$. Physically, the reason for $Y_L \equiv Y_l - Y_{l^c}$ to evolve into a negative value is that, of the two violating interactions active $(\chi\chi \leftrightarrow l^c l^c)$ and $(\bar{\chi}\bar{\chi} \leftrightarrow ll)$, the one producing antileptons is the one that will have a larger rate even if the cross-sections are the same. This is because the rate is proportional to the number density as

$$\Gamma(\chi\chi \leftrightarrow l^c l^c) = n_\chi \langle\sigma v\rangle_{DL2}$$

$$\Gamma(\bar{\chi}\bar{\chi} \leftrightarrow ll) = n_{\bar{\chi}} \langle\sigma v\rangle_{DL2}$$

and due to the initial asymmetry in dark matter we have $n_\chi > n_{\bar{\chi}}$.

- The opposite case is shown in Fig. 4.5b, where the system is solved for cross-sections $\langle\sigma v\rangle_{\text{ann}} = 10^{-18} \text{ GeV}^{-2}$, $\langle\sigma v\rangle_{DL1} = 3 \times 10^{-19} \text{ GeV}^{-2}$ and $\langle\sigma v\rangle_{DL2} = 0$. Now the only active violating interactions are those corresponding to $\langle\sigma v\rangle_{DL1}$, which preserve $D+L$. Similarly to the previous case, both asymmetries follow the same evolution, but they have opposite tendencies, as the coefficient in Eq. (4.1.15) is now -1 . The right plots in Figs. 4.5a and 4.5b are mirrored, and in this second case the evolution takes place following a $D+L$ preserving path, parallel to the red line. The interaction with the higher rate now is $(\chi\chi \leftrightarrow ll)$, which produces leptons, versus $(\bar{\chi}\bar{\chi} \leftrightarrow l^c l^c)$, as

$$\Gamma(\chi\chi \leftrightarrow ll) = n_\chi \langle\sigma v\rangle_{DL1}$$

$$\Gamma(\bar{\chi}\bar{\chi} \leftrightarrow l^c l^c) = n_{\bar{\chi}} \langle\sigma v\rangle_{DL1}$$

and $n_\chi > n_{\bar{\chi}}$. Therefore we end up with a positive lepton asymmetry.

- In Fig. 4.5c the system is solved for cross-sections $\langle\sigma v\rangle_{\text{ann}} = 10^{-18} \text{ GeV}^{-2}$, $\langle\sigma v\rangle_{DL1} = 8 \times 10^{-18} \text{ GeV}^{-2}$ and $\langle\sigma v\rangle_{DL2} = 0$. This is analogous to 4.5b but for illustrative purposes we took a larger $\langle\sigma v\rangle_{DL1}$, which produces an almost total transmission of D into L .
- Finally, in Fig. 4.5d the system is solved for cross-sections $\langle\sigma v\rangle_{\text{ann}} = 10^{-17} \text{ GeV}^{-2}$, $\langle\sigma v\rangle_{DL1} = 2 \times 10^{-18} \text{ GeV}^{-2}$ and $\langle\sigma v\rangle_{DL2} = 10^{-18} \text{ GeV}^{-2}$. Here both cross-sections $\langle\sigma v\rangle_{DL1}$ and $\langle\sigma v\rangle_{DL2}$ are non-zero, producing a combined effect. In this particular case $\langle\sigma v\rangle_{DL1} > \langle\sigma v\rangle_{DL2}$, so the resulting Y_L is positive. The asymmetries have evolutions with opposite signs, but this time with a scaling of -3 according to Eq. (4.1.15). In the right plot of this figure, we can also see that the evolution of the quantum numbers preserves neither $D-L$ nor $D+L$.

Case 8: Breaking dark number D , lepton number L and CP

We could now also review the last case in our systematic analysis, the one in which all symmetries D , L and CP are violated. This scenario would also succeed in the asymmetry transfer. However, this case does not add any particular interesting features to the transmission of the asymmetry and we would like to continue our analysis with the minimal set of conditions necessary: D and L violation.

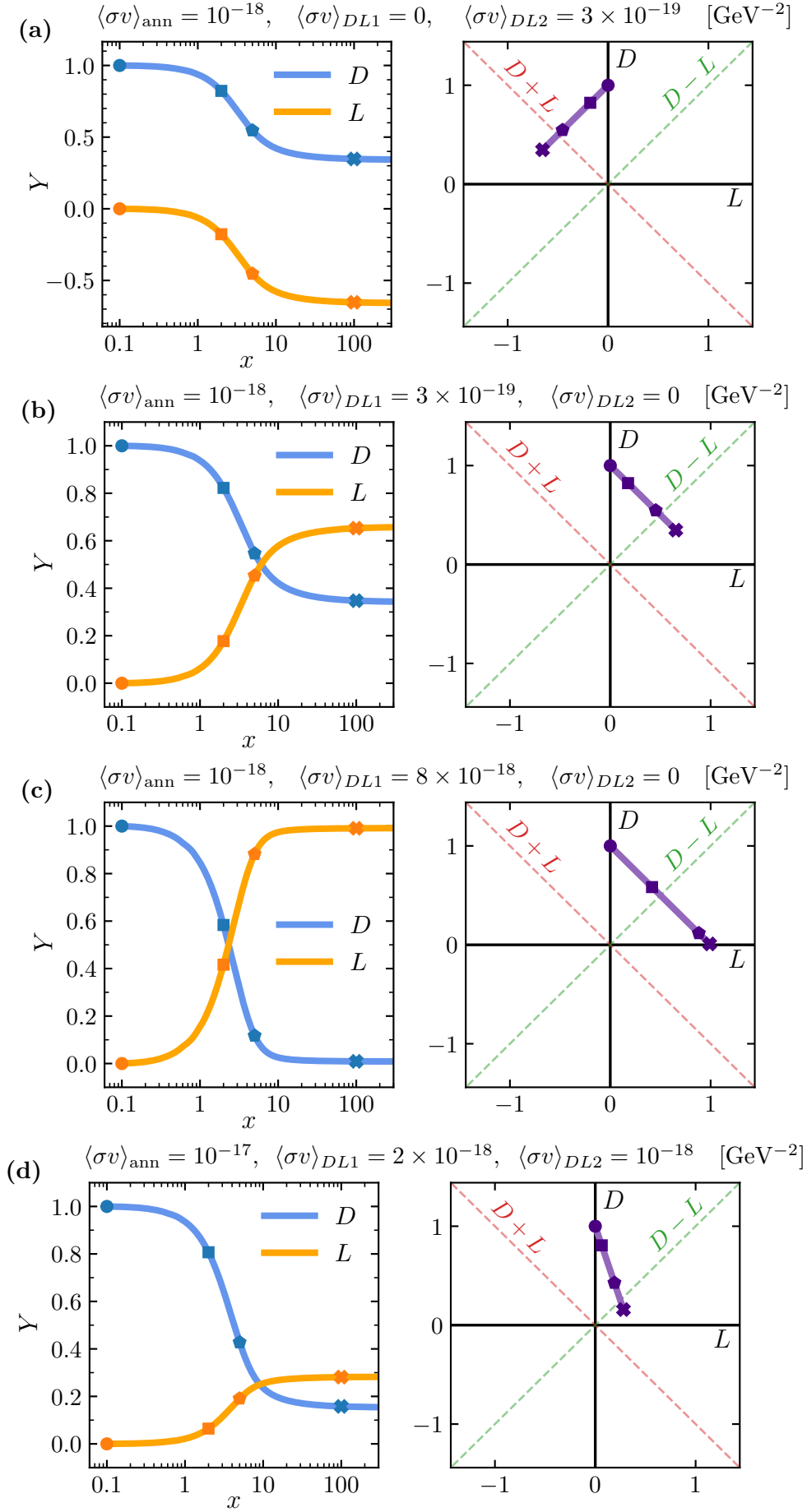


Fig. 4.5: Evolution of the dark matter asymmetry Y_D ($\equiv D$) and the lepton asymmetry Y_L ($\equiv L$) in **Case 7**, assuming $m_\chi = 100$ GeV. The system is solved for different values of $\langle\sigma v\rangle_{\text{ann}}$, $\langle\sigma v\rangle_{DL1}$ and $\langle\sigma v\rangle_{DL2}$, specified on each figure, $\langle\sigma v\rangle_L = \langle\sigma v\rangle_D = 0$, and initial asymmetries $Y_D^{\text{in}} = 10^{-11}$ and $Y_L^{\text{in}} = 0$. The vertical axis on the left plots and both axes on the right plots are scaled by a factor of 10^{-11} . The markers correspond to $x = 0.1, 2, 5$ and 100 . The notations are the same as in Fig. 4.2.

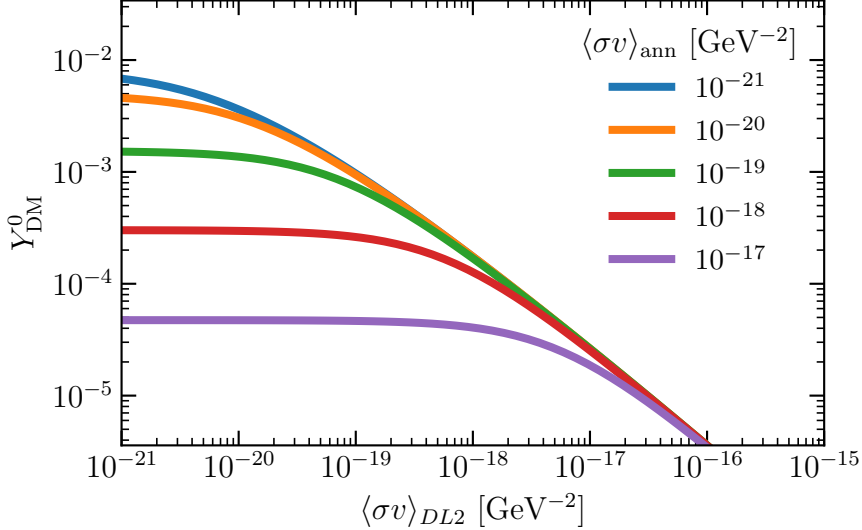


Fig. 4.6: The final dark matter yield $Y_{\text{DM}}^0 \equiv Y_{\chi}^0 + Y_{\bar{\chi}}^0$ as a function of the cross-section $\langle\sigma v\rangle_{DL2}$ for different values of $\langle\sigma v\rangle_{\text{ann}}$, in the case where only these two cross-sections are non-zero. Here we take $m_{\chi} = 800$ GeV and $Y_D^{\text{in}} = 2.5 \times 10^{-10}$. We can see how for each value of $\langle\sigma v\rangle_{\text{ann}}$, there are two regimes. The first regime is where Y_{DM}^0 is constant with $\langle\sigma v\rangle_{DL2}$ and the second regime is where Y_{DM}^0 is linear with $\langle\sigma v\rangle_{DL2}$ in logarithmic scale.

4.1.2 Analytic analysis

It is realistic to think that some of the cross-sections present in the Boltzmann equations will dominate over the rest. In this case we can try to understand analytically how the system will behave, analogous to the usual non-violating scenario.

We remember from Fig. 3.1 that the final abundance of a species is inversely proportional to the annihilation cross-section. This relation is clearly seen from the instantaneous freeze-out approximation, where freeze-out occurs at $\Gamma(x_f) = H(x_f)$, and which implies that the number density is $n \simeq H/\langle\sigma v\rangle$. This is a good approximation when one of the two cross-sections involved in Eqs. (4.1.13) of Case 7 is negligible compared to the others. If we take, for example $\langle\sigma v\rangle_{DL2}$ to be the dominating cross-section, only the second term in the χ and $\bar{\chi}$ equations will be relevant, and we will have that

$$n_{\chi, \bar{\chi}} \propto \frac{1}{\langle\sigma v\rangle_{DL2}}. \quad (4.1.16)$$

The inverse proportionality translates into a linear relation at logarithmic scale. We can see this in Fig. 4.6, where we considered a case where only $\langle\sigma v\rangle_{DL2}$ and $\langle\sigma v\rangle_{\text{ann}}$ are non-zero. We solved the system for many different values of the cross-sections in order to see this linear dependence. We can see how for each value of $\langle\sigma v\rangle_{\text{ann}}$, there are two regimes. The first regime is that where Y_{DM}^0 is constant with $\langle\sigma v\rangle_{DL2}$. This is because $\langle\sigma v\rangle_{\text{ann}} \gg \langle\sigma v\rangle_{DL2}$, and therefore $\langle\sigma v\rangle_{\text{ann}}$ dominates the evolution of $Y_{\chi, \bar{\chi}}^0$. The second regime is where Y_{DM}^0 is linear with $\langle\sigma v\rangle_{DL2}$ in logarithmic scale, as $\langle\sigma v\rangle_{\text{ann}} \ll \langle\sigma v\rangle_{DL2}$ and $\langle\sigma v\rangle_{DL2}$ dominates the evolution of $Y_{\chi, \bar{\chi}}^0$. We see how in the linear regime, all lines converge to the same values, as the contribution of $\langle\sigma v\rangle_{\text{ann}}$ is negligible.

4.2 Transmission from Lepton to Baryon Asymmetries by Sphalerons

In the previous section, we have successfully shown that an asymmetry in a dark sector can be transmitted to the leptonic sector of the standard model if we have interactions that simultaneously break the global symmetry $U(1)_D$ associated to dark matter and the global lepton number asymmetry $U(1)_L$. Now we would like to see if we can transmit the asymmetry from the leptonic sector to the baryonic one. In section 2.2.2 we already explained what electroweak sphaleron processes are, and here we will attempt to transmit the asymmetry from L to B making use of these processes. Until now, we have treated the leptons to which dark matter couples as generic, knowing that they should be neutral in order not to violate electromagnetic charge when we break L . The setting we will study now is the particular case where these product leptons are the standard left-handed neutrinos.

In this thesis, the model building of the mechanism will not be addressed. It might be concerning that before the electroweak phase transition, the left-handed neutrinos are part of a $SU(2)_L$ doublet including the charged leptons, and that we cannot write an interaction term in terms of ν_L without breaking the $SU(2)_L$ symmetry. One option would be trying to transmit the asymmetry in the small window of temperatures in which the Higgs VEV is already non-zero but the Sphalerons have not yet switched off. Nevertheless, here we are going to consider a different scenario. We know we could build a model, for example similar to the ‘verifiable radiative Seesaw mechanism of neutrino mass and dark matter’ model described in Ref. [62], which allows dark matter to couple to ν_L without breaking any essential symmetry groups, by making dark matter part of a $SU(2)_L$ doublet too. Knowing that such a mechanism or some other similar one could serve to our purposes, we proceed assuming that dark matter could be coupled to the SM neutrinos well before electroweak phase transition.

4.2.1 Sphaleron rate and chemical equilibrium

It is important now to understand at which temperature, T_{sph} , electroweak sphalerons come out of thermal equilibrium, meaning that their rate is not rapid enough compared to the expansion of the universe and they are effectively switched off. From this moment on, the quantum numbers B and L will be conserved by all the standard model interactions. Even if L is still violated in the interactions with the dark matter, there are not any interactions that can change B , and therefore Y_B will freeze out at T_{sph} . The value of the baryon asymmetry after the sphaleron freeze-out is the one that we would observe today.

In Ref. [63] they perform large-scale lattice simulations to compute the rate of baryon number violating processes (sphaleron rate) across the electroweak phase transition. They find that these processes are not completely effective at all times: the rate decays exponentially when the temperature gets close to the sphaleron freeze-out. The parametrization in terms of temperature is

$$\Gamma_{\text{sph}} \simeq \begin{cases} T^4 \cdot 8 \times 10^{-7}, & \text{in the symmetric phase,} \\ T^4 \cdot \exp(-147.7 + 0.83 T / \text{GeV}), & \text{in the Higgs phase.} \end{cases} \quad (4.2.1)$$

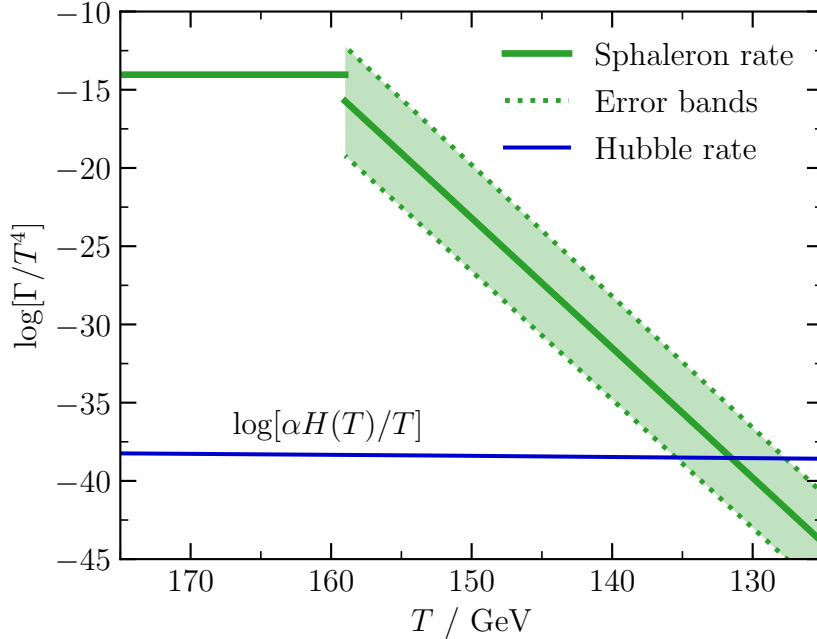


Fig. 4.7: Sphaleron rate in the symmetric and broken phase as parametrized in Eq. (4.2.1) taken from Ref. [63] (in green), compared to the appropriately scaled Hubble rate (in blue), where $\alpha = 0.1015$. This scaling is taken from Ref. [64]. The shaded area is the error band, dominated mainly by systematics, also obtained from Ref. [63], which in the symmetric phase is too small to appear in the figure.

In Fig. 4.7 we see this evolution graphically, and also the comparison with the appropriately scaled Hubble rate. In the moment when the sphaleron rate falls below the blue line, which quantifies the expansion of the universe, sphalerons are considered to be out of equilibrium and their interactions switch off. To carry out an exhaustive study of the B generation, we would need to plug the rate Γ_{sph} into the Boltzmann equations. For the purposes of this thesis we will take the simplified assumption that sphaleron processes are highly effective above a critical temperature T_{sph} , and then they switch off instantly below it. Taking the sphalerons to be fully effective means taking Y_B to closely follow Y_B^{eq} , therefore the instantaneous freeze-out approximation corresponds to taking $Y_B(T) = Y_B^{\text{eq}}(T_{\text{sph}})$ for $T < T_{\text{sph}}$.

The different interactions that are active during a certain temperature range, impose some relations among the chemical potentials of said particles. Relating the number densities to the chemical potential of each species, and then relating the baryon and lepton numbers to these number densities, gives an equilibrium relation

$$Y_B = c(Y_{B-L}) \equiv c(Y_B - Y_L).$$

The constant c depends on which interactions are in equilibrium at the moment when the sphalerons are switched off, and on the particle content of the SM. This relation is usually found in the literature using the notation $B = c(B - L)$. For three SM generations and one Higgs boson, and for the case in which sphalerons fall out of equilibrium after electroweak symmetry breaking [65], this constant takes the value $c = 36/111$. A detailed analysis of how this relation is derived, based on Ref. [66], can be found in appendix C.

According to [65], Y_B is found to deviate from the equilibrium at a temperature $T_{\text{dev}} \simeq 140$ GeV. A good choice for our purposes is therefore to take this temperature for the instantaneous freeze-out approximation. Below $T_{\text{sph}} \equiv T_{\text{dev}}$, the change in the baryon asymmetry does not contribute much, so this simplified treatment is good enough for our scenario.

4.2.2 Boltzmann equations and numerical resolution

The generic form of the Boltzmann equations for the different asymmetry yields, now adding the evolution of Y_B , and taking into account the electroweak sphaleron conversion, is

$$\begin{aligned}\frac{dY_D}{dx} &= f(x), \\ \frac{dY_L}{dx} &= g(x) + \frac{dY_L^{\text{EW}}}{dx}, \\ \frac{dY_B}{dx} &= \frac{dY_B^{\text{EW}}}{dx},\end{aligned}\tag{4.2.2}$$

where the functions $f(x)$ and $g(x)$ correspond to the evolution of our dark matter and lepton asymmetries depending on the scenario that we choose, based the symmetries we choose to break. The terms of the form $\frac{dY^{\text{EW}}}{dx}$ correspond to the transmission due to electroweak sphalerons. Since these processes preserve $B - L$, one has

$$\frac{dY_L^{\text{EW}}}{dx} = \frac{dY_B^{\text{EW}}}{dx} \equiv \frac{dY^{\text{EW}}}{dx}.$$

With the considerations of section 4.2.1 regarding instantaneous sphaleron conversion from L to B , and instantaneous freeze-out of Y_B and temperature T_{sph} , we derive the following relation

$$\begin{aligned}Y_B &= -\frac{c}{1-c}Y_L \\ \frac{dY_B}{dx} &= -\frac{c}{1-c}\frac{dY_L}{dx} \equiv \frac{dY^{\text{EW}}}{dx} \\ \frac{dY_L}{dx} &= g(x) - \frac{c}{1-c}\frac{dY_L}{dx} \quad \longrightarrow \quad \frac{1}{1-c}\frac{dY_L}{dx} = g(x) \quad \longrightarrow \quad \frac{dY_L}{dx} = (1-c)g(x)\end{aligned}$$

where $c = 36/111$ for $T > T_{\text{sph}}$ and $c = 0$ for $T < T_{\text{sph}}$. Here we already assumed $Y_B^{\text{in}} = 0$ as the initial condition. Finally, for [Case 7](#), our set of Boltzmann equations including the baryon asymmetry take the form

$$\begin{aligned}
\frac{dY_D}{dx} &= -\frac{2\lambda}{x^2} \left(\langle \sigma v \rangle_D + \langle \sigma v \rangle_{DL1} + \langle \sigma v \rangle_{DL2} \right) \left(Y_\chi^2 - Y_{\bar{\chi}}^2 - Y_{\chi, \text{eq}}^2 + Y_{\bar{\chi}, \text{eq}}^2 \right), \\
\frac{dY_L}{dx} &= (1-c) \frac{2\lambda}{x^2} \left(\langle \sigma v \rangle_{DL1} - \langle \sigma v \rangle_{DL2} \right) \left(Y_\chi^2 - Y_{\bar{\chi}}^2 - Y_{\chi, \text{eq}}^2 + Y_{\bar{\chi}, \text{eq}}^2 \right), \\
\frac{dY_B}{dx} &= -\frac{c}{1-c} \frac{dY_L}{dx},
\end{aligned} \tag{4.2.3}$$

where again $c = 36/111$ for $T > T_{\text{sph}}$ and $c = 0$ for $T < T_{\text{sph}}$.

We are now ready to solve the system of differential equations that will give us the evolution of the asymmetries in these three sectors, taking into account the interplay among them. In Fig. 4.8 we have solved the system for two different choices of the dark matter mass, and also different values of the cross-sections $\langle \sigma v \rangle_{DL1}$ and $\langle \sigma v \rangle_{DL2}$. There we show the evolution of the three asymmetries with the decrement of temperature, and also the evolution in the DL and BL planes.

The choice of the dark matter mass plays a very important role in the generation of a B asymmetry, because it affects the moment in which dark matter stops being relativistic and therefore, the range of temperatures in which the transmission from D to L does happen. In the moment when the electroweak sphalerons freeze-out, $x_{\text{sph}} \equiv m_\chi/T_{\text{sph}}$, the transmission from L to B is interrupted. The higher x_{sph} is, the later this happens relative to the transmission from D to L . We can see in Fig. 4.8 and the rest of plots where the asymmetry is being transmitted, that most of the evolution happens approximately at $1 \lesssim x \lesssim 10$, which translates into temperatures of $m_\chi \gtrsim T \gtrsim 0.1 m_\chi$. If m_χ is too small, the sphalerons will freeze out before we can generate any L and we will not be able to generate a baryon asymmetry B . The greater the mass is, the more asymmetry will be transmitted to B before it freezes-out. For large enough masses, the D to L transmission will be completed before the sphaleron freeze-out, being this the case in which a greater part of the asymmetry will be converted into B .

In Fig. 4.8a we have chosen $m_\chi = 500$ GeV, while in 4.8b the mass is larger, $m_\chi = 800$ GeV. As discussed, this results in a lower transmission from L to B in 4.8a as x_{sph} is lower. Apart from this, the choice of active interactions is different in each case: in Fig. 4.8a the non-zero cross-section is $\langle \sigma v \rangle_{DL2}$ while in Fig. 4.8b the non-zero cross-section is taken to be $\langle \sigma v \rangle_{DL1}$ for illustrative purposes. The effects of this choice are described in Case 7. If both cases had the same masses, the behaviour in the DL and BL planes would be mirrored (flip of B and L axes). As the generated L is being partially converted into B , we can see graphically in the DL middle plots how before x_{sph} (from the circle to the pentagon marker in the figures) the evolution is not exactly parallel to the $D + L$ or $D - L$ lines any more. This is because now these quantities are no longer conserved due to the sphaleron processes. After x_{sph} (from the pentagon to the cross marker) the evolution becomes again parallel to the correspondent line.

We can also see graphically in Fig. 4.8 how the sphalerons being completely effective prior to their departure from equilibrium translates into the evolution in the BL asymmetry plane to follow the equilibrium black dashed line of $B = c(B - L)$. This equilibrium line is described by the relations among the chemical potentials of the particle species inside the thermal plasma, as exposed in the previous section and derived in appendix

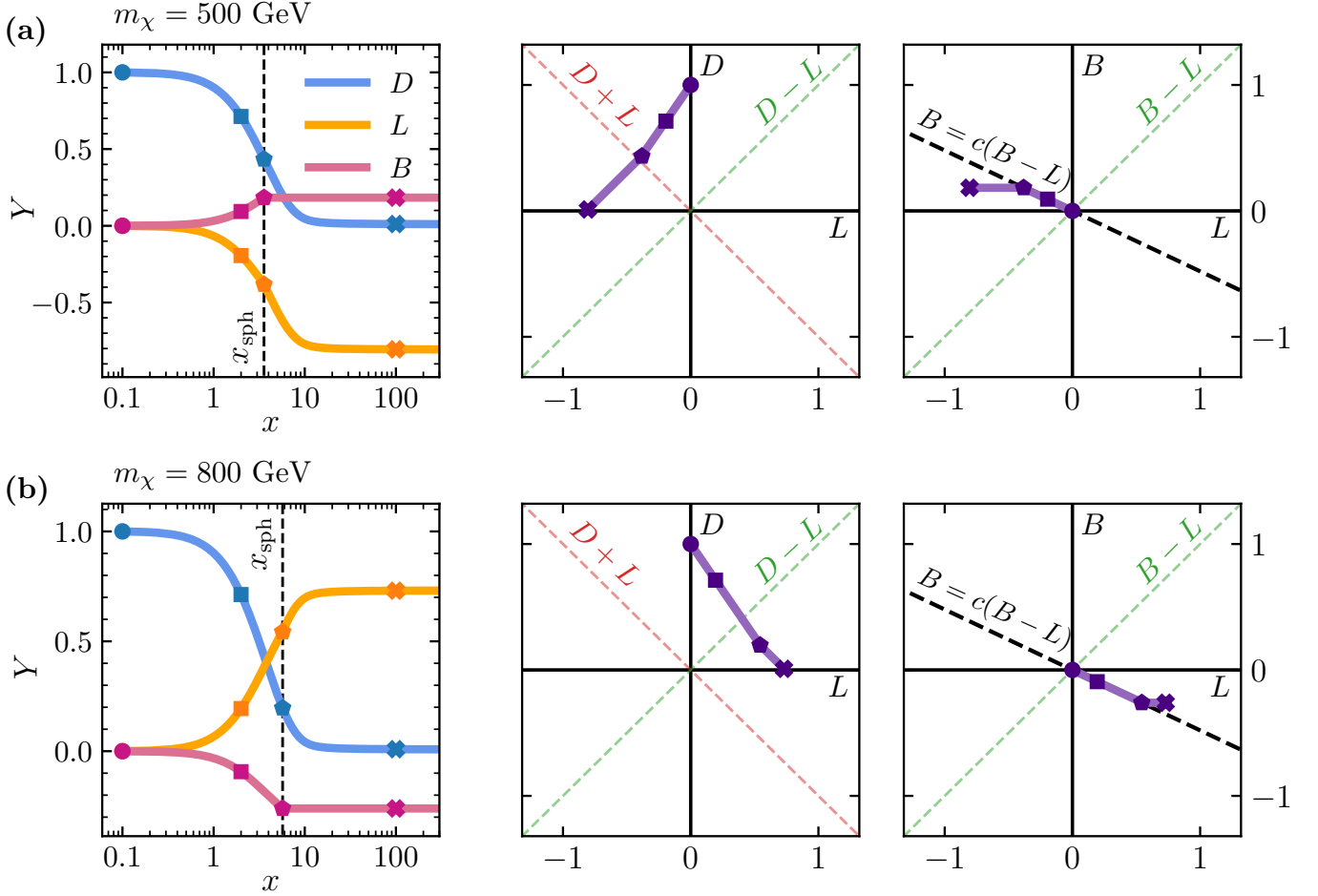


Fig. 4.8: Evolution of the dark matter asymmetry $Y_D (\equiv D)$, the lepton asymmetry $Y_L (\equiv L)$ and the baryon asymmetry $Y_B (\equiv B)$ for dark matter masses m_χ specified above each figure and for cross-sections $\langle\sigma v\rangle_{\text{ann}} = 10^{-16} \text{ GeV}^{-2}$, $\langle\sigma v\rangle_L = \langle\sigma v\rangle_D = 0$ and in (a) $\langle\sigma v\rangle_{DL1} = 0$ and $\langle\sigma v\rangle_{DL2} = 5 \times 10^{-17} \text{ GeV}^{-2}$ while in (b) $\langle\sigma v\rangle_{DL1} = 5 \times 10^{-17} \text{ GeV}^{-2}$ and $\langle\sigma v\rangle_{DL2} = 0$. The initial values are $Y_D^{\text{in}} = 10^{-11}$ and $Y_L^{\text{in}} = Y_B^{\text{in}} = 0$. All the axes corresponding to yield asymmetries are scaled by a factor of 10^{-11} . The dashed vertical line on the left plot corresponds to $x_{\text{sph}} = m_\chi / (T^{\text{sph}} = 140 \text{ GeV})$, the point where sphalerons instantaneously freeze-out and with them the baryon asymmetry Y_B . The value of x_{sph} changes in each case due to the different m_χ , in (a) it is $x_{\text{sph}} \simeq 3.57$ and in (b) it is $x_{\text{sph}} \simeq 5.71$. The rest of notations are the same as in Fig. 4.2, and the additional right plot corresponds to the equivalent BL plane, where the black dashed line corresponds to the equilibrium distribution imposed by the chemical equilibration in the plasma for the value of $c = 36/111$. The markers correspond to $x = 0.1, 2, x_{\text{sph}}$ and 100 .

C. After x_{sph} (pentagon marker), B freezes out and only L is generated in this plane. Because the generated B and L asymmetries have opposing signs, we conclude that we will need a non-zero $\langle\sigma v\rangle_{DL2}$ to generate a positive baryon asymmetry.

4.2.3 Comparison with observations

Now that we managed to describe a mechanism to possibly account for the baryon asymmetry generation, we want to check if we can obtain results which are compatible with the CMB measurements within our scenario. The observations we need to address are the baryon asymmetry η_B , which effectively contains the same information as the baryon energy density Ω_b , and the dark matter energy density Ω_{DM} .

Comparison with η_B

Previously, in section 2.2.1, we presented the value of the baryon-to-photon number density ratio in the universe, $\eta_B = (6.12 \pm 0.04) \times 10^{-10}$ [2], measured from the CMB. We also saw why this is too a measure of the matter-antimatter asymmetry, see Eq. (2.2.2). In order to compare this value with our result in the form of the baryon asymmetry yield after sphaleron freeze-out, Y_B^{sph} , we can write

$$\eta_B^0 \equiv \frac{n_b^0}{n_\gamma^0} = \frac{n_B^0}{n_\gamma^0} = \frac{Y_B^0 s^0}{n_\gamma^0} \simeq \frac{Y_B^{\text{sph}} s^0}{n_\gamma^0}, \quad (4.2.4)$$

using the fact that Y_B stays constant after T^{sph} . We also know that the η_B measured in the CMB is the same as the one today, as the number of degrees of freedom $g_{*,S}$ has not changed since then. The superindex 0 refers to the values of these magnitudes today. The number density of photons, integrating the Bose-Einstein distribution in Eq. (3.1.1) is

$$n_\gamma = \frac{2\zeta(3)}{\pi^2} T^3 \quad (4.2.5)$$

where we used that $\mu_\gamma = 0$ and $g_\gamma = 2$. $\zeta(s)$ is the Riemann zeta function. The value of the entropy of the universe today is $s^0 \simeq 2.21 \times 10^{-38} \text{ GeV}^3$ [2]. It is straightforward to deduce from Eq. (4.2.4) and the observed value of η_B that the value of the final baryon asymmetry should be $Y_B^{\text{sph}} \simeq 8.7 \times 10^{-11}$.

Comparison with Ω_{DM} and Ω_b

In section 2.1.1, we introduced the measured value for the dark matter density in the universe today, $\Omega_{\text{DM}} = 0.265(7)$. The most precise baryon density measure, also coming from the CMB is $\Omega_b = 0.0484(10)$ [2]. To connect these values with the yields of dark matter and baryons after they freeze-out, we write

$$\Omega_b \equiv \frac{\rho_b}{\rho_{\text{crit}}} = \frac{m_p n_b^0}{\rho_{\text{crit}}} = \frac{m_p Y_b^0 s^0}{\rho_{\text{crit}}} = \frac{m_p Y_B^0 s^0}{\rho_{\text{crit}}} \simeq \frac{m_p Y_B^{\text{sph}} s^0}{\rho_{\text{crit}}}, \quad (4.2.6)$$

and

$$\Omega_{\text{DM}} \equiv \frac{\rho_{\text{DM}}}{\rho_{\text{crit}}} = \frac{m_\chi n_{\text{DM}}^0}{\rho_{\text{crit}}} = \frac{m_\chi Y_{\text{DM}}^0 s^0}{\rho_{\text{crit}}} = \frac{m_\chi (Y_\chi^0 + Y_{\bar{\chi}}^0) s^0}{\rho_{\text{crit}}}, \quad (4.2.7)$$

where $m_p \simeq 0.938 \text{ GeV}$ and $\rho_{\text{crit}} \simeq 3.66 \times 10^{-47} \text{ GeV}^4$ for $h = 0.674$ [2].

From Eq. (4.2.6) we find that the value of Y_B^{sph} required to match the measured Ω_b is $Y_B^{\text{sph}} \simeq 8.7 \times 10^{-11}$, the same as the one obtained from η_B . This is what we expected, as η_B and Ω_b contain the same information. Similarly, we can estimate the expected dark matter yield from Eq. (4.2.7) and the measured Ω_{DM} , but the result in this case depends on the dark matter mass m_χ . We find that $Y_{\text{DM}}^0 \equiv Y_\chi^0 + Y_{\bar{\chi}}^0 \simeq 4.4 \times 10^{-10}/m_\chi \text{ GeV}$.

4.2.4 Our scenario and some considerations

We now have all the necessary tools to attempt to reproduce the measured dark matter and baryon densities in the universe. We will focus on the minimal scenario for the asymmetry transfer, where the only parameters are the dark matter mass, m_χ , the initial dark matter asymmetry, Y_D^{in} , and the $D - L$ preserving cross-section, $\langle\sigma v\rangle_{DL2}$. The rest of violating cross-sections will be taken to be zero. This could be justified by imposing $D - L$ conservation in the interactions. In this case, also the annihilation cross-section, $\langle\sigma v\rangle_{\text{ann}}$, would be non-zero. We rename $\langle\sigma v\rangle_{DL2} \equiv \langle\sigma v\rangle_{D-L}$ from here on.

We will make use of the analytical arguments detailed at the end of section 4.1.2 to obtain our results. As described in Footnote 1, there are some numerical issues when using cross-sections larger than $\sim 10^{-15} \text{ GeV}^{-2}$ in our set of Boltzmann equations. Nevertheless, we understand well the physics for smaller values and we are confident that we can extrapolate this knowledge to larger cross-sections. As Sakharov conditions evidence, being in thermal equilibrium washes out any existing asymmetries of the species involved. Now, here we have a slightly more complex scenario, because we have an interplay between two types of processes: $\langle\sigma v\rangle_{\text{ann}}$ and $\langle\sigma v\rangle_{D-L}$. In this minimal scenario, we remember that the Boltzmann equations for χ , $\bar{\chi}$ and the dark asymmetry Y_D in this case are

$$\begin{aligned} \frac{dY_\chi}{dx} &= -\frac{\lambda}{x^2} \left[\langle\sigma v\rangle_{\text{ann}} (Y_\chi Y_{\bar{\chi}} - Y_{\chi,\text{eq}} Y_{\bar{\chi},\text{eq}}) + 2\langle\sigma v\rangle_{D-L} (Y_\chi^2 - Y_{\chi,\text{eq}}^2) \right], \\ \frac{dY_{\bar{\chi}}}{dx} &= -\frac{\lambda}{x^2} \left[\langle\sigma v\rangle_{\text{ann}} (Y_\chi Y_{\bar{\chi}} - Y_{\chi,\text{eq}} Y_{\bar{\chi},\text{eq}}) + 2\langle\sigma v\rangle_{D-L} (Y_{\bar{\chi}}^2 - Y_{\bar{\chi},\text{eq}}^2) \right], \\ \frac{dY_D}{dx} &= -\frac{2\lambda}{x^2} \langle\sigma v\rangle_{D-L} (Y_\chi^2 - Y_{\bar{\chi}}^2 - Y_{\chi,\text{eq}}^2 + Y_{\bar{\chi},\text{eq}}^2). \end{aligned} \quad (4.2.8)$$

Both $\langle\sigma v\rangle_{\text{ann}}$ and $\langle\sigma v\rangle_{D-L}$ contribute to bringing the dark matter into thermal equilibrium, but only $\langle\sigma v\rangle_{D-L}$ can transmit the asymmetry. The asymmetry will therefore be totally transmitted for the cases in which dark matter is in thermal equilibrium, along with the condition that $\langle\sigma v\rangle_{D-L}$ is relatively high compared to $\langle\sigma v\rangle_{\text{ann}}$. In the case where the contribution of $\langle\sigma v\rangle_{\text{ann}}$ is larger than that of $\langle\sigma v\rangle_{D-L}$, the system will be in thermal equilibrium but the asymmetry will remain within the dark sector. For the purposes of asymmetry transmission and for making use of the analytical considerations specified, we will take $\langle\sigma v\rangle_{\text{ann}}$ to be negligible compared to $\langle\sigma v\rangle_{DL2}$.

Consequently, we can be sure that for large cross-sections, if the condition regarding the relative size of $\langle\sigma v\rangle_{\text{ann}}$ and $\langle\sigma v\rangle_{D-L}$ is met, the asymmetry will be completely transmitted from D to L and B . We then end up with a universe where $D = 0$, corresponding to symmetric dark matter which then freezes-out as in the WIMP scenario.

We focus our attention in the second regime of Fig. 4.6, where the asymmetry will be fully transmitted. We can very accurately obtain the final dark matter abundances for large values of $\langle\sigma v\rangle_{D-L}$ by extrapolating from small values of $\langle\sigma v\rangle_{D-L}$. The initial value of the asymmetry, Y_D^{in} , does not influence the relic abundance of dark matter for the range of values we consider, as the asymmetry is very quickly washed-out and we end up with symmetric dark matter. Nevertheless, Y_L^0 and Y_B^0 will be very sensitive to Y_D^{in} . They will also sensitively depend on m_χ , which determines the moment of B freeze-out relative to the transmission from D to L .

We now will look for values of $\langle\sigma v\rangle_{D-L}$ which give the expected Y_{DM}^0 , for specific m_χ and Y_D^{in} . We always assume that $\langle\sigma v\rangle_{\text{ann}}$ will be negligible compared to $\langle\sigma v\rangle_{D-L}$ for our analysis, but of course the scenario in which the this condition is not fulfilled and the asymmetry is not completely transmitted is also possible.

4.2.5 Parameters and results

As we already analysed in the previous subsection, our scenario has four parameters that affect the values of η_B and Ω_{DM} . These parameters and their effect on the observations are summarized in Table 4.3. Remember that η_B (and therefore Ω_b) will be determined by Y_B^0 , while Ω_{DM} will be determined by Y_{DM}^0 .

Parameters	Effect on observations
m_χ	It strongly affects Y_B^0 by determining the moment of the D transmission relative to the sphaleron freeze-out. It also slightly affects Y_{DM}^0 as it is a parameter in the Boltzmann equations. Ω_{DM} is not only determined by Y_{DM}^0 , but it is also proportional to m_χ .
Y_D^{in}	It strongly affects Y_B^0 , as we will be working on a regime where the asymmetry Y_D is completely transmitted. It does not affect Y_{DM}^0 as it will be effectively washed out.
$\langle\sigma v\rangle_{D-L}$	It strongly affects Y_{DM}^0 , as it determines the moment for the dark matter freeze-out. It does not affect Y_B^0 in our case as we assume it to be large enough for the asymmetry to be fully transmitted.
$\langle\sigma v\rangle_{\text{ann}}$	It does not affect Y_{DM}^0 nor Y_B^0 , as in our case it will be negligible compared to $\langle\sigma v\rangle_{D-L}$.

Table 4.3: List of the parameters in our scenario and how they affect Y_{DM}^0 , which determines Ω_{DM} , and Y_B^0 , which determines η_B and Ω_b . The effect on the final abundances is given for the regime where $\langle\sigma v\rangle_{\text{ann}} \ll \langle\sigma v\rangle_{D-L}$, implying that the asymmetry will be fully transmitted.

We can now set bounds on some of the parameters, particularly on m_χ and Y_D^{in} . For a given m_χ , there will be a minimum Y_D^{in} which is able to reproduce η_B . This minimum Y_D^{in} gives the measured baryon asymmetry in the optimal case of complete transmission of the dark asymmetry D . For smaller values of Y_D^{in} , it is not possible to reproduce the observed η_B . For higher Y_D^{in} , the observations could be matched in the case of a partial transmission of D . These bounds are plotted in Fig. 4.9, where we show the three regions that can be distinguished inside the excluded area.

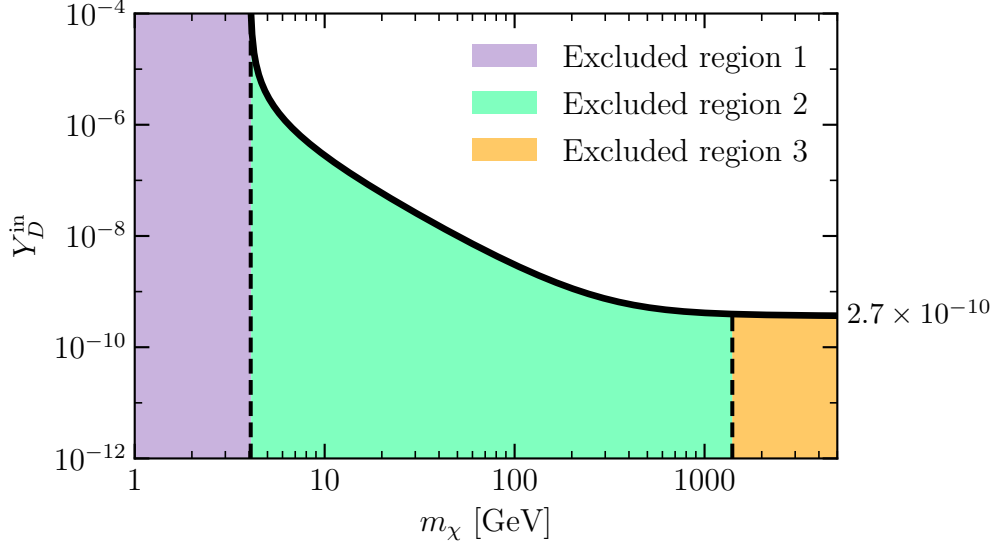


Fig. 4.9: Bounds on the $m_\chi - Y_D^{\text{in}}$ parameter space. The colored zone is the excluded area. The solid black line corresponds to the lowest Y_D^{in} necessary to reproduce the measured η_B for a certain m_χ . This bound is obtained assuming a complete transmission of the asymmetry. Dashed lines separate three different regions inside the excluded area. These separations are plotted at $m_\chi = 4$ GeV and $m_\chi = 1400$ GeV. See main text for more information on the different regions.

- Region 1, shown in purple. For masses $m_\chi \lesssim 4$ GeV there is no possible value of Y_D^{in} that could reproduce the observed asymmetry. This is because the sphaleron processes would switch off before the transmission of D began. All the dark asymmetry would be transmitted to the leptons and none to the baryons.
- Region 2, shown in turquoise. For masses of 4 GeV $\lesssim m_\chi \lesssim 1400$ GeV. Here the minimum Y_D^{in} changes with m_χ , as the sphaleron freeze-out happens while the asymmetry is being transmitted from D to the visible sector. The lower the mass is, the less asymmetry is transmitted.
- Region 3, shown in orange. For masses $m_\chi \gtrsim 1400$ GeV, the minimum Y_D^{in} stays constant. This is because the transmission happens completely before sphaleron freeze-out. The bound in this region is also the general bound for all parameter space, which is $Y_D^{\text{in}} \simeq 2.7 \times 10^{-10}$.

Being in the allowed area from the $m_\chi - Y_D^{\text{in}}$ parameter space would not guarantee that the baryon asymmetry could be reproduced in this way. Here the other two parameters, $\langle\sigma v\rangle_{\text{ann}}$ and $\langle\sigma v\rangle_{D-L}$, come into play. $\langle\sigma v\rangle_{D-L}$ needs to be large enough, and also large enough relative to $\langle\sigma v\rangle_{\text{ann}}$ in order to transmit enough of the asymmetry.

Making use of the extrapolation method detailed in subsection 4.2.4, we can find sets of parameters that can reproduce simultaneously η_B and Ω_{DM} . The cross-section $\langle\sigma v\rangle_{D-L}$ will be chosen in order to reproduce the dark matter density and $\langle\sigma v\rangle_{\text{ann}}$ will be by choice negligible in comparison to $\langle\sigma v\rangle_{D-L}$. The values of m_χ and Y_D^{in} will be chosen from the lower bound (solid line in Fig. 4.9) as we are choosing the regime in which the asymmetry is fully transmitted. Some examples of sets of parameters compatible with the observations are

$$\begin{aligned}
m_\chi = 50 \text{ GeV}, & \quad Y_D^{\text{in}} = 9.7 \times 10^{-9} \quad \text{and} \quad \langle \sigma v \rangle_{D-L} = 1.55 \times 10^{-8} \text{ GeV}^{-2}, \\
m_\chi = 100 \text{ GeV}, & \quad Y_D^{\text{in}} = 2.6 \times 10^{-9} \quad \text{and} \quad \langle \sigma v \rangle_{D-L} = 1.20 \times 10^{-8} \text{ GeV}^{-2}, \\
m_\chi = 500 \text{ GeV}, & \quad Y_D^{\text{in}} = 3.3 \times 10^{-10} \quad \text{and} \quad \langle \sigma v \rangle_{D-L} = 8.1 \times 10^{-9} \text{ GeV}^{-2}, \\
m_\chi = 800 \text{ GeV}, & \quad Y_D^{\text{in}} = 2.8 \times 10^{-10} \quad \text{and} \quad \langle \sigma v \rangle_{D-L} = 7.4 \times 10^{-9} \text{ GeV}^{-2}, \\
m_\chi = 1000 \text{ GeV}, & \quad Y_D^{\text{in}} = 2.7 \times 10^{-10} \quad \text{and} \quad \langle \sigma v \rangle_{D-L} = 7.2 \times 10^{-9} \text{ GeV}^{-2}.
\end{aligned}$$

The size of $\langle \sigma v \rangle_{D-L}$ that we obtain is quite close to the WIMP cross-section and therefore also to the weak interaction of the SM, which is $\sim 2.6 \times 10^{-9} \text{ GeV}^{-2}$. The mediator of these processes would be around $\sim 30 \text{ GeV}$, which is not such a large value. The size of these cross-sections are also not ruled out by the current bounds for dark matter annihilation to neutrinos [67], which in our range of masses set an upper limit of order $\sim 10^7 \text{ GeV}^{-2}$.

The values of the lepton asymmetry Y_L^0 are also allowed by the bounds for the example cases we provided. As we saw on Eq. (2.2.10), these bounds are around 7 orders of magnitude more relaxed than those on the baryon asymmetry. The lepton asymmetry bounds could set an upper limit on the initial dark asymmetry Y_D^{in} , but only for the case of total D transmission. As it is always possible to have cross-sections which do not completely transfer D , we cannot set an upper limit on Y_D^{in} . This is why lepton asymmetry constraints are not shown in Fig. 4.9.

Chapter 5

Conclusions

The motivation of this thesis was to address two of the main fundamental open problems in modern physics: dark matter and the baryon asymmetry of the universe, both of them reviewed in Chapter 2. The measured energy densities of the dark matter and the baryons are very similar, see Eq. (2.3.1). This fact suggests that the dark sector might also be asymmetric, and hints a possible common origin or connection between the two asymmetries.

In this work we focussed on the transmission of an asymmetry initially residing in the dark sector, to the visible sector. Our mechanism connects dark matter to the leptonic sector via interactions of the type $(\text{DM DM} \leftrightarrow \nu_L \nu_L)$. In section 4.1 we performed a systematic analysis of the different symmetry-violating processes that could be present, in order to find the minimal set of conditions for the asymmetry transfer. We concluded that even though some scenarios were successful in the generation or wash-out of the asymmetries, for the purpose of transmission there must be simultaneous D and L violation, see Case 7. CP-violation is not necessary in the interactions connecting both sectors, but it is already present in the initial condition of a dark asymmetry. Once we achieved the transmission from D to L , we also reviewed the simultaneous transmission from L to B via electroweak sphalerons in section 4.2. It is necessary that the sphaleron freeze-out, and therefore B freeze-out, takes place after some part of (or all) the asymmetry has already been transferred to the leptons.

We found that our mechanism could be reduced to three indispensable parameters that play a role in the asymmetry transmission: the dark matter mass, m_χ , the initial dark asymmetry, Y_D^{in} , and the D - and L -violating but $D-L$ preserving cross-section, $\langle\sigma v\rangle_{D-L}$. Also the annihilation cross-section, $\langle\sigma v\rangle_{\text{ann}}$, plays a role in the dynamics of our mechanism, but it does not necessarily need to be non-zero. For a summary of these parameters and their effect on the observations see Table 4.3.

Analysing the role of each of these parameters in subsections 4.2.4 and 4.2.5, we then tried to find the conditions for our scenario to be able to match the CMB measurements: the observed baryon asymmetry encoded in η_B (and also in Ω_b), and the dark matter energy density Ω_{DM} . We managed to find some constraints in the $m_\chi - Y_D^{\text{in}}$ plane, shown in Fig. 4.9, consisting in the minimum Y_D^{in} to reproduce the baryon asymmetry for each m_χ . We then also showed some examples of sets of parameters which simultaneously explain both η_B and Ω_{DM} , assuming the complete transmission of D .

We conclude that our mechanism is capable, with only three parameters, of connecting the dark matter and the baryon asymmetry in a way that relates their energy densities, explaining the ratio $\Omega_{\text{DM}}/\Omega_{\text{b}} \simeq 5$. It is a plausible scenario, because there are no constraints that prevent a dark matter asymmetry to be originated in the early universe, previous to the energy scales at which our mechanism takes place. The existence of interactions mediated by some particle of a mass not far from the electroweak energy scale is also plausible.

In this thesis we have set the minimal conditions for the transmission of an asymmetry from the dark sector to the baryons, via the leptonic sector. We have developed the computational tools to analyse this scenario, and we have proved that it could explain the observations from the CMB. Now the mechanism is ready to be implemented into a complete physical model which would describe the entire dark sector physics including the asymmetry generation.

Chapter 6

Outlook

In this thesis we developed a mechanism that could possibly explain the baryon asymmetry of the universe and the closeness of the baryon and dark matter energy densities. However, there are many possible directions towards which this scenario could be further developed. Here we review some of the possible completions for the mechanism and aspects that we did not fully address in this work.

- **Development of a complete model which includes this scenario.** In order to design a complete model for dark matter and asymmetry transfer, there are some features that need to be developed. Some of these features are the following.
 1. **Dark sector completion.** It is very likely that, similarly to the visible sector, the dark sector has a rich structure. This includes many different fundamental particles, interactions among them and with the visible sector, and a symmetry group which all interactions obey. One of the multiple dark sector particles would constitute the dark matter that we detect. An important aspect for our mechanism would be the full description of the Lagrangian interaction terms which give rise to the processes of the type $(\text{DM DM} \leftrightarrow \nu_L \nu_L)$ that we consider. The design of a plausible dark sector structure is a crucial aspect when developing a model for dark matter.
 2. **Asymmetry generation.** We assumed an initial dark asymmetry, but for the sake of completeness we would need a mechanism for the generation of this asymmetry (darkogenesis). The knowledge about the dark sector is still very scarce, so the design of such a mechanism is not very constrained. This darkogenesis mechanism could be a dark-sector analogy to electroweak baryogenesis or leptogenesis, among many other possibilities.
 3. **Neutrino masses.** In the design of our scenario, we considered that the leptons into which dark matter annihilates are the neutrinos of the SM. We could also connect the neutrino masses problem with our work. We mentioned in section 4.2 the verifiable radiative seesaw mechanism for neutrino masses and dark matter, introduced in Ref. [62]. This mechanism or a similar one could both describe the $(\text{DM DM} \leftrightarrow \nu_L \nu_L)$ interactions and account for the masses of active neutrinos.
- **Testability.** Another important aspect for future works would consist on analysing the testability of our mechanism. The cross-sections needed to reproduce Ω_{DM} are not weaker than that of the electroweak interaction, meaning that the interactions with visible matter are not notably small. This is favorable for collider searches. For dark matter annihilation to SM neutrinos, the current upper bounds on cross-sections in the

range of m_χ we consider are $\sim 10^{-7} \text{ GeV}^{-2}$ [67]. The values that we found are around one order of magnitude weaker. This means that our scenario could be ruled out in future neutrino detection experiments.

In the radiative seesaw mechanism mentioned above, the dark matter, χ^0 , would be a part of a $SU(2)$ doublet $(\chi^- \chi^0)$, which interacts with the left handed lepton doublet of the SM. Instead of focussing on the $(\chi^0 \chi^0 \leftrightarrow \nu_L \nu_L)$ processes, we could also try to detect the also present $(\chi^- \chi^- \leftrightarrow e^- e^-)$ processes. This could be done in electron colliders, trying to find the decay products of χ^- , for example $\chi^- \rightarrow \chi^0 \pi^-$ or $\chi^- \rightarrow \chi^0 W^- \rightarrow \chi^0 e^- \nu$.

Our scenario is capable of generating large lepton asymmetries. The generation of lepton asymmetries close to the current bound of order $\sim 10^{-3}$ would happen if we have a large Y_D^{in} and a small enough m_χ so that little part of the asymmetry is transmitted to the baryons. In this case, the large lepton asymmetries could leave further signals in BBN and might be detected in the future.

Finally, if the dark matter mass would be experimentally determined in the future and turned out to be much lower than our bound of $m_\chi \lesssim 4 \text{ GeV}$, this could rule out our mechanism.

- **Other annihilation products.** Further work could explore the different possibilities regarding the particles dark matter annihilates into, like sterile neutrinos. This would require adding all the physics regarding the sterile neutrino decays and scatterings, which is also present in the leptogenesis scenario. The option of dark matter directly decaying into baryonic matter could also be explored. It is important that the annihilation products charge- and color-neutral, if we want to violate B without breaking $U(1)_{\text{EM}}$ or $SU(3)_C$. Plausible options to be considered could be annihilation into neutrons, other heavier baryons, or mesons. The annihilation would have to take place at temperatures $T < T_{\text{QCD}} \sim 150 \text{ MeV}$. Annihilation into 3-bodies might also be an option.
- **Different initial abundance.** A similar ADM context but with an initial zero abundance rather than a thermal initial condition and with a later freeze-in (see section 2.1.3) could also be an alternative worth exploring.
- **Co-annihilations.** Another possible scenario to take into consideration would be a set of particles in the dark sector which co-annihilate with the dark matter into lighter particles [68].

To summarize, we have put forward and explored a mechanism to explain and connect the dark matter and baryon abundances of the Universe. However, as discussed in this section, there are many aspects of the scenario that remain to be explored and that we believe deserve further investigation.

Appendix A

Equilibrium Number Density Expressions

In this appendix we show the derivation of the equilibrium number density of a particle species as a function of T . The calculation is made for relativistic and non-relativistic particles, and also in the general case. We will assume the Maxwell-Boltzmann (MB) approximation, treating fermions and bosons equally. The MB distribution phase space distribution is

$$f_{\text{MB}} = \exp\left(-\frac{E - \mu}{T}\right).$$

Following the definition of the number density in Eq. (3.1.2), the integral expression for the MB number density becomes

$$n_{\text{MB}} = \frac{g}{(2\pi)^3} e^{\mu/T} \int d^3p e^{-E/T}.$$

- **Relativistic particles.** The energy can be approximated to $E \approx |\vec{p}|$. In this appendix we will use the notation $|\vec{p}| \equiv p$. We write

$$\begin{aligned} n_{\text{MB}}^{\text{rel}} &= \frac{g}{(2\pi)^3} e^{\mu/T} \int d^3p e^{-p/T} = \frac{g}{(2\pi)^3} e^{\mu/T} 4\pi \int_0^\infty dp p^2 e^{-p/T} = \\ &= \frac{g}{(2\pi)^3} e^{\mu/T} 4\pi 2T^2 = \frac{g}{\pi^2} T^3 e^{\mu/T}. \end{aligned} \tag{A.1}$$

- **Non-relativistic particles.** The energy can be approximated to $E \approx m + \frac{p^2}{2m}$. We then have

$$\begin{aligned} n_{\text{MB}}^{\text{NR}} &= \frac{g}{(2\pi)^3} e^{\mu/T} \int d^3p e^{-m/T} e^{-p^2/(2mT)} = \frac{g}{(2\pi)^3} e^{-m/T} e^{\mu/T} 4\pi \int_0^\infty dp p^2 e^{-p^2/(2mT)} = \\ &= \frac{g}{(2\pi)^3} e^{-m/T} e^{\mu/T} 4\pi \sqrt{\frac{\pi}{2}} (mT)^{\frac{3}{2}} = g e^{-(m-\mu)/T} \left(\frac{mT}{2\pi}\right)^{\frac{3}{2}}. \end{aligned} \tag{A.2}$$

- **General case.** The energy is $E = \sqrt{m^2 + p^2}$. Then

$$\begin{aligned}
 n_{\text{MB}} &= \frac{g}{(2\pi)^3} e^{\mu/T} 4\pi \int_0^\infty dp p^2 e^{-E/T} = \frac{g}{(2\pi)^3} e^{\mu/T} 4\pi m^2 T K_2\left(\frac{m}{T}\right) = \\
 &= \frac{g}{2\pi^2} m^2 T K_2\left(\frac{m}{T}\right) e^{\mu/T} = \frac{g}{2\pi^2} x^2 T^3 K_2(x) e^{\mu/T},
 \end{aligned}
 \tag{A.3}$$

with $x \equiv m/T$.

Appendix B

Calculations for the Boltzmann Equation

B.1 Liouville Operator in terms of Number Density

To go from the Liouville operator for the FLRW metric as shown in Eq. (3.2.2) to the Boltzmann equation in the form of (3.2.3), we need to recall the definition of the number density in terms of the phase space density in (3.1.2). We use the relation $E dE = |\vec{p}| d|\vec{p}|$, and integrate the Liouville operator by parts

$$\begin{aligned}
\frac{g}{(2\pi)^3} \int \frac{d^3 p}{E} \hat{L}[f] &= \frac{g}{(2\pi)^3} \int d^3 p \frac{\partial f}{\partial t} - \frac{g}{(2\pi)^3} \int \frac{d^3 p}{E} H |\vec{p}|^2 \frac{\partial f}{\partial E} = \\
&= \frac{dn}{dt} - \frac{g}{(2\pi)^3} H \int d^3 p |\vec{p}|^2 \frac{\partial f}{E \partial E} = \\
&= \dot{n} - \frac{g}{(2\pi)^3} H \int d^3 p |\vec{p}| \frac{\partial f}{\partial |\vec{p}|} = \dot{n} - \frac{4\pi g}{(2\pi)^3} H \int d|\vec{p}| |\vec{p}|^3 \frac{\partial f}{\partial |\vec{p}|} = \\
&= \dot{n} - \frac{4\pi g}{(2\pi)^3} H \left[\int d|\vec{p}| \frac{\partial}{\partial |\vec{p}|} (|\vec{p}|^3 f) - \int d|\vec{p}| \frac{\partial |\vec{p}|^3}{\partial |\vec{p}|} f \right] \\
&= \dot{n} + \frac{4\pi g}{(2\pi)^3} H \int d|\vec{p}| 3|\vec{p}|^2 f = \dot{n} + 3H \frac{g}{(2\pi)^3} \int d^3 p f = \dot{n} + 3Hn.
\end{aligned}$$

Now we can introduce this into Eq. (3.2.1) and we find the relation (3.2.3).

B.2 Liouville Operator in terms of Yield

We start from the left-hand side of Eq. (3.2.7). Having defined the yield as $Y \equiv n/s$, we write

$$\begin{aligned}\dot{n} + 3Hn &= \frac{d(sY)}{dt} + 3HsY = Y\dot{s} + s\dot{Y} + 3HsY = Y\frac{d}{dt}(sa^3a^{-3}) + s\dot{Y} + 3HsY = \\ &= Ysa^3\frac{d}{dt}(a^{-3}) + s\dot{Y} + 3HsY = -3Ys\frac{\dot{a}}{a} + s\dot{Y} + 3HsY = s\dot{Y}.\end{aligned}$$

B.3 Thermal Average for Decay

In this appendix we will explicitly show how one gets from the general Boltzmann equation in Eq. (3.2.13) to the integrated expression for the simplest case, the decay of a particle a into two particles i and j .

In this case, the initial particle a is heavy and may or may not be in thermal equilibrium. The product particles i and j are lighter (later assumed to be massless) and remain in equilibrium with the thermal plasma at all temperatures relevant for the evolution of n_a . We further assume that the particles i and j have negligible chemical potentials $\mu_i = \mu_j = 0$ so that their phase space distributions become

$$f_i = \exp(-E_i/T) \quad f_j = \exp(-E_j/T).$$

Using detailed balance as in section 3.3.1, we have that $f_i = f_i^{\text{eq}}$, $f_j = f_j^{\text{eq}}$ and $f_i^{\text{eq}}f_j^{\text{eq}} = f_a^{\text{eq}}$. With the relations above and knowing that $|M|$ is constant for a decay, we arrive to

$$\begin{aligned}\dot{n}_a + 3Hn_a &= -g_a|M|^2 \int d\Pi_a d\Pi_i d\Pi_j (2\pi)^4 \delta^4(p_a - p_i - p_j) (f_a - f_a^{\text{eq}}) \\ &= -g_a \frac{(2\pi)^4}{(2\pi)^9} |M|^2 \int \frac{d^3p_a}{2E_a} (f_a - f_a^{\text{eq}}) \int \frac{d^3p_i}{2E_i} \int \frac{d^3p_j}{2E_j} \delta(E_a - E_i - E_j) \delta^3(\vec{p}_a - \vec{p}_i - \vec{p}_j).\end{aligned}\tag{B.3.1}$$

Now we introduce the two-body phase space, defined as

$$\int d\Phi_2(p_i, p_j) \equiv \int \frac{d^3p_i}{(2\pi)^3 2E_i} \int \frac{d^3p_j}{(2\pi)^3 2E_j} (2\pi)^4 \delta^4(p_a - p_i - p_j).$$

This expression is Lorentz invariant, and therefore we can solve it for the center of mass frame and introduce the result into the integral Boltzmann equation. In the center of mass of particle a , we have $\vec{p}_a = 0$ and $E_a = M_a$. We have then

$$\int d\Phi_2(p_i, p_j) = \frac{1}{(2\pi)^2} \int \frac{d^3p_i}{2E_i} \int \frac{d^3p_j}{2E_j} \delta(M_a - E_i - E_j) \delta^3(\vec{p}_i + \vec{p}_j).$$

Solving the momenta delta and renaming $\vec{p}_i = \vec{p}_j \equiv \vec{p}$, we get to

$$\int d\Phi_2(p_i, p_j) = \frac{1}{(2\pi)^2} \int \frac{d^3p}{4\sqrt{\vec{p}^2 + m_i^2}\sqrt{\vec{p}^2 + m_j^2}} \delta\left(M_a - \sqrt{\vec{p}^2 + m_i^2} - \sqrt{\vec{p}^2 + m_j^2}\right).$$

Now, in order to solve the delta function, we use the identity

$$\delta(f(x)) = \sum_i \frac{\delta(x - x_i)}{\left|\frac{\partial f}{\partial x}(x_i)\right|}.$$

Obtaining the root of the function,

$$\begin{aligned} M_a - \sqrt{\vec{p}^2 + m_i^2} - \sqrt{\vec{p}^2 + m_j^2} = 0 &\rightarrow M_a^2 + \vec{p}^2 + m_i^2 - 2M_a\sqrt{\vec{p}^2 + m_i^2} = \vec{p}^2 + m_j^2 \\ \rightarrow (M_a^2 + m_i^2 + m_j^2)^2 = 4M_a^2\vec{p}^2 + 4M_a^2m_i^2 &\rightarrow \vec{p}^2 = \frac{(M_a^2 + m_i^2 + m_j^2)^2 - 4M_a^2m_i^2}{4M_a^2} \\ \rightarrow \dots \rightarrow |\vec{p}| = \frac{M_a}{2} \sqrt{1 - \frac{2(m_i^2 + m_j^2)^2}{M_a^2} + \frac{(m_i^2 + m_j^2)^2}{M_a^4}} &\equiv \frac{M_a}{2}\beta, \end{aligned}$$

and the derivative

$$\frac{\partial f}{\partial |\vec{p}|} = -|\vec{p}| \left(\frac{1}{E_i} + \frac{1}{E_j} \right),$$

the delta function finally becomes

$$\delta\left(M_a - \sqrt{\vec{p}^2 + m_i^2} - \sqrt{\vec{p}^2 + m_j^2}\right) = \frac{\delta(|\vec{p}| - \frac{M_a}{2}\beta)}{\left| -|\vec{p}| \left(\frac{1}{E_i} + \frac{1}{E_j} \right) \right|_{|\vec{p}| = \frac{M_a}{2}\beta}}.$$

Going back to the two-body phase space, we find

$$\begin{aligned} \int d\Phi_2(p_i, p_j) &= \frac{1}{(2\pi)^2} \int \frac{d|\vec{p}||\vec{p}|^2 d\Omega}{4\sqrt{\vec{p}^2 + m_i^2}\sqrt{\vec{p}^2 + m_j^2}} \frac{\delta(|\vec{p}| - \frac{M_a}{2}\beta)}{\frac{M_a}{2}\beta \left(\frac{1}{\sqrt{(\frac{M_a}{2}\beta)^2 + m_i^2}} + \frac{1}{\sqrt{(\frac{M_a}{2}\beta)^2 + m_j^2}} \right)} = \\ &= \frac{1}{(2\pi)^2} \int d\Omega \frac{\frac{M_a}{2}\beta}{4 \left(\sqrt{(\frac{M_a}{2}\beta)^2 + m_j^2} + \sqrt{(\frac{M_a}{2}\beta)^2 + m_i^2} \right)} = \frac{1}{(2\pi)^2} \int d\Omega \frac{\frac{M_a}{2}\beta}{4(E_j + E_i) \Big|_{|\vec{p}| = \frac{M_a}{2}\beta}} = \\ &= \frac{1}{(2\pi)^2} \int d\Omega \frac{\frac{M_a}{2}\beta}{4M_a} = \frac{4\pi}{4\pi^2} \frac{\beta}{8} = \frac{\beta}{8\pi}. \end{aligned}$$

In the particular case in which the two decay products are massless particles, then $\beta = 1$. Plugging this into the Boltzmann equation (B.3.1), we obtain

$$\dot{n}_a + 3Hn_a = -\frac{g_a}{(2\pi)^3}|M|^2 \frac{1}{8\pi} \int \frac{d^3p_a}{2E_a} (f_a - f_a^{\text{eq}}). \quad (\text{B.3.2})$$

Using now the relation (3.2.11), we can turn our equation into

$$\frac{dY_a}{dx} = -\frac{1}{sxH(x)} \frac{g_a}{(2\pi)^3} \frac{|M|^2}{8\pi} \int \frac{d^3p_a}{2E_a} (f_a - f_a^{\text{eq}}),$$

and rewriting $|M|^2$ in terms of the decay rate $\Gamma_{\text{D}} = |M|^2/(16\pi M_a)$, we have

$$\frac{dY_a}{dx} = -\frac{g_a}{(2\pi)^3} \int d^3p_a \frac{1}{sxH(x)} \frac{2M_a\Gamma_{\text{D}}}{2E_a} (f_a - f_a^{\text{eq}}).$$

The factor M_a/E_a is the interaction suppression for the particle a being non-relativistic. The remaining integral gives a modified Bessel function of the second kind and of order 1, $K_1(x)$,

$$\begin{aligned} \int \frac{d^3p_a}{E_a} (f_a - f_a^{\text{eq}}) &= 4\pi \int_0^\infty \frac{d|\vec{p}_a||\vec{p}_a|^2}{E_a} (f_a - f_a^{\text{eq}}) = 4\pi \int_{M_a}^\infty dE_a \sqrt{E_a^2 - M_a^2} (f_a - f_a^{\text{eq}}) = \\ &= 4\pi M_a (T_a - T_{\text{eq}}) K_1(x). \end{aligned}$$

This leaves us with

$$\frac{dY_a}{dx} = -\frac{4\pi g_a}{(2\pi)^3} \frac{1}{sxH(x)} M_a \Gamma_{\text{D}} M_a (T_a - T_{\text{eq}}) K_1(x).$$

Moreover, we can prove that

$$\frac{Y_a}{Y_a^{\text{eq}}} = \frac{n_a}{n_a^{\text{eq}}} = \frac{\int d^3p_a f_a}{\int d^3p_a f_a^{\text{eq}}} = \frac{4\pi \int dp_a p_a^2 e^{-E_a/T_a}}{4\pi \int dp_a p_a^2 e^{-E_a/T_{\text{eq}}}} = \frac{M_a^2 T_a K_2(x)}{M_a^2 T_{\text{eq}} K_2(x)} = \frac{T_a}{T_{\text{eq}}},$$

and using this back in our Boltzmann equation, we write

$$\begin{aligned} \frac{dY_a}{dx} &= -\frac{4\pi g_a}{(2\pi)^3} \frac{M_a^2 \Gamma_{\text{D}}}{sxH(x)} K_1(x) \frac{M_a}{x} \frac{(T_a - T_{\text{eq}})}{T_{\text{eq}}} = -\frac{4\pi g_a}{(2\pi)^3} \frac{M_a^3 \Gamma_{\text{D}}}{sx^2 H(x)} K_1(x) \left(\frac{n_a}{n_a^{\text{eq}}} - 1 \right) = \\ &= -\frac{4\pi g_a}{(2\pi)^3} \frac{M_a^3 \Gamma_{\text{D}}}{sx^2 H(x)} K_1(x) \frac{n_a - n_a^{\text{eq}}}{n_a^{\text{eq}}} = -\frac{4\pi g_a}{(2\pi)^3} \frac{M_a^3 \Gamma_{\text{D}}}{sx^2 H(x)} K_1(x) \frac{Y_a - Y_a^{\text{eq}}}{Y_a^{\text{eq}}}. \end{aligned}$$

Taking into account the expression in Eq. (3.2.9) for s and the equilibrium yield obtain using Eq. (A.3),

$$Y_a^{\text{eq}} = \frac{45g_a}{4\pi^4 g_{\star s}} x^2 K_2(x),$$

we write

$$\begin{aligned}
\frac{dY_a}{dx} &= -\frac{4\pi g_a}{(2\pi)^3} \frac{M_a^3 \Gamma_D}{x^2 H(x)} \frac{K_1(x)}{\frac{2\pi^2}{45} g_{*s} T_{\text{eq}}^3 \frac{45 g_a}{4\pi^4 g_{*s}} x^2 K_2(x)} (Y_a - Y_a^{\text{eq}}) \\
&= -\frac{4\pi 4\pi^4}{(2\pi)^3 2\pi^2} \frac{\Gamma_D M_a^3}{x^4 H(x) T_{\text{eq}}^3} \frac{K_1(x)}{K_2(x)} (Y_a - Y_a^{\text{eq}}) = -\frac{\Gamma_D}{x H(x)} \frac{K_1(x)}{K_2(x)} (Y_a - Y_a^{\text{eq}}).
\end{aligned}$$

We arrive then to the expression we were looking for: the Boltzmann equation for a decay of a heavy particle a into two massless particles

$$\frac{dY_a}{dx} = -\frac{\Gamma_D}{x H(x)} \frac{K_1(x)}{K_2(x)} (Y_a - Y_a^{\text{eq}}).$$

Appendix C

Chemical Equilibration: Baryon and Lepton Asymmetries

In this appendix we present a detailed analysis for the chemical equilibration in the thermal plasma, based on Ref. [66].

Particle asymmetries can be expressed in terms of their chemical potentials. Assuming that all the particles are ultrarelativistic, which at temperatures above the Electroweak Phase Transition (EWPT) should be a good approximation, this relation is given by

$$n_i - n_{\bar{i}} = \frac{g_i T^3}{6} \begin{cases} \beta\mu_i + \mathcal{O}((\beta\mu_i)^3) & \text{fermions,} \\ 2\beta\mu_i + \mathcal{O}((\beta\mu_i)^3) & \text{bosons,} \end{cases} \quad (\text{C.1})$$

where n_i is the equilibrium number density of a given particle species, $n_{\bar{i}}$ that of the CP-conjugate species, g_i its internal degrees of freedom and μ_i its chemical potential. We also assume that $|\mu/T| \ll 1$, as the baryon and lepton chemical potentials are expected to be of order $|\mu| \sim 10^{-10}T$, and $|\mu| < m$ (no Bose condensation).

We now know that the electroweak sphaleron processes are rapid ($\Gamma_{\text{sph}} \gg H$) at temperatures both above the EWPT and below it. However, we will perform different analyses for the case in which sphalerons go out of equilibrium before and after this phase transition, for theoretical purposes. We will be working in a generalized model consisting of N_F generations of quarks and leptons, m complex Higgs doublets (ϕ_i^+, ϕ_i^0), and the gauge bosons of $SU(3)_C \otimes SU(2)_L \otimes U(1)_Y$. The chemical potentials are assigned to be

- μ_{u_L} for all the left-handed up-quark fields and μ_{u_R} for all the right-handed up-quark fields;
- μ_{d_L} for all the left-handed down-quark fields and μ_{d_R} for all the right-handed down-quark fields;
- $\mu_{e_L i}$ for the left-handed charged lepton fields and $\mu_{e_R i}$ for the right-handed charged lepton fields;
- $\mu_{\nu i}$ for the left-handed neutrino fields;
- μ_W for W^- (and therefore $-\mu_W$ for W^+);

- μ_0 for all the ϕ_0 Higgs fields and μ_- for all ϕ^+ Higgs fields.

The eight gluon fields and the W^0 and B^0 bosons have vanishing chemical potentials and therefore we may ignore them.

We recall that whenever a reaction is occurring rapidly, the sum of the chemical potentials of the incoming particles must equal that of the outgoing particles. According to this, the vanishing chemical potentials of the gluons ensures equal chemical potentials for the different colors of quarks. Also, Cabibbo mixing and the vanishment of the chemical potentials of the neutral electroweak bosons maintains the equality of the various generations of up- and down-quark fields, respectively. At temperatures above the EWPT, the bosons W^\pm will also have vanishing potentials as we will show, which will ensure the equality of the chemical potentials for fields in the same electroweak doublet, via the Yukawa interactions. For now we will take the general approach as we will also be studying the case below the critical temperature. In general, in absence of flavour-mixing neutrino interactions, the lepton generations will not have equal chemical potentials. Finally, we can assume that the chemical potentials of the m Higgs doublets are going to be equal due to mixing among them.

Rapid electroweak interactions in the early universe impose the following equilibrium relations

$$\mu_W = \mu_- + \mu_0 \quad (W^- \leftrightarrow \phi^- + \phi^0), \quad (\text{C.2})$$

$$\mu_{d_L} = \mu_{u_L} + \mu_W \quad (W^- \leftrightarrow \bar{u}_L + d_L), \quad (\text{C.3})$$

$$\mu_{e_{Li}} = \mu_{\nu_i} + \mu_W \quad (W^- \leftrightarrow \bar{\nu}_{Li} + e_{Li}), \quad (\text{C.4})$$

$$\mu_{u_R} = \mu_0 + \mu_{u_L} \quad (\phi^0 \leftrightarrow \bar{u}_L + u_R), \quad (\text{C.5})$$

$$\mu_{d_R} = -\mu_0 + \mu_{d_L} \quad (\phi^0 \leftrightarrow d_L + \bar{d}_R), \quad (\text{C.6})$$

$$\mu_{e_{Ri}} = -\mu_0 + \mu_{e_{Li}} \quad (\phi^0 \leftrightarrow e_{Li} + \bar{e}_{Ri}). \quad (\text{C.7})$$

The last three processes correspond to the Yukawa interactions, which for temperatures $T \lesssim 10^8$ GeV are in equilibrium for all the generations, even for the lightest ones [69]. By making use of these relations we can express all the chemical potentials in terms of $3 + N_F$ chemical potentials, which are chosen to be μ_W , μ_0 , μ_{u_L} and μ_{ν_i} . It is also convenient to define the sum of the neutrino chemical potentials $\mu_\nu = \sum_i \mu_{\nu_i}$.

As long as the electroweak sphalerons are rapid, they impose the following relation

$$N_F(\mu_{u_L} + 2\mu_{d_L}) + \sum_i \mu_{\nu_i} = 0, \quad (\text{C.8})$$

coming from the creation of a $u_L d_L d_L \nu_L$ state from each generation out of the vacuum. Using the relation (C.5) we can rewrite this condition as

$$3N_F \mu_{u_L} + 2N_F \mu_W + \mu_\nu = 0. \quad (\text{C.9})$$

Now we express the baryon and lepton number densities in terms of the chosen chemical potentials, making use of (C.1) and the relations (C.3), (C.5) and (C.6). From now on we

will use the common notation $n_B \equiv B$ and $n_L \equiv L$, and the subindexed B_i and L_i will represent the quantum baryon and lepton number of a species i . The relations are

$$\begin{aligned} B &= \sum_b B_b(n_b - n_{\bar{b}}) = \frac{g_q T^2}{6} B_q [N_F(\mu_{u_L} + \mu_{u_R}) + N_F(\mu_{d_L} + \mu_{d_R})] = \\ &= \frac{3 \cdot 2 T^2}{6} \frac{1}{3} N_F(2\mu_{u_L} + \mu_0 + \mu_{u_L} + \mu_W - \mu_0 + \mu_{u_L} + \mu_W), \end{aligned}$$

arriving at

$$B = \frac{T^2}{3} (4N_F \mu_{u_L} + 2N_F \mu_W). \quad (\text{C.10})$$

Analogously:

$$\begin{aligned} L &= \sum_l L_l(n_l - n_{\bar{l}}) = \frac{g_l T^2}{6} L_l \sum_i (\mu_{\nu i} + \mu_{e_L i} + \mu_{e_R i}) = \\ &= \frac{2T^2}{6} \cdot 1 \cdot \sum_i (\mu_{\nu i} + \mu_{\nu i} + \mu_W - \mu_0 + \mu_{\nu i} + \mu_W), \\ L &= \frac{T^2}{3} (3\mu_\nu + 2N_F \mu_W - N_F \mu_0). \end{aligned} \quad (\text{C.11})$$

We can also express the number densities of charge Q and of the third component of weak isospin I_3 ,

$$\begin{aligned} Q &= \frac{T^2}{6} \left[g_u N_F(\mu_{u_L} + \mu_{u_R}) q_u + g_d N_F(\mu_{d_L} + \mu_{d_R}) q_d + \sum_i g_e (\mu_{e_L i} + \mu_{e_R i}) q_e + \right. \\ &\quad \left. + 2g_W(\mu_{W^+} q_{W^+} + \mu_{W^-} q_{W^-}) + 2g_{\phi^+} m \mu_{\phi^+} \right], \end{aligned}$$

where we have taken into account the extra factor 2 that appears in the relation (C.1) for bosons. Now, substituting the adequate charges for each particle and the degrees of freedom $g_u = g_d = 6$, $g_e = g_W = g_{\phi^+} = 2$ (which we take before the EWPT, but this should not change the result as charge is conserved), and using again the relations (C.2–C.7) we arrive to

$$Q = \frac{4T^2}{3} [N_F \mu_{u_L} - \mu_\nu - (2N_F + m + 2)\mu_W + (2N_F + m)\mu_0]. \quad (\text{C.12})$$

And similarly

$$\begin{aligned} I_3 &= \frac{T^2}{6} \left[g_q N_F \left(\frac{1}{2} \mu_{u_L} + \left(-\frac{1}{2} \right) \mu_{u_R} \right) + g_l \sum_i \left(\frac{1}{2} \mu_{\nu i} + \left(-\frac{1}{2} \right) \mu_{e_L i} \right) \right. \\ &\quad \left. + 2g_W \left(-\mu_{W^+} (+1) + \mu_{W^-} (-1) \right) + 2g_{\phi^+} m \left(-\mu_{\phi^+} \frac{1}{2} + \mu_0 \left(-\frac{1}{2} \right) \right) \right], \end{aligned}$$

where we have already used the values of the third component of weak isospin for all the involved particles, and their degrees of freedom. Rearranging, we get to

$$I_3 = -\frac{T^2}{12} (2N_F + m + 4) \mu_W. \quad (\text{C.13})$$

Above the critical temperature: In this regime, both the total charges Q and I_3 of the plasma must vanish. As the relation (C.13) shows, this implies $\mu_W = 0$. Making use of the relation imposed by electroweak sphaleron transitions (C.9) and the vanishment of electromagnetic charge number density (C.12), we get the following conditions among the chemical potentials,

$$\begin{aligned} 2N_F \mu_{u_L} - 2\mu_\nu + (4N_F + 2m)\mu_0 &= 0, \\ 3N_F \mu_{u_L} + \mu_\nu &= 0. \end{aligned}$$

We can express B and L in terms of one single chemical potential, taken to be μ_{u_L} ,

$$\begin{aligned} B &= \frac{T^2}{3} 4N_F \mu_{u_L}, \\ L &= -\frac{T^2}{3} \frac{14N_F + 9N_F m}{2N_F + m} \mu_{u_L}, \end{aligned}$$

and also

$$B - L = \frac{T^2}{3} \frac{22N_F^2 + 13N_F m}{2N_F + m} \mu_{u_L}.$$

Finally, we get to relate the B and L number densities with the sphaleron-conserved quantity $B - L$,

$$B = \frac{8N_F + 4m}{22N_F + 13m} (B - L), \quad (\text{C.14})$$

$$L = -\frac{14N_F + 9m}{22N_F + 13m} (B - L). \quad (\text{C.15})$$

These relations would be to be used in the case that sphalerons go out of equilibrium before EWPT (for example if EWPT had been strongly first order or if they are suppressed by some mechanism). In the case of the SM, with $N_F = 3$ and $m = 1$, the above relations acquire the values: $B = \frac{28}{79} B - L$, and $L = \frac{51}{79} B - L$.

Under the critical temperature: In this regime Q still must be zero, but I_3 no longer needs to vanish, since $SU(2)_L$ has been broken and it is not a symmetry of the model any more. This translates in $\mu_W \neq 0$. However, because of the vacuum condensate of ϕ^0 Higgs bosons, μ_0 must vanish in this case. The charge vanishment and the electroweak sphaleron relation impositions take in this case the form

$$2N_{\text{F}}\mu_{u_L} - 2\mu_\nu - (4N_{\text{F}} + 2m + 4)\mu_W = 0,$$

$$3N_{\text{F}}\mu_{u_L} + 2N_{\text{F}}\mu_W + \mu_\nu = 0.$$

Rewriting everything again in terms of μ_{u_L} , we get to

$$B = \frac{T^2}{3} \frac{8N_{\text{F}}^2 + 4N_{\text{F}}(m + 2)}{m + 2} \mu_{u_L},$$

$$L = -\frac{T^2}{3} \frac{16N_{\text{F}}^2 + 9N_{\text{F}}(m + 2)}{m + 2} \mu_{u_L},$$

$$B - L = \frac{T^2}{3} \frac{24N_{\text{F}}^2 + 13N_{\text{F}}(m + 2)}{m + 2} \mu_{u_L},$$

and then to the relations

$$B = \frac{8N_{\text{F}} + 4(m + 2)}{24N_{\text{F}} + 13(m + 2)} (B - L), \quad (\text{C.16})$$

$$L = -\frac{16N_{\text{F}} + 9(m + 2)}{24N_{\text{F}} + 13(m + 2)} (B - L). \quad (\text{C.17})$$

These relations are valid in the case where electroweak sphalerons are rapid both above and below the EWPT. In the particular case of our SM with $N_{\text{F}} = 3$ and $m = 1$, then the B and L numbers today are given by $B = \frac{36}{111}B - L$, and $L = \frac{75}{111}B - L$.

Bibliography

- [1] B. Schulz, *Review on the quantization of gravity*, [1409.7977](#).
- [2] PARTICLE DATA GROUP collaboration, P. Zyla et al., *Review of Particle Physics*, *PTEP* **2020** (2020) 083C01.
- [3] C. Csáki and P. Tanedo, *Beyond the Standard Model*, in *2013 European School of High-Energy Physics*, pp. 169–268, 2015, [1602.04228](#), DOI.
- [4] E. W. Kolb and M. S. Turner, *The Early Universe*, vol. 69. 1990.
- [5] R. D. Peccei and H. R. Quinn, *CP conservation in the presence of pseudoparticles*, *Phys. Rev. Lett.* **38** (1977) 1440.
- [6] J. E. Kim and G. Carosi, *Axions and the Strong CP Problem*, *Rev. Mod. Phys.* **82** (2010) 557 [[0807.3125](#)].
- [7] SUPERNOVA SEARCH TEAM collaboration, A. G. Riess et al., *Observational evidence from supernovae for an accelerating universe and a cosmological constant*, *Astron. J.* **116** (1998) 1009 [[astro-ph/9805201](#)].
- [8] M. J. Mortonson, D. H. Weinberg and M. White, *Dark Energy: A Short Review*, [1401.0046](#).
- [9] G. Bertone, D. Hooper and J. Silk, *Particle dark matter: Evidence, candidates and constraints*, *Phys. Rept.* **405** (2005) 279 [[hep-ph/0404175](#)].
- [10] K. Freese, *Review of Observational Evidence for Dark Matter in the Universe and in upcoming searches for Dark Stars*, *EAS Publ. Ser.* **36** (2009) 113 [[0812.4005](#)].
- [11] F. Zwicky, *Die Rotverschiebung von extragalaktischen Nebeln*, *Helv. Phys. Acta* **6** (1933) 110.
- [12] V. C. Rubin and W. K. J. Ford, *Rotation of the Andromeda Nebula from a Spectroscopic Survey of Emission Regions*, *Astrophysical Journal* **159** (1970) 379.
- [13] K. G. Begeman, A. H. Broeils and R. H. Sanders, *Extended rotation curves of spiral galaxies: dark haloes and modified dynamics*, *Monthly Notices of the Royal Astronomical Society* **249** (1991) 523.
- [14] E. W. Greisen, K. Spekkens and G. A. van Moorsel, *Aperture synthesis observations of the nearby Spiral NGC 6503: modeling the thin and thick H I disks*, *The Astronomical Journal* **137** (2009) 4718.
- [15] H. Hoekstra, H. Yee and M. Gladders, *Current status of weak gravitational lensing*, *New Astron. Rev.* **46** (2002) 767 [[astro-ph/0205205](#)].

- [16] D. Clowe, M. Bradac, A. H. Gonzalez, M. Markevitch, S. W. Randall, C. Jones et al., *A direct empirical proof of the existence of dark matter*, *Astrophys. J. Lett.* **648** (2006) L109 [[astro-ph/0608407](#)].
- [17] M. Markevitch, *Chandra observation of the most interesting cluster in the universe*, *ESA Spec. Publ.* **604** (2006) 723 [[astro-ph/0511345](#)].
- [18] PLANCK collaboration, N. Aghanim et al., *Planck 2018 results. VI. Cosmological parameters*, *Astron. Astrophys.* **641** (2020) A6 [[1807.06209](#)].
- [19] P. J. E. Peebles, *Growth of the nonbaryonic dark matter theory*, *Nature Astron.* **1** (2017) 0057 [[1701.05837](#)].
- [20] L. J. Hall, K. Jedamzik, J. March-Russell and S. M. West, *Freeze-In Production of FIMP Dark Matter*, *JHEP* **03** (2010) 080 [[0911.1120](#)].
- [21] Y. Hochberg, E. Kuflik, T. Volansky and J. G. Wacker, *Mechanism for Thermal Relic Dark Matter of Strongly Interacting Massive Particles*, *Phys. Rev. Lett.* **113** (2014) 171301 [[1402.5143](#)].
- [22] M. Fabbrichesi, E. Gabrielli and G. Lanfranchi, *The Dark Photon*, [2005.01515](#).
- [23] K. Benakli, Y. Chen, E. Dudas and Y. Mambrini, *Minimal model of gravitino dark matter*, *Phys. Rev. D* **95** (2017) 095002 [[1701.06574](#)].
- [24] B. Carr, F. Kuhnel and M. Sandstad, *Primordial Black Holes as Dark Matter*, *Phys. Rev. D* **94** (2016) 083504 [[1607.06077](#)].
- [25] S. Joudaki et al., *KiDS-450: Testing extensions to the standard cosmological model*, *Mon. Not. Roy. Astron. Soc.* **471** (2017) 1259 [[1610.04606](#)].
- [26] S. Dodelson, *The Real Problem with MOND*, *Int. J. Mod. Phys. D* **20** (2011) 2749 [[1112.1320](#)].
- [27] J. L. Feng, *Dark Matter Candidates from Particle Physics and Methods of Detection*, *Ann. Rev. Astron. Astrophys.* **48** (2010) 495 [[1003.0904](#)].
- [28] G. Steigman, B. Dasgupta and J. F. Beacom, *Precise Relic WIMP Abundance and its Impact on Searches for Dark Matter Annihilation*, *Phys. Rev. D* **86** (2012) 023506 [[1204.3622](#)].
- [29] G. Jungman, M. Kamionkowski and K. Griest, *Supersymmetric dark matter*, *Phys. Rept.* **267** (1996) 195 [[hep-ph/9506380](#)].
- [30] L. Roszkowski, E. M. Sessolo and S. Trojanowski, *WIMP dark matter candidates and searches—current status and future prospects*, *Rept. Prog. Phys.* **81** (2018) 066201 [[1707.06277](#)].
- [31] D. J. E. Marsh, *Axion Cosmology*, *Phys. Rept.* **643** (2016) 1 [[1510.07633](#)].
- [32] M. Archidiacono, S. Hannestad, A. Mirizzi, G. Raffelt and Y. Y. Y. Wong, *Axion hot dark matter bounds after Planck*, *JCAP* **10** (2013) 020 [[1307.0615](#)].
- [33] J. E. Kim, *Weak-interaction singlet and strong CP invariance*, *Phys. Rev. Lett.* **43** (1979) 103.

- [34] M. Shifman, A. Vainshtein and V. Zakharov, *Can confinement ensure natural cp invariance of strong interactions?*, *Nuclear Physics B* **166** (1980) 493.
- [35] A. Ringwald, *Exploring the Role of Axions and Other WISPs in the Dark Universe*, *Phys. Dark Univ.* **1** (2012) 116 [[1210.5081](#)].
- [36] F. Chadha-Day, J. Ellis and D. J. E. Marsh, *Axion Dark Matter: What is it and Why Now?*, [2105.01406](#).
- [37] B. Pontecorvo, *Mesonium and antimesonium*, *Zhur. Eksptl'. i Teoret. Fiz.*
- [38] R. N. Mohapatra, *Seesaw mechanism and its implications*, in *SEESAW25: International Conference on the Seesaw Mechanism and the Neutrino Mass*, pp. 29–44, 12, 2004, [hep-ph/0412379](#), DOI.
- [39] S. Dodelson and L. M. Widrow, *Sterile-neutrinos as dark matter*, *Phys. Rev. Lett.* **72** (1994) 17 [[hep-ph/9303287](#)].
- [40] A. Boyarsky, M. Drewes, T. Lasserre, S. Mertens and O. Ruchayskiy, *Sterile neutrino Dark Matter*, *Prog. Part. Nucl. Phys.* **104** (2019) 1 [[1807.07938](#)].
- [41] J. Heisig, M. Korsmeier and M. W. Winkler, *Dark matter or correlated errors: Systematics of the AMS-02 antiproton excess*, *Phys. Rev. Res.* **2** (2020) 043017 [[2005.04237](#)].
- [42] A. G. Cohen, A. De Rujula and S. L. Glashow, *A Matter - antimatter universe?*, *Astrophys. J.* **495** (1998) 539 [[astro-ph/9707087](#)].
- [43] A. D. Sakharov, *Violation of CP Invariance, C asymmetry, and baryon asymmetry of the universe*, *Pisma Zh. Eksp. Teor. Fiz.* **5** (1967) 32.
- [44] G. 't Hooft, *Symmetry breaking through bell-jackiw anomalies*, *Phys. Rev. Lett.* **37** (1976) 8.
- [45] D. Bodeker and W. Buchmuller, *Baryogenesis from the weak scale to the grand unification scale*, *Rev. Mod. Phys.* **93** (2021) 035004 [[2009.07294](#)].
- [46] T. Akiba, H. Kikuchi and T. Yanagida, *Relaxation of Baryon Number in the Standard Electroweak Model*, *Prog. Theor. Phys.* **83** (1990) 671.
- [47] M. Dine and A. Kusenko, *The Origin of the matter - antimatter asymmetry*, *Rev. Mod. Phys.* **76** (2003) 1 [[hep-ph/0303065](#)].
- [48] I. Affleck and M. Dine, *A new mechanism for baryogenesis*, *Nuclear Physics B* **249** (1985) 361.
- [49] A. G. Cohen, D. B. Kaplan and A. E. Nelson, *Progress in electroweak baryogenesis*, *Ann. Rev. Nucl. Part. Sci.* **43** (1993) 27 [[hep-ph/9302210](#)].
- [50] V. Kuzmin, V. Rubakov and M. Shaposhnikov, *On anomalous electroweak baryon-number non-conservation in the early universe*, *Physics Letters B* **155** (1985) 36.
- [51] K. Kajantie, M. Laine, K. Rummukainen and M. E. Shaposhnikov, *The Electroweak phase transition: A Nonperturbative analysis*, *Nucl. Phys. B* **466** (1996) 189 [[hep-lat/9510020](#)].

- [52] M. B. Gavela, P. Hernandez, J. Orloff and O. Pene, *Standard model CP violation and baryon asymmetry*, *Mod. Phys. Lett. A* **9** (1994) 795 [[hep-ph/9312215](#)].
- [53] D. E. Morrissey and M. J. Ramsey-Musolf, *Electroweak baryogenesis*, *New J. Phys.* **14** (2012) 125003 [[1206.2942](#)].
- [54] N. Terasawa and K. Sato, *Lepton and Baryon Number Asymmetry of the Universe and Primordial Nucleosynthesis*, *Progress of Theoretical Physics* **80** (1988) 468.
- [55] E. Castorina, U. Franca, M. Lattanzi, J. Lesgourgues, G. Mangano, A. Melchiorri et al., *Cosmological lepton asymmetry with a nonzero mixing angle θ_{13}* , *Phys. Rev. D* **86** (2012) 023517 [[1204.2510](#)].
- [56] C. Pitrou, A. Coc, J.-P. Uzan and E. Vangioni, *Precision big bang nucleosynthesis with improved Helium-4 predictions*, *Phys. Rept.* **754** (2018) 1 [[1801.08023](#)].
- [57] K. Petraki and R. R. Volkas, *Review of asymmetric dark matter*, *Int. J. Mod. Phys. A* **28** (2013) 1330028 [[1305.4939](#)].
- [58] K. M. Zurek, *Asymmetric Dark Matter: Theories, Signatures, and Constraints*, *Phys. Rept.* **537** (2014) 91 [[1308.0338](#)].
- [59] V. A. Rubakov and D. S. Gorbunov, *Introduction to the Theory of the Early Universe: Hot big bang theory*. World Scientific, Singapore, 2017, [10.1142/10447](#).
- [60] A. D. Dolgov, *Neutrinos in cosmology*, *Phys. Rept.* **370** (2002) 333 [[hep-ph/0202122](#)].
- [61] H. Iminniyaz, M. Drees and X. Chen, *Relic abundance of asymmetric dark matter*, *Journal of Cosmology and Astroparticle Physics* **2011** (2011) 003–003.
- [62] E. Ma, *Verifiable radiative seesaw mechanism of neutrino mass and dark matter*, *Phys. Rev. D* **73** (2006) 077301 [[hep-ph/0601225](#)].
- [63] M. D’Onofrio, K. Rummukainen and A. Tranberg, *Sphaleron Rate in the Minimal Standard Model*, *Phys. Rev. Lett.* **113** (2014) 141602 [[1404.3565](#)].
- [64] Y. Burnier, M. Laine and M. Shaposhnikov, *Baryon and lepton number violation rates across the electroweak crossover*, *JCAP* **02** (2006) 007 [[hep-ph/0511246](#)].
- [65] S. Eijima, M. Shaposhnikov and I. Timiryasov, *Freeze-out of baryon number in low-scale leptogenesis*, *JCAP* **11** (2017) 030 [[1709.07834](#)].
- [66] J. A. Harvey and M. S. Turner, *Cosmological baryon and lepton number in the presence of electroweak fermion number violation*, *Phys. Rev. D* **42** (1990) 3344.
- [67] C. A. Argüelles, A. Diaz, A. Kheirandish, A. Olivares-Del-Campo, I. Safa and A. C. Vincent, *Dark matter annihilation to neutrinos*, *Rev. Mod. Phys.* **93** (2021) 035007 [[1912.09486](#)].
- [68] K. Griest and D. Seckel, *Three exceptions in the calculation of relic abundances*, *Phys. Rev. D* **43** (1991) 3191.
- [69] E. Nardi, Y. Nir, J. Racker and E. Roulet, *On Higgs and sphaleron effects during the leptogenesis era*, *JHEP* **01** (2006) 068 [[hep-ph/0512052](#)].